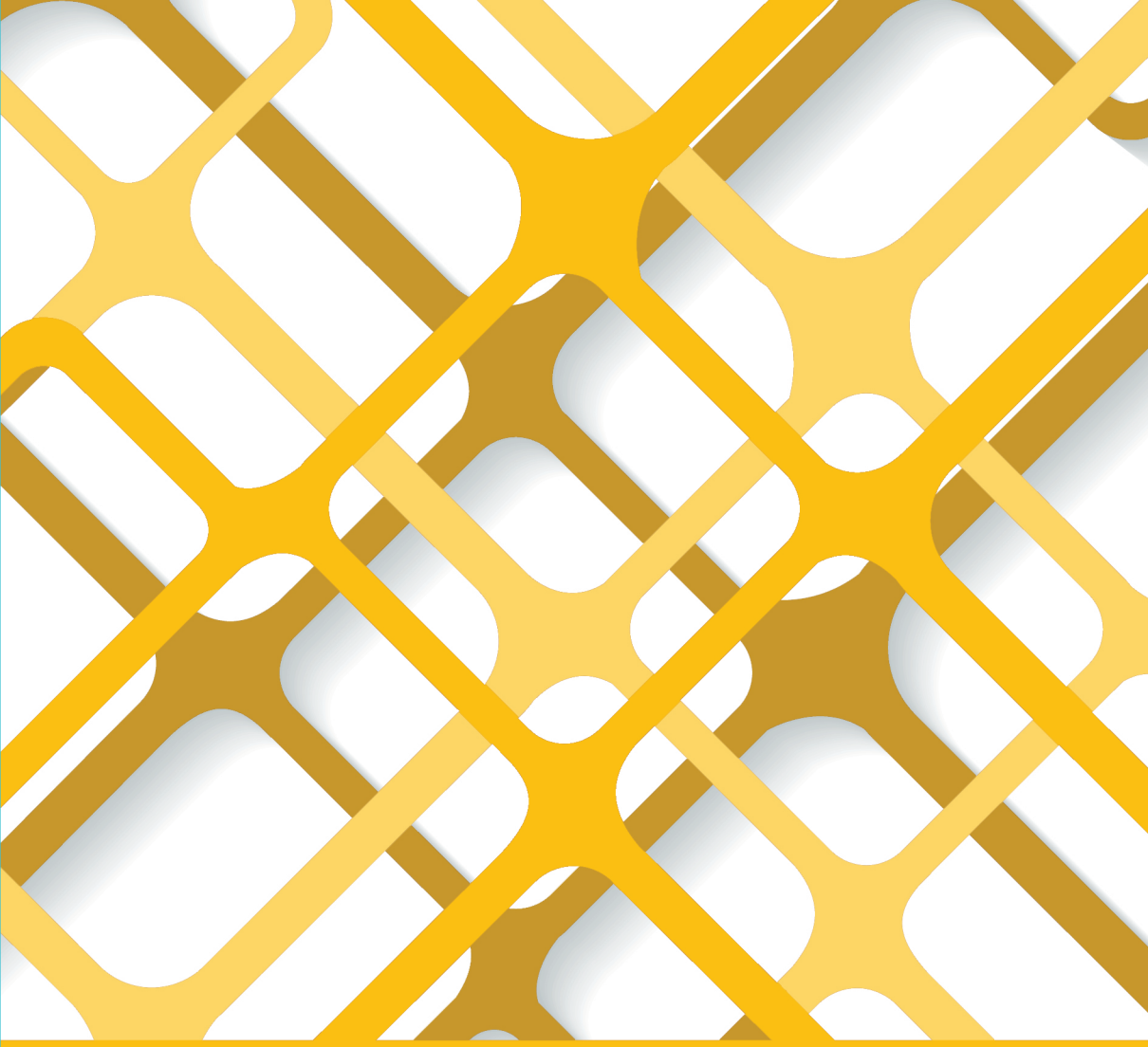

RESEARCH & REVIEWS IN SCIENCE AND MATHEMATICS

SEPTEMBER/2021

EDITORS
PROF. DR. HASAN AKGÜL
PROF. DR. MURAT KÜTÜK

gece kitaplığı

İmtiyaz Sahibi / Publisher • Yaşar Hız
Genel Yayın Yönetmeni / Editor in Chief • Eda Altunel
Kapak & İç T asarım / Cover & Interior Design • Gece Kitaplığı
Editörler / Editors • Prof. Dr. Hasan Akgül
Prof. Dr. Murat Kütük
Birinci Basım / First Edition • © Eylül 2021
ISBN • 978-625-8002-41-6

Gece Kitaplığı / Gece Publishing
Türkiye Adres / Turkey Address: Kızılay Mah. Fevzi Çakmak 1. Sokak Ümit Apt. No: 22/A Çankaya / Ankara / TR
Telefon / Phone: +90 312 384 80 40
web: www.gecekitapligi.com
e-mail: gecekitapligi@gmail.com

Baskı & Cilt / Printing & Volume
Sertifika / Certificate No: 47083

RESEARCH & REVIEWS IN SCIENCE AND MATHEMATICS

September / 2021

EDITORS

PROF. DR. HASAN AKGÜL

PROF. DR. MURAT KÜTÜK

gece kitaplığı

CONTENTS

Chapter 1

BROWN DWARFS

E. Nihal ERCAN[1]

1 Prof. Dr. E.Nihal Ercan, Boğaziçi University, Physics Department

I. Introduction

Figure 1 Color of an isolated Brown Dwarf See (3)

Brown dwarfs, as they are most known, are substellar objects that fail to become planets or stars. Their existence was introduced before the 1980s. In the 1960s, Shiv S. Kumar called them "black dwarfs" (1), contrary to its now-known name, but in astronomy, the "Black Dwarf" term was used because they represented another object. Black dwarfs are a concept related to cold white dwarfs, which do not emit significant light and heat anymore. In the astronomical world, several ideas have been put forward about what to call these objects: red dwarfs represent the smallest and coldest star in the main sequence stars, and thus this name is also rejected because it fuses hydrogen, unlike Brown Dwarfs. Although names such as "Planetar" and "Substar" have been proposed, in 1975 Jill Tarter come up with the term "Brown Dwarf" because brown is an approximate color, and this strange and mysterious object is named in this way (49) (3) (50). Although their name gives the impression that they are brown, this is not true, they have a color scale that varies according to the temperature they have. The hotter ones are seen between red and orange, but the cold ones have a color that plays magenta. (3)

To better understand the definition of brown dwarfs, it is necessary to know their specific characteristics and how stars form. Astronomers who studied how very low-mass stars form and evolve revealed the existence of brown dwarfs in the 1960s (2). The stars' massive clouds of molecular gas collapse due to gravity, increasing the temperature and pressure in the center. As a result of this temperature and intensity, nuclear fusion reactions that convert hydrogen into helium begin. This process forms one of the most fundamental differences between a star and a planet. On planets inside and outside of the solar system, the process takes place first in the form of the formation of the nucleus and then in the collection of material. On most

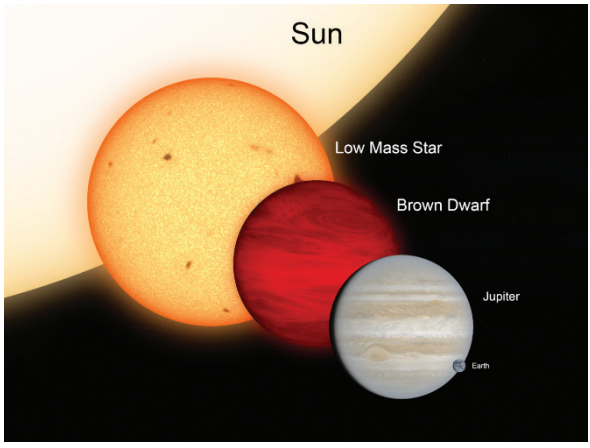

Figure 2 See(48)

large-mass planets, the nucleus has enough mass to steal gas from the pre-star disk; that is how gas giants like Jupiter and Saturn form. However, brown dwarfs form like stars; they collapse like a star in a cloud of gas. However, at the end of the process, they do not turn into stars. According to the theory about low-mass stars, there is a certain mass limit for objects to fuse hydrogen. Thus, brown dwarfs do not fuse hydrogen and are therefore also called, *failed stars*. Brown dwarfs are thought to fuse deuterium or lithium depending on their mass. Brown dwarfs have a mass between the most massive gas giant planets and the least massive stars (51) (52). They are thought to be between 10 and 84 Jupiter masses. The minimum mass for burning deuterium is 13 Jupiter masses, and below that value lies planets. Also, they are called *super Jupiter* since they are massive gas structures. The smallest brown dwarfs cannot fuse anything. However, if they could start fusion reaction even for a small moment, they can store that energy for billion years in their cores.

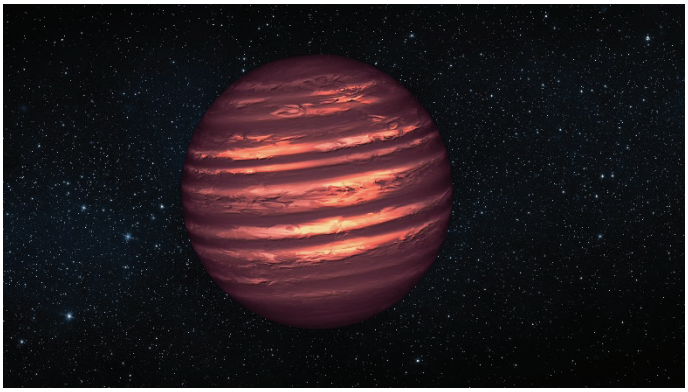

Figure 3 See (47)

The way brown dwarfs are defined also was a topic of discussion. Ideas have been put forward that it would be more accurate to identify them with their formation processes rather than mass limits on nuclear reactions. Accordingly, brown dwarfs are the lowest mass product of the star formation process, while planets as they are known, form in gases and dust around stars (2). Objects with a mass of less than 13 M_j were discovered, resulting in uncertainty about whether they are brown dwarfs or rogue planets[1]. Therefore, such an opinion has been put forward.

The first brown dwarf searches were conducted, in part, with speculation that they could be the main component of dark matter (though not true). In theory, their existence was revealed in the 1960s, however, they were not discovered until the mid-1990s. This was not because they were rare objects in the universe, but because they were not bright objects. Since they have relatively low surface temperatures, they do not emit much

1 A *rogue planet* term is used for the planets that do not orbit a star. (46)

at visible light wavelength, mostly emit at infrared wavelength. Devices to observe the brown dwarfs and methods are found and developed in the late 1980s. Some of the methods are imaging studies for faint companions of main sequence stars and white dwarfs and searches in young star clusters[2]. Hundreds of brown dwarfs are discovered since then.

Table 6.1 Spectral Classes

Spectral Class	Approximate Temperature (K)	Hydrogen Balmer Lines	Other Spectral Features	Naked-Eye Example
O	40,000	Weak	Ionized helium	Meissa (O8)
B	20,000	Medium	Neutral helium	Achernar (B3)
A	10,000	Strong	Ionized calcium weak	Sirius (A1)
F	7,500	Medium	Ionized calcium weak	Canopus (F0)
G	5,500	Weak	Ionized calcium medium	Sun (G2)
K	4,500	Very weak	Ionized calcium strong	Arcturus (K2)
M	3,000	Very weak	TiO strong	Betelgeuse (M2)

Figure 4 Resource: ASTRO, chapter 6: see (47)

Astronomers classify self-luminous objects according to the lines and bands in their spectrum, which they call spectral classes. Although normal stars are in the O, B, A, F, G, K, M classes according to their surface temperature, new classes, L, T, and Y have been added with the discovery of brown dwarfs because the surface temperatures of brown dwarfs are much lower than in other classes in the table. Brown dwarfs are in M, L, T, and Y classes (2) (53). In addition, brown dwarfs pass through later spectral types as they age because they do not have stable hydrogen fusion like other stars, and they cool down over time. (M => L => T => Y)

II. Observational Properties of Brown Dwarfs

We mentioned in the previous section that the existence of brown dwarfs has been known since the 1960s and received this name in 1975. Astronomers began an intensive search for brown dwarfs in the mid-1980s, but these first attempts went fruitless. In 1995, the first definitive conclusion of their existence was obtained. It was a well-known fact that brown dwarfs were not bright objects because, like stars, they did not have nuclear energy reactions to be bright. Astronomers began looking around known stars to find such faint objects. In our galaxy, half the stars are in binary systems, and astronomers have suspected that there may be a brown dwarf close to the stars that appear to be alone. In this way, they have limited the places they can look for a brown dwarf. This strategy also paid off. In 1988, astronomers Ben Zuckerman and Eric Becklin discovered a brown dwarf candidate called GD 165B. However, they could not be sure that this red object accompanying a white dwarf was a brown dwarf because its mass was on the mass boundary of low-mass stars and

2 https://en.wikipedia.org/wiki/Brown_dwarf#cite_note-Cain-6

brown dwarfs. There were advantages to looking for brown dwarfs in a binary system. Because in this way, they could be found through periodic changes in the movement of the other star in which they orbit. The Doppler shift in their spectrum gave them this opportunity. At the same time, their mass, which was greater than the planet, was advantageous in this method. However, still, brown dwarfs were not easy to find and were considered rare at that time. In 1988, David W. Latham found a brown dwarf candidate using the doppler method, but this was likely to be a low-mass star because the doppler method provided only a lower limit for the companion's mass. Another way astronomers were looking for brown dwarfs, was to look at star clusters because brown dwarfs were brightest at the time when they were young, and star clusters were the ideal place to look at young objects. In this way, many brown dwarf candidates were found, but none of them were brown dwarfs. They were usually found to be red dwarfs or low-mass stars. Then the idea of the lithium test to distinguish low-mass stars from brown dwarfs was proposed, and in 1995 the first brown dwarf, Teide 1 was discovered in the Pleiades cluster, with the help of this idea. (9)

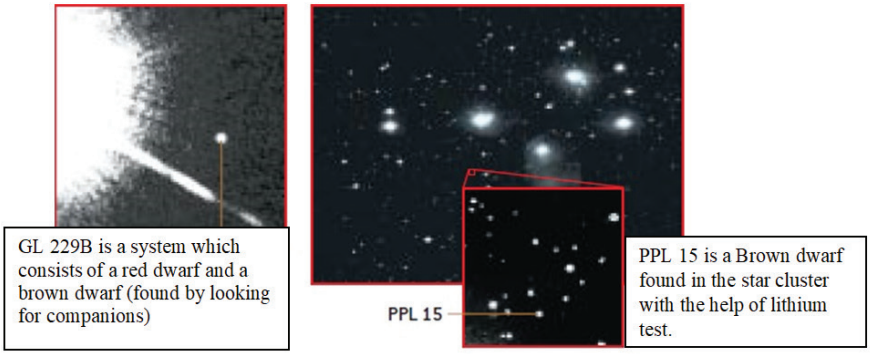

Figure 5.See (9)

In 2006, an interesting binary system was detected using ESO's large telescope: the white dwarf and the brown dwarf system. Pierre Maxted, the lead author of the study, says "Its existence proves that the brown dwarf came out almost unaltered from an episode in which it was swallowed by a red giant". (20) Right now, the distance between them is a few thousand times the distance between the Sun and the Earth. However, they were not this close in the past. The star, now a white dwarf when it was a red giant, swallows the brown dwarf and the brown dwarf draws a spiral towards the nucleus. When the outer layers of the red giant drift away from the nucleus, it leaves behind a pair of the white dwarf and brown dwarf with a close orbit. (20)

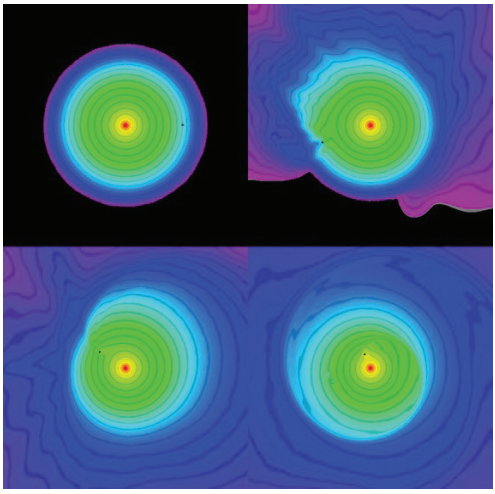

Figure 6 Brown dwarf swallowed by red giant ,see(20).

Today, new methods continue to be found in this area. In 2020, a brown dwarf was discovered for the first time using a radio telescope. We said another name for brown dwarfs was super Jupiters. Large planets like Jupiter emit radio light because of their magnetic dynamos. Brown dwarfs are like Jupiter; thus, they emit radio light in the same way. The conducted study captured a radio signal detected from a brown dwarf with LOFAR, a low-frequency radio telescope. In this way, the discovery was made for the first time using only radio lights. Soon, many more brown dwarfs can also be found with this method. (44)

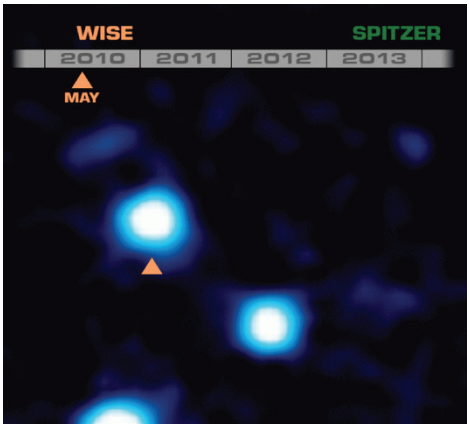

Figure 7 coldest brown dwarf see(13)

Nasa's Wide-field Infrared Survey Explorer (WISE) was launched in 2009 and studied the entire sky in infrared light in 2010. One of WISE's missions was to study brown dwarfs. According to WISE data, there may be six stars for one brown dwarf. In 2014, WISE and Spitzer Space Telescope discovered the coldest brown dwarf known. With 7.2 light-years away, it is the fourth closest system to our Sun. This new brown dwarf found was named WISE J085510.83-071442.5. The temperature ranged from -48 to -13 degrees. (14)

In March 2013, Luhman's analysis of the pictures taken by WISE uncovered warmer brown dwarfs 6.5 light-years away. With this distance, it deserves to be the third closest system to our Sun.See Figure 8.

In 2013, 27 brown dwarfs, including 16 L type dwarf and 11 T type dwarf, were observed in the study conducted with the infrared observation telescope AKARI. 16 of this observation provide good quality spectra, 5

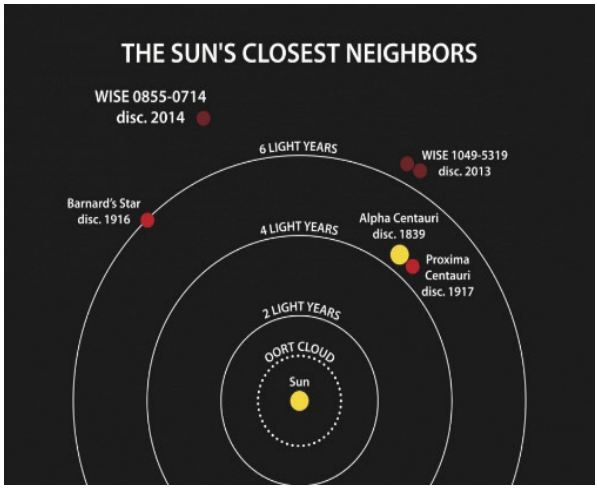

Figure 8 .(13)

of them was T type and 11 of them was L type. As a result of this study, the radius of 16 brown dwarfs was calculated and found to be largely compatible with pre-existing theories. According to the study, the average radius of brown dwarfs is 0.83 R_j[3]. The radius range of brown dwarfs is found to be 0.64 R_j to 1.13 R_j. In 2001, Burrows theoretically calculated radius, and this data matched this ratio, but there was a great discrepancy in mid and late-L dwarfs because, in the study, they found out that the radius of mid and late-L dwarfs is smaller than the theoretical one. However, they could not solve the reason behind this and left this question to later studies. (8) The data found in the study given in the figures (9, as their 2 and 3) *.

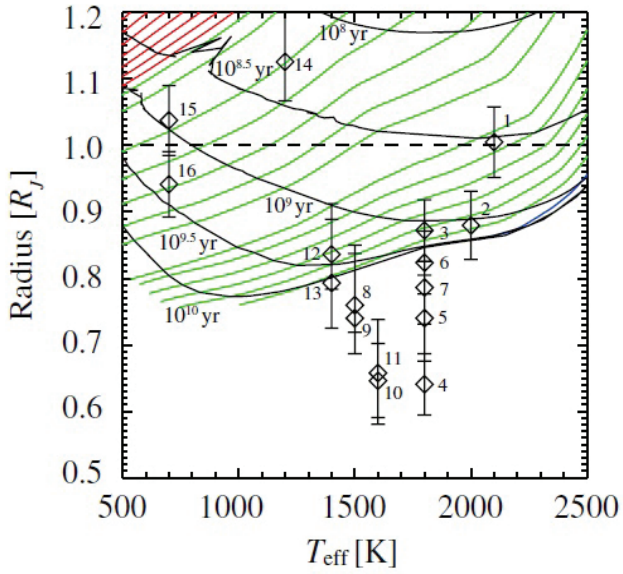

Figure 2. Radii of *AKARI* observed brown dwarfs are plotted on the theoretical prediction of the relation between T_{eff} and radii at different masses from 11 M_J to 0.085 $M_\odot$. Red are less massive objects with 11, 12, 13, and 15 M_J, blue are massive objects 0.08 and 0.085 $M_\odot$, and green are intermediate mass objects with 0.02, 0.025, 0.03, 0.035, 0.04, 0.045, 0.05, 0.055, 0.06, 0.065, 0.07, and 0.075 $M_\odot$. The numerical data for the evolutionary model was provided by A. Burrows (in private communication). The numbers are in object index in Table 2.

3 Radius of Jupiter = 69.911 km

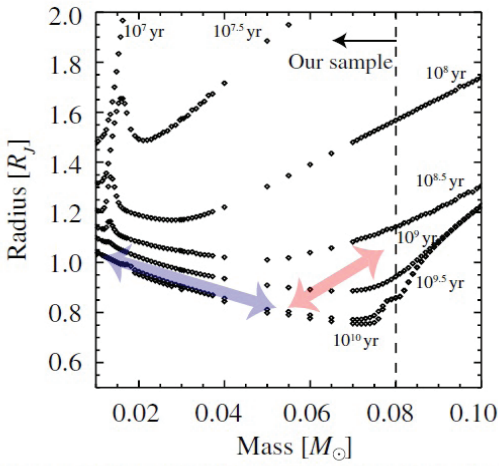

Figure 3. Theoretical prediction of the relation between the radius and mass of brown dwarfs at different ages. The radii of relatively light and young objects are small and rather stable throughout their lifetimes. On the other hand, the radii of massive dwarfs $\geqslant 0.06\,M_\odot$ are large when they are young, but ultimate radii are smaller than those of less massive objects. The radii of early-type objects in our sample tend to depend on their ages (shown by the red arrow), while those of late-type objects tend to depend more on their masses than their ages (shown by the blue arrow). The data was provided by A. Burrows (2012, private communication).

Table 2
The Radius of *AKARI* Objects

Object Name	Sp. Type	Radius(Error) (R_J)	Number in Figure 2
2MASS J1439+1929	L1	1.01(0.05)	1
2MASS J0036+1821	L4	0.88(0.05)	2
2MASS J2224−0158	L4.5	0.87(0.05)	3
GJ 1001B	L5	0.64(0.05)	4
SDSS J1446+0024	L5	0.74(0.06)	5
SDSS J0539−0059	L5	0.82(0.05)	6
2MASS J1507−1627	L5	0.79(0.06)	7
2MASS J0825+2115	L6	0.76(0.09)	8
2MASS J1632+1904	L7.5	0.74(0.10)	9
2MASS J1523+3014	L8	0.65(0.09)	10
SDSS J0830+4828	L9	0.66(0.08)	11
SDSS J1254−0122	T2	0.84(0.05)	12
SIMP J0136+0933	T2.5	0.80(0.12)	13
2MASS J0559−1404	T4.5	1.13(0.18)	14
Gl 570D	T8	1.04(0.05)	15
2MASS J0415−0935	T8	0.94(0.05)	16

Also, the theory predicts that there is an inverse relation between radius-mass and radius-age in brown dwarfs older than 10^8 years old. The result of this study also proves that theoretical prediction.

*Figures are taken from: https://iopscience.iop.org/article/10.1088/0004-637X/767/1/77/pdf

Wind Speed of a Brown Dwarf

Using NASA's Spitzer Space Telescope and National Science Foundation's Karl G. Jansky Very Large Array (VLA), astronomers measured the wind speed of a brown dwarf called 2MASS J10475385+2124234. They conducted their experiments on a brown dwarf about the size of Jupiter, which is 34 times more massive than Jupiter. Astronomers have noticed that the rotational period in observations of Jupiter's radio waves is different from the rotational period in observations made in infrared and visible waves. The reason for this difference is that; radio waves interact with Jupiter's magnetic field, which is related to the interior, but infrared waves are associated with the top surface of the atmosphere. The atmosphere rotates faster than the planet's interior, and this difference in speed is due to atmospheric winds. Using NASA's Spitzer Space Telescope and VLA data, astronomers showed that the same situation applies to the brown dwarfs. They calculated the speed of atmospheric winds as1425

miles per hour. This method is also a good development for understanding the atmospheric properties of extrasolar planets. (25)

First Direct Brown Dwarf Mass Measurement

Today, astronomers do mass calculations separately because there is no general theory or relationship between mass and luminosity. Astronomers who conduct a study for 4 years, achieved the first direct calculation of the mass of a brown dwarf in the binary system called 2MASSW J0746425+2000321 in 2004. First, the stellar orbits and physical separation of the objects in the binary system, which were observed from different positions for 4 years, were calculated. Using this information and Kepler's Laws, they found the total mass of the system, which is less than 0.15 $M_{\odot}$. Using photometric data and spectrum with appropriate models, astronomers calculated the surface temperatures of objects. They found that two objects share the same value, approximately 1,800 Kelvins, which is cold indeed for a star. Then, using theoretical models, they found the ages and individual masses of the objects. The more massive one has a mass of 0.075-0.095 $M_{\odot}$, while the other has a mass of between 0.05-0.07 $M_{\odot}$. Since objects with masses below 0.072 (in some sources 0.08) are considered brown dwarfs, astronomers have measured the mass of a brown dwarf directly for the first time. (26)

Atmospheric Properties of Brown Dwarfs

The surface temperature of known brown dwarfs is between 750 - 2200 Kelvins. (27) Unlike stars, brown dwarfs cool over time, since they do not have an energy source like hydrogen fusing. More massive brown dwarfs cool more slowly compared to brown dwarfs with less mass. Brown dwarfs, like planets, have climate and clouds. These clouds are mostly composed of dust from minerals such as Enstatite and Corundum. The size of these particles is 0.5 micrometers. In wo855-0714, the brown dwarf was found to have clouds of frozen sulfide and water ice; gases such as Methane, Hydrogen Sulfide, and Ammonia are assumed to be present. In addition, there are indications of extreme hurricanes, a lot of lightning activity, and melt sand or iron rain in brown dwarfs with patch-like cloud structures. (35)

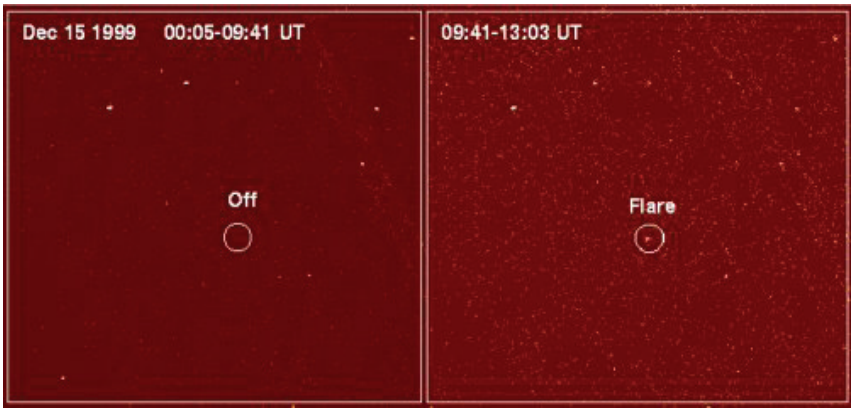

Figure 10. LP 944-20 in non-flare and flare picture ,see (29)

X-Ray Flares from Brown Dwarfs

X-ray flares were detected from brown dwarfs in 1999 (30). This may be due to changing magnetic fields. Brown dwarfs do not have a strong energy source like stars, they do not fuse hydrogen. The interior of brown dwarfs is also convective. With these conditions and a fast rotational speed, convection provides appropriate conditions for the formation of a strong and mixed magnetic field close to the surface in brown dwarfs. The flare Chandra observed from LP 944-20 may have been caused by magnetized hot material beneath the surface of brown dwarfs. This situation below the surface can cause heat to be transmitted to the atmosphere and current to form. In this way, x-ray flares may occur. The absence of x-rays in LP 944-20 during the period that does not flare also indicates the lowest observational limit of X-ray power produced by the brown dwarf. In addition, this situation indicates that the presence of coronas stops as it cools to below about 2800K and becomes electrically neutral. (28)

Exoplanet Around Brown Dwarf

In 2004, astronomers discovered a planet about five times the mass of Jupiter and gravitationally bound to a brown dwarf. This planet, called 2M1207b, is also the first planet to be observed outside the solar system. (36) The planet is more than

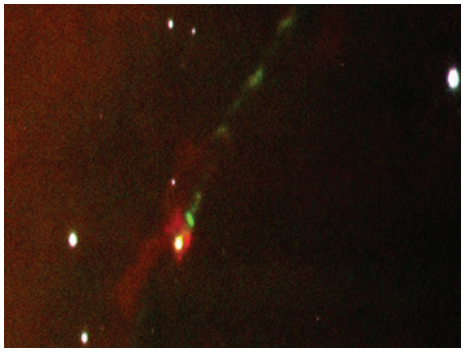

Figure 11

100 times fainter than the brown dwarf, 2M1207a. The distance between them is 55 times the distance between Earth and Sun. This system, which was observed for a year, also confirmed the findings from the previous year in 2005. These objects, which are gravitationally bound, seem to remain that way. In this way, the possibility of forming a planet that can orbit the brown dwarf from the accretion disc around the brown dwarf has been confirmed. (32) See Figure 11 above.

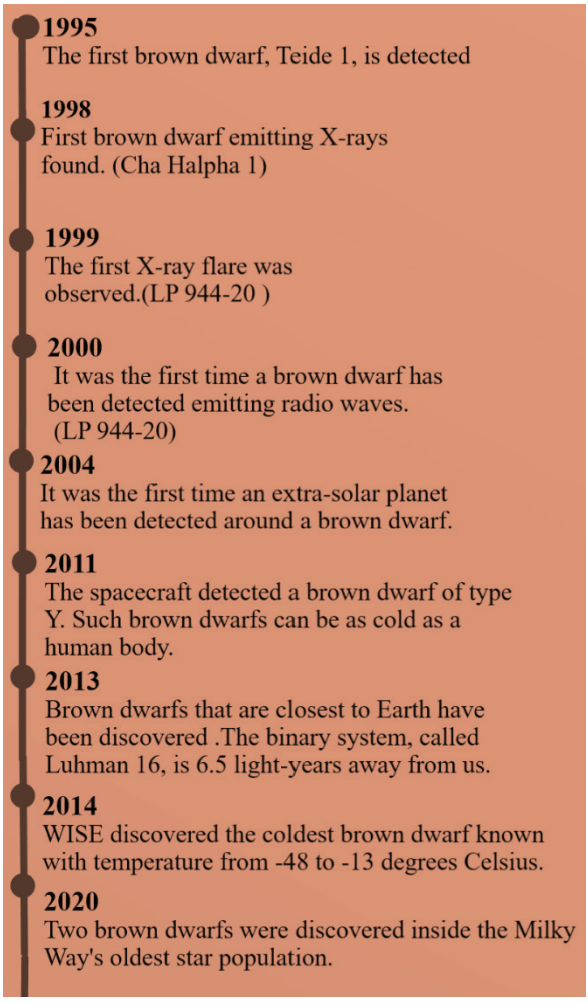

<---Timing Diagram of Brown Dwarfs

Figure 12 The picture of 2M1207 system (reddish one is planet, the blueish one is the brown dwarf),see (32)

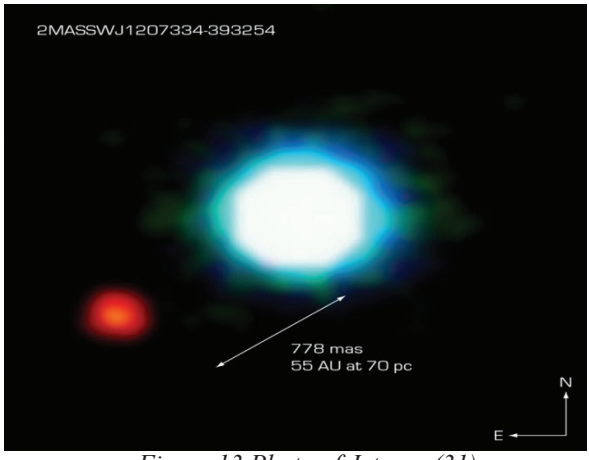

Figure 13 Photo of Jet ,see (31)

Observing the SOAR telescope at the Cerro Tololo Inter-American Observatory, astronomers discovered a jet that had expanded from a young brown dwarf in 2017. Usually, young stars launch jets, and this is the first time this brown dwarf has had a similar event. This supports the idea that brown dwarfs form like stars. Jet, HH 1165; is launched from a brown dwarf named Mayrit 1701117. As it is viewed with singly ionized sulfur, we see a green color extending to the northwest of the brown dwarf in the photo. The jet extends to 0.7 light-years (corresponding to 0.2 pc). The red nebula to the southeast is also caused by the reflection nebula. The knots seen in the jet may indicate that the mass loss is time-dependent and may be the result of episodic accretion in the brown dwarf. This discovery shows that brown dwarfs launch jet like stars, and their mass is built in the episodic and unsteady process like stars. (31)

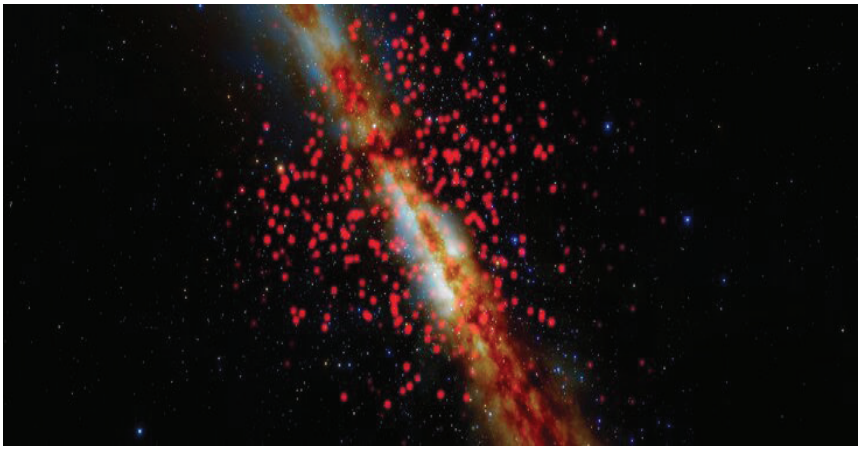

Ninety-five brown dwarfs were discovered around the Sun as part of the Backyard Worlds: Planet 9 project, which was carried out with the help of NASA and professional scientists and volunteers. These objects are presumed to be brown dwarfs because they are too large to be planets and too small to be stars. The brown dwarfs found are an important development for the astronomical world because they give insight into how exoplanets form and their atmosphere. At the same time, these brown dwarfs are quite cold, even one of them has a very close temperature to the earth's temperature, so they can have clouds of water in their atmosphere. Of course, the fact that brown dwarfs are so cold can leave doubt as to whether they are exoplanets. Whatever the result is, the brown dwarfs found to continue to give us clues about their nature. (33)

As the project progressed further, a map and list of all the brown dwarfs found in the vicinity of the Sun so far were published. This map contains 525 brown dwarfs and 38 have just been found. These brown dwarfs are located within 65 light-years to the Sun. A 3D map was created by calculating the distances of all objects. As indicated in the previous sections, there is the coldest brown dwarf known at 6.5 light-years from the Sun. Astronomers had expected to find several more like this one within 65 light-years of the Sun, but efforts to do so were inconclusive. (34)

III. Theoretical Aspects of Brown Dwarfs

Formation of Brown Dwarfs

Brown dwarfs blur the line between the planets and the stars since they are neither planets nor stars, making us question what we know about the planets and the stars. The way brown dwarfs form is no different from the way low mass stars form in the aspect in the aspects of statistical properties of brown dwarfs (mass function, clustering properties, kinematics, binary statistics, accretion rates, etc.) as indicated in the study done by Anthony Whitworth, Matthew R. Bate, Ake Nordlund, Hans Zinnceker, and Bo Reipurth. (*16*) The presence of brown dwarfs in the 1960s was also revealed by astronomers who studied how low-mass stars formed. Therefore, we should know what a star is, what is not a star.

What is a Star?

Stars are a globe of gas that, by definition, held together with their gravity and are supported by the pressure of hot gas in them and produce their energy through nuclear reactions. Stars are formed by the impact of gravity, disintegration, and large clouds of gas and dust contract and fragmentation. As these clouds fragment, the potential energy of gravity is released in the form of radiation and heat. This causes the temperature of

the star's core to increase. If this temperature is more than approximately 3 x 10^6 Kelvins, nuclear reactions begin. Fusion reactions that convert hydrogen to helium occur in stars. These reactions are the primary energy sources of stars and the reason they shine. The energy released as a result of this fusion reaction closes the energy lost by radiation, and the pressure of the fusing core halts the contraction caused by gravity. The pressure of hot gases and this gravitational pressure of the star are very important for the star and keep it stable. In this way, hydrodynamic and thermal balance is achieved, and the life of the star begins. (2) How long the stars live depends on their mass. If we classify stars by mass:

- *Very-low-mass stars*
- *Low-mass stars*
- *Intermediate-mass stars*
- *Massive stars*

The mass of our star, Sun is about 2 x 10^{30} kg and represents with symbol $M_{\odot}$.

Stars release gravitational energy as it contracts, which affects the temperature in the star's core. This released energy depends on the mass of the star and how many contracts the star. Accordingly, low-mass stars must be contracted further to reach the temperature required to start fusing hydrogen. The density of the core of stars, whose mass is approximately one-tenth of the mass of the sun, is high enough to make free electrons start filling the lowest-energy Fermi states. The highest momentum states of degenerated electrons provide counter pressure support to gravitational contraction and in this way, they prevent the star's radius from shrinking below Jupiter's radius. (2) In objects with a mass of less than 0.072 $M_{\odot}$ (in some resources, 0.080 $M_{\odot}$), this degenerate pressure stops construction before the critical temperature of the core reaches the temperature required to fuse hydrogen. Hydrodynamic equilibrium is established, but thermal equilibrium is not established. These objects that begin to collapse to become stars but cannot be stars are brown dwarfs. (2008)

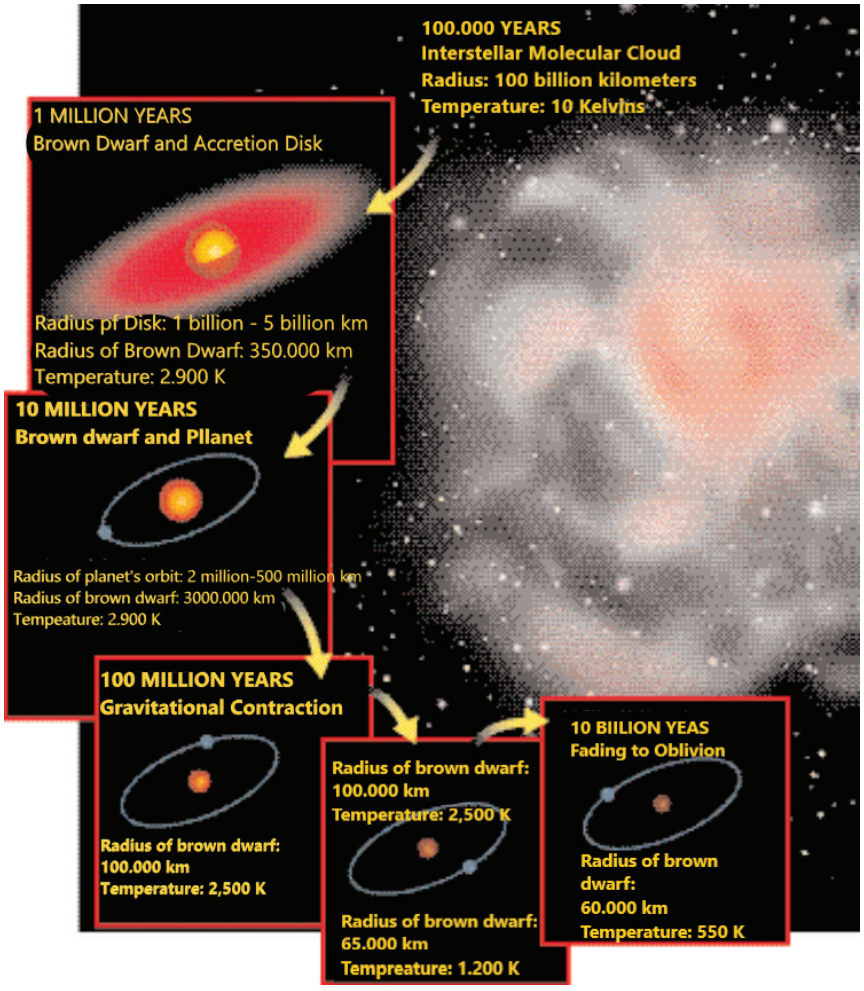

Figure 13 In the picture, assumed that a planet formed beside the brown dwarf. Brown dwarf assumed to have 40 Jupiter Mass. (Image is edited, not original picture),see (9)

Mechanisms for Brown Dwarf Forming

In the study done by Anthony Whitworth, Matthew R. Bate, Ake Nordlund, Hans Zinnceker, and Bo Reipurth. (*16*) states 5 mechanisms for forming brown dwarfs.

According to study, these mechanisms are:

(1) Turbulent fragmentation of molecular clouds, producing very-low-mass prestellar cores by shock compression, (*16*)

(2) Collapse and fragmentation of more massive prestellar cores, (*16)*

(3) Disk fragmentation, (*16*)

(4) Premature ejection of protostellar embryos from their natal cores, (*16*)

(5) Photo erosion of pre-existing cores overrun by HII regions. (*16*)

These five mechanisms are not exclusive mutually (16), thus if one is happening, we cannot say it cannot be the other. As mentioned in the study, it is necessary to look at the extent to which these mechanisms contribute to the formation of brown dwarfs. According to the study, these relative contributions may depend on the environment, metallicity, and epoch, and may therefore lead to local and/or cosmological variations in the ratio of brown dwarfs to H-burning stars, and in the binary and accretion statistics of brown dwarfs (16). To find out which mechanism is dominant; scientists do simulations using required physical information. Here is a simulation given in the research paper of study about the brown dwarfs forming from the fragmentation of dense filaments of molecular gas and disk fragmentation. (16)

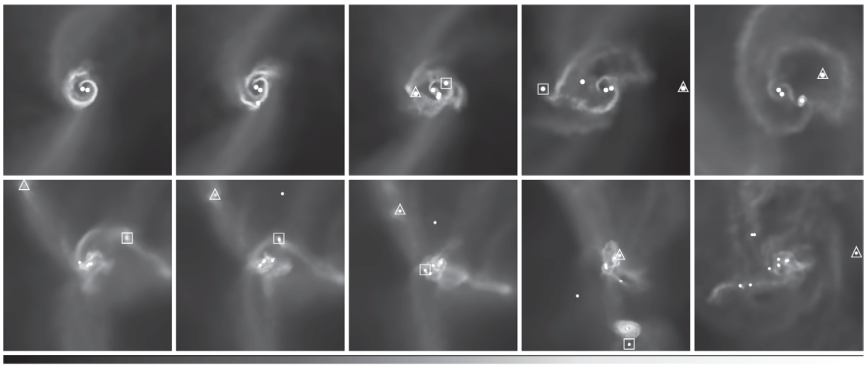

Figure 14 As stated in the study, the upper sequence shows two brown dwarfs (square and triangle) forming in a circumbinary disk, while the lower sequence shows two brown dwarfs (square and triangle) forming in a filament.See (16)

They also tried to calculate the minimum mass for brown dwarfs. They found the minimum mass may be between the range 0.001–0.004 $M_{\odot}$. Accordingly, it may be a range in which the masses of the planets and the masses of brown dwarfs overlap. In hotter places and earlier times, this minimum mass may be larger, and therefore brown dwarfs may be less common. (16)

What is a Planet?

In general, a planet is an astronomical object orbiting a star or remnant of stars that is large enough to remain round thanks to its gravity but not

large enough to initiate fusion reactions like stars (17). According to the study done in 2007, there may be a range that intersects between the mass of planets and the mass of brown dwarfs as indicated in previous sections. So how do we distinguish planets from stars or brown dwarfs?

First of all, planets; do not form like a brown dwarf or a star. According to the theory put forward by Russian astronomer Viktor Safronov, the gas giant planets are made up of planetesimals. Planetesimal is called small rock, dust, or icy objects. According to this theory, before a planetary system formed, there was a disk of material from the nebula in which it formed, and this material formed small chunks under the influence of gravity. Planetesimals are formed from growing chunks. These planetesimals form the cores of the planets, and that core becomes molten when it reaches enough heat. These cores attract large gas envelopes over the years. This theory was developed in accordance with our solar system, and the gas giant planets should be at distant orbits according to theory. However, this theory was also damaged when planets outside the solar system were discovered in the following years because those planets found were traveling in close orbit. It was later even revealed that lonely planets could be found. This has created problems with how to distinguish brown dwarfs and planets. We can observe brown dwarfs accompanying another star or brown dwarf, and this also applies to planets. An alternative solution is to see if the object has ever started a nuclear reaction. Deuterium reactions occur above about 13 Jupiter masses, and brown dwarfs are thought to have a deuterium reaction. In this way, a mass-based distinction can be made. (9)

Older brown dwarfs like Gliese 229B seem to be closer to gas giant planets as numerical values. On the other hand, younger brown dwarfs like Teide 1, are relatively close to low-mass stars such as Glisse 229A. Brown dwarfs and low-mass stars are completely convective as shown in the left figure (9). So, how to distinguish the low-mass stars and brown dwarfs? The answer is Lithium test.

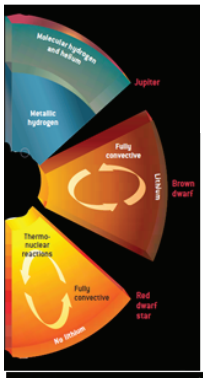

Name	Jupiter	Gliese 229B	Teide 1	Gliese 229A	Sun
Type of object	Gas-giant planet	Brown dwarf	Brown dwarf	Red dwarf star	Yellow dwarf star
Mass (Jupiter-masses)	1	30–40	55	300	1,000
Radius (kilometers)	71,500	65,000	150,000	250,000	696,000
Temperature (kelvins)	100	1,000	2,600	3,400	5,800
Age (years)	4.5 billion	2–4 billion	120 million	2–4 billion	4.5 billion

Figure 15 All pictures are taken from: (9)

13 M_j mass limit between the planet and the brown dwarf are an accepted value rather than a physically measured or proven quantity. In 2011, the Extrasolar Planets Encyclopedia included objects up to 25 M_j. In 2016, based on a study about the mass-density relationship, this limit increased to 60 M_j (21) (54). The Exoplanet Data Explorer also included objects up to the mass of 24 M_j (56). Nasa Exoplanet Archive also contains objects up to a mass of 30 M_j (55).

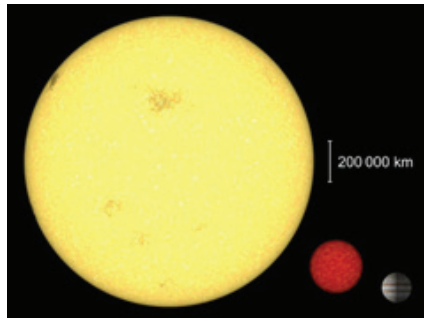

Figure16 Size comparison between the Sun, a young sub-brown dwarf, and Jupiter ,see(24)

Objects that fall below this 13 M_j mass limit are called sub-brown dwarf or planetary-mass brown dwarf (23). They do not fuse deuterium because they do not reach sufficient mass. These objects, like stars and brown dwarfs, are formed by the collapsing of the gas and dust cloud.

Lithium Test

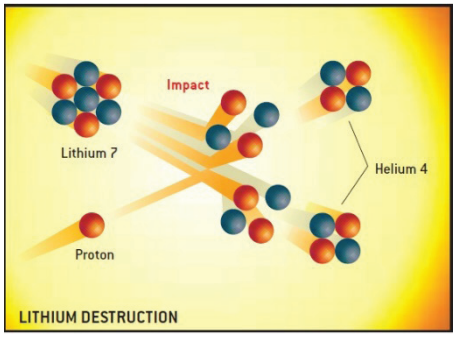

Figure17 Reaction of lithium (9)

Lithium is used to distinguish brown dwarfs from low-mass stars, which is called a lithium test. Generally, lithium is completely depleted in stars. The temperature required to fuse the lithium is just below the temperature required to burn hydrogen. Therefore, it is normal to not expect lithium in the stars. Convection in the stars also contributes to this situation. In this reaction, lithium-7 and proton collide, resulting in 2 helium-4 atoms. Brown dwarfs are not hot enough to perform this reaction, and therefore we can see this element in their spectral lines. This gives a strong clue that the observed object is a brown dwarf.

However still, the lithium test does not give excellent results because lithium is also found in young stars who have not had time to fully fuse it yet. In heavier stars such as our sun, lithium remains in the outer layers because it is not hot enough for this reaction and convection is inadequate here. However, in terms of their light and size, these stars can be distinguished from brown dwarfs. In addition, brown dwarfs with large masses can consume their lithium when they are young. As a result, lithium testing is a good method, but it is not perfect.

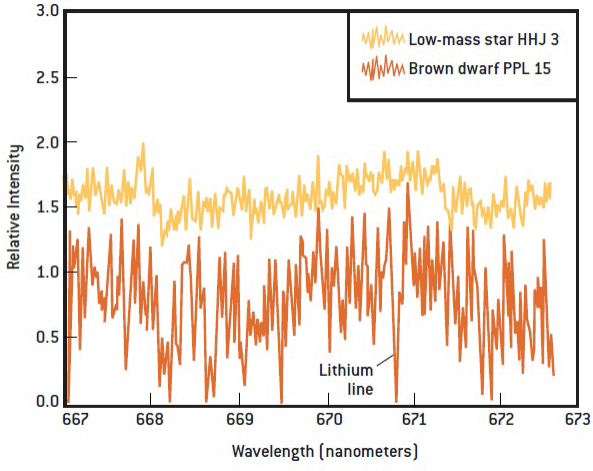

Figure 18. In spectrum of low mass star, there is no sign of lithium unlike the brown dwarf,see (9)

Radius Calculation of Brown Dwarfs

The calculation of the radius of brown dwarfs is not an easy subject observationally, it is usually done using binary systems. In 2001, Burrows conducted a theoretical study on this subject. According to this study, some brown

dwarfs are smaller than Jupiter, although they are called super Jupiter. Brown dwarfs older than 10^9 years and has a mass between 0.3 to 70 M_j have a radius of roughly 0.7 to 1.1 R_j, of course within the error. Considering this error, the result of this theoretical study is matched by the AKARI observation studies carried out in 2013.[4] (2013)

Types of Brown Dwarf

Stars are divided into spectral classes according to their temperature. These classes are; O, B, A, F, G, K, M. The hottest ones correspond to the O class, and the coldest stars correspond to class M. M class includes red dwarf stars, but there are also some young brown dwarfs here. Classes L, T, and Y were included in this classification because brown dwarfs are much colder than stars. These spectral classes are divided into 10 according to their temperature. Number 0 corresponds to the hottest ones; number 9 is used for the coldest ones.

Spectral Class M

This group is also called M-dwarfs. Red dwarfs are usually here, but young brown dwarfs like Teide 1 are also in this class. The brown dwarfs here begin with M-6.5.

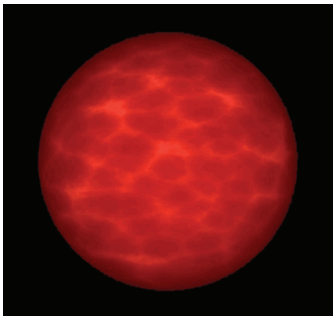

Figure 19. Illustration of a L type Brown Dwarf,see (39)

Spectral Class L

Brown Dwarfs, which are colder than M-type objects, are located here. They have temperatures in the range of 1300 to 2000 Kelvins and are usually of a color between red and brown. An example of this type is the GD 165B dwarf. Such dwarfs show themselves with metal hydride emission lines (FeH, CrH, MgH, CaH) and prominent alkali metal lines (Na I, K I, Cs I, Rb I). At the same time, not only brown dwarfs are in this class, but also the coldest main sequence stars. (37) (38)

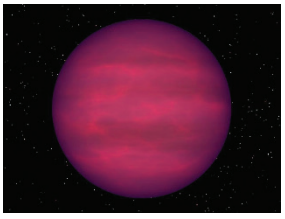

Figure 20. Illustration of T type Brown Dwarf,see (41)

Spectral Class T

Brown dwarfs with surface temperatures in the range of 700 to 1300 Kelvin are in this class. Their color is dark magenta. Gliese 229b is an example of this class brown dwarf. In their spectrum, methane absorption lines are dominant and have very wide absorption

4 Burrows, A., Hubbard, W. B., Lunine, J. I., & Liebert, J. 2001,

properties from Alkaline metals Na and K. In addition, FeH and CrH lines exhibited by L-type dwarfs are not observed in this class. 355 class T dwarfs are known, as of 2013. According to the developments made in the Near-Infrared Classification scheme, class T is attributed only to brown dwarfs, but class L includes both very low-mass stars and brown dwarfs. (37) (40)

Spectral Class Y

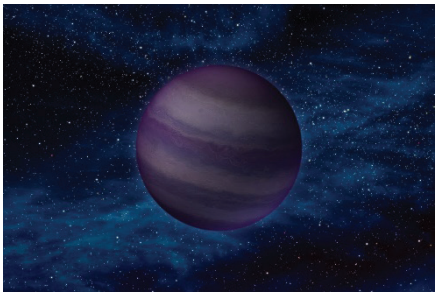

Figure 21. Illustration of Y type Brown Dwarf,see (42)

Class Y is a theoretical class for brown dwarfs, which are colder than type T. Surface temperatures of these brown dwarfs is thought to be lower than 600 Kelvins. Over the years, brown dwarfs that may belong to this class have been observed and candidates are found. In 2011, NASA discovered six brown dwarfs with the Wise telescope, whose temperatures dropped to 25 degrees Celsius, and these brown dwarfs were classified as Y (43). In 2014, the coldest brown dwarf known was detected and included in this class.

IV. Discussion

The existence of brown dwarfs was first introduced in the 1960s by astronomers working on low-mass stars (2). In 1975, these objects were called *brown dwarfs* because their color was approximately brown. However, their color is not exactly brown, they can be between red and orange depending on their temperature, or in a color that plays to the magenta. Although the existence of brown dwarfs was introduced in the 1960s, it was possible to find them in 1995. The reason they are hard to detect is that they do not have nuclear energy sources like stars. In 1995, the first brown dwarf named Teide 1 was found. (9)

Brown dwarfs are divided into M, L, T, or Y types according to their temperature. In class M, there are younger brown dwarfs, such as Teide 1. The hottest of these classes is M; the coldest is class Y. Since brown dwarfs do not fuse hydrogen like stars, they cannot keep themselves hot enough and cool down over time. Deuterium reactions also do not provide enough energy for this. That is why brown dwarfs get colder and change classes as they get older. (M => L => T => Y)

Brown dwarfs are objects that do not fit the definition of planets or stars. With these features, they shed light on new aspects of star and planet formation. They are formed primarily by the collapse of gas and dust particles like stars, but they do not fuse hydrogen like stars because their nuclei do not reach the temperature and density required for this while forming. To make this reaction, 0.072 solar mass is needed. (0.08 in some sources)

5 mechanisms for brown dwarf formation were proposed in the study done by Anthony Whitworth, Matthew R. Bate, Ake Nordlund, Hans Zinnceker, and Bo Reipurth. These are: turbulent fragmentation of molecular clouds, producing very-low-mass prestellar cores by shock compression; collapse and fragmentation of more massive prestellar cores; disk fragmentation; premature ejection of protostellar embryos from their natal cores; photo erosion of pre-existing cores overrun by HII regions as stated in the research. (*16*)

At the same time, the minimum mass of brown dwarfs was calculated in this study and was found in the range of 0.001–0.004 $M_{\odot}$ (16). There are also planets within this mass range. In this sense, brown dwarfs and planets can be confused. However, the planets do not have nuclear reactions in any way. Brown dwarfs, on the other hand, can fuse deuterium if it is of sufficient mass. The mass required is 13 Jupiter masses. In this sense, it can be understood whether it is a planet or a brown dwarf by looking at whether the object initiated any reactions. In 2004, for the first time, the mass of a brown dwarf was measured directly. The mass of the brown dwarf in the binary system called 2MASSW J0746425+2000321 is calculated to be between 0.05 and 0.07 solar mass. (26)

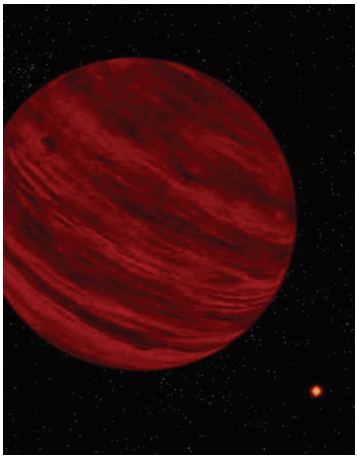

Figure 22. (9)

Brown dwarfs have many aspects that resemble low-mass stars. They form like them, and they launch jets like them, according to a 2017 study (31). In this sense, how to distinguish between brown dwarfs and low-mass stars is an important issue. One of these ways is the lithium test. Stars consume all the lithium they have because they are at the appropriate temperature for this. However, brown dwarfs are not able to do this because they are colder, and because of that, they have lithium in them. In this sense, looking for lithium in

I would like to thank Elif Kızılkaya, one of my undergraduate students, who did a very good job in helping me to prepare this review type of search article.

V. References

1. Kumar, Shiv S. “Study of Degeneracy in Very Light Stars.” 1. https://ui.adsabs.harvard.edu/abs/1962AJ.....67S.579K/abstract, n.d.

2. June 2008 : Brown Dwarfs: Failed Stars Article : https://web.archive.org/web/20130508182012/http://astro.berkeley.edu/~gmarcy/astro160/papers/brown_dwarfs_failed_stars.pdf .

Burgasser, A. J. (June 2008). “Brown dwarfs: Failed stars, super Jupiters” (PDF). Physics Today. 61 (6): 70–71. Bibcode:2008PhT....61f..70B. doi:10.1063/1.2947658. Archived from the original (PDF) on 8 May 2013. Retrieved 11 January 2016.

3. 2009: Color: If Brown Isn’t a Color, What Color are Brown Dwarfs? https://www.universetoday.com/23247/if-brown-isnt-a-color-what-color-are-brown-dwarfs/#:~:text=But%20you%20can’t%20have,impossible%20to%20emit%20brown%20light .

4. “Rogue Planet.” Wikipedia. Wikimedia Foundation, June 25, 2021. https://en.wikipedia.org/wiki/Rogue_planet .

5. Burrows, A., Heng, K., & Nampaisarn, T. 2011, ApJ, 736, 47

6. Burrows, A., Hubbard, W. B., Lunine, J. I., & Liebert, J. 2001, RvMP, 73, 719

7. Burrows, A., Marley, M., Hubbard, W. B., et al. 1997, ApJ, 491, 856

8. Sorahana, S., I. Yamamura, and H. H. Murakami. “ON THE RADII OF BROWN DWARFS MEASURED WITH AKARI NEAR-INFRARED SPECTROSCOPY,” April 10, 2013. https://iopscience.iop.org/article/10.1088/0004-637X/767/1/77/pdf .(2013)

9. Basri, G. (2000, April). *The Discovery of Brown Dwarf*. Www.Sciam.Com. https://w.astro.berkeley.edu/~basri/bdwarfs/SciAm-book.pdf .

10. Greicius, Tony. “Welcome to the Sun’s Neighborhood.” NASA. NASA, April 24, 2014. https://www.nasa.gov/jpl/wise/spitzter/pia18003/#.YLvj_fkzYuQ .

11. Dunbar, Brian. “WISE Finds Few Brown Dwarfs Close To Home.” NASA. NASA. Accessed June 25, 2021. https://www.nasa.gov/mission_pages/WISE/news/wise20120608.html .

12. Greicius, Tony. “Cold and Quick: a Fast-Moving Brown Dwarf.” NASA. NASA, April 25, 2014. https://www.nasa.gov/jpl/wise/spitzter/pia18002/#.YNZOyegzYuR .

13. Greicius, Tony. “NASA’s Spitzer and WISE Telescopes Find Close, Cold Neighbor of Sun.” NASA. NASA, February 18, 2015. https://www.nasa.gov/jpl/wise/spitzer-coldest-brown-dwarf-20140425 . (2014)

14. Dunbar, Brian. “WISE Finds Few Brown Dwarfs Close To Home.” NASA. NASA. Accessed June 25, 2021. https://www.nasa.gov/mission_pages/WISE/news/wise20120608.html .

15. Dunbar, Brian. “WISE Finds Few Brown Dwarfs Close To Home.” NASA. NASA. Accessed June 25, 2021. https://www.nasa.gov/mission_pages/WISE/news/wise20120608.html .

16. Whitworth, A., M. R. Bate, Å. Nordlund, B. Reipurth, and H. Zinnecker. “The Formation of Brown Dwarfs: Theory.” NASA/ADS, January 1, 1970. https://ui.adsabs.harvard.edu/abs/2007prpl.conf..459W/abstract#:~:text=We%20review%20five%20mechanisms%20for,protostellar%20embryos%20from%20their%20nat .

17. “Gezegen.” Wikipedia. Wikimedia Foundation, June 19, 2021. https://tr.wikipedia.org/wiki/Gezegen . (*definition of a planet*)

18. Cessna, Abby. “Planetesimals.” Universe Today, December 25, 2015. https://www.universetoday.com/35974/planetesimals/ .

19. “Planetesimal.” Encyclopædia Britannica. Encyclopædia Britannica, inc. Accessed June 25, 2021. https://www.britannica.com/science/planetesimal.

20. Information@eso.org. “A Sub-Stellar Jonah - Brown Dwarf Survives Being Swallowed.” www.eso.org. Accessed June 25, 2021. https://www.eso.org/public/news/eso0628/ .

21. Exoplanets versus brown dwarfs: the CoRoT view and the future, Jean Schneider, 4 Apr 2016.

22. Hatzes Heike Rauer, Artie P. (2015). “A Definition for Giant Planets Based on the Mass-Density Relationship”. The Astrophysical Journal. 810 (2): L25.

23. Working Group on Extrasolar Planets – Definition of a “Planet” Archived 2012-07-02 at the Wayback MachinePosition statement on the definition of a “planet” (IAU)

24. “Brown Dwarf.” Wikipedia. Wikimedia Foundation, June 24, 2021. https://en.wikipedia.org/wiki/Brown_dwarf#/media/File:Sol_Cha-110913-773444_Jupiter.jpg . (*image*)

25. TheNRAO. “Astronomers Measure Wind Speed on a Brown Dwarf.” EurekAlert! Accessed June 25, 2021. https://www.eurekalert.org/pub_releases/2020-04/nrao-amw040620.php .

26. Information@eso.org. “Weighing Ultra-Cool Stars - Large Ground-Based Telescopes and Hubble Team-Up to Perform First Direct Brown Dwarf Mass Measurement.” www.eso.org. Accessed June 25, 2021. https://www.eso.org/public/news/eso0420/ .

27. Burrows; et al. (2001). “The theory of brown dwarfs and extrasolar giant planets”. Reviews of Modern Physics. 73 (3): 719–65.

28. "X-rays from a Brown Dwarf's Corona". April 14, 2003. Archived from the original on December 30, 2010. Retrieved March 19, 2010.

29. "Brown Dwarf." Wikipedia. Wikimedia Foundation, June 24, 2021. https://en.wikipedia.org/wiki/Brown_dwarf#/media/File:Lp94420_duo_m.jpg . (*image*)

30. Rutledge, Robert E.; Basri, Gibor; Martín, Eduardo L.; Bildsten, Lars (1 August 2000). "Chandra Detection of an X-Ray Flare from the Brown Dwarf LP 944-20". The Astrophysical Journal. 538 (2): L141–L144.

31. Info@noirlab.edu. "Punching Above Its Weight - A Brown Dwarf Launches a Parsec-Scale Jet." www.noirlab.edu. Accessed June 25, 2021. https://noirlab.edu/public/news/noao1701/ .

32. Information@eso.org. "Yes, It Is the Image of an Exoplanet - Astronomers Confirm the First Image of a Planet Outside of Our Solar System." www.eso.org. Accessed June 25, 2021. https://www.eso.org/public/news/eso0515/ .

33. Gohd, Chelsea. "Volunteers Spot Almost 100 Cold Brown Dwarfs near Our Sun." Space.com. Space, August 19, 2020. https://www.space.com/citizen-scientists-discover-95-brown-dwarfs.html .

34. Info@noirlab.edu. "Mapping Our Sun's Backyard - Astronomers and Citizen Scientists Produce the Most Complete 3D Map of Cool Brown Dwarfs in the Sun's Neighborhood." www.noirlab.edu. Accessed June 25, 2021. https://noirlab.edu/public/news/noirlab2105/ .

35. All About Space Mart/2021 Magazine, "Kahverengi Cüceler ve Süper Jüpiterler", 68-72.

36. The Distance to the 2M1207 System" Archived 2008-01-24 at the Wayback Machine, Eric Mamajek, November 8, 2007. Accessed on line June 15, 2008.

37. Hillyard, William. Type L, T & Y Brown Dwarfs. Accessed June 25, 2021. http://www.whillyard.com/science-pages/type-lty-dwarfs.html .

38. Smart, R. L.; Bucciarelli, B.; Jones, H. R. A.; Marocco, F.; Andrei, A. H.; Goldman, B.; Mendez, R. A.; d'Avila, V. A.; Burningham, B.; Camargo, J. I. B.; Crosta, M. T. (December 2018). "Parallaxes of Southern Extremely Cool objects III: 118 L and T dwarfs". MNRAS. 481 (3): 3548–3562.

39. "Brown Dwarf." Wikipedia. Wikimedia Foundation, June 24, 2021. https://en.wikipedia.org/wiki/Brown_dwarf#/media/File:L-dwarf-nasa-hurt.png . (*image*)

40. Kirkpatrick, Davy; Burgasser, Adam (6 November 2012). "Photometry, spectroscopy, and astrometry of M, L, and T dwarfs". DwarfArchives.org. Pasadena, CA: California Institute of Technology. Retrieved 2012-12-28. (M=536, L=918, T=355, Y=14)

41. "Brown Dwarf." Wikipedia. Wikimedia Foundation, June 24, 2021. https://en.wikipedia.org/wiki/Brown_dwarf#/media/File:T-dwarf-nasa-hurt.png . (*image*)

42. "Brown Dwarf." Wikipedia. Wikimedia Foundation, June 24, 2021. https://en.wikipedia.org/wiki/Brown_dwarf#/media/File:WISE_1828+2650_Brown_dwarf.jpg . (*image*)

43. Plait, Phil (24 August 2011). "WISE finds coolest brown dwarfs ever seen!". Discover Magazine.

44. Koberlein, Brian. "Brown Dwarf Discovered with a Radio Telescope for the First Time." Universe Today, November 10, 2020. https://www.universetoday.com/148746/brown-dwarf-discovered-with-a-radio-telescope-for-the-first-time/ .

45. "Rogue Planet." Wikipedia. Wikimedia Foundation, June 25, 2021. https://en.wikipedia.org/wiki/Rogue_planet#cite_note-shostak-1 . *(Definition of rogue planet is taken from website)*

46. ASTRO, chapter 6: The Family of Stars *(table taken from lecture slides)*

47. "Brown Dwarf." Wikipedia. Wikimedia Foundation, June 24, 2021. https://en.wikipedia.org/wiki/Brown_dwarf#/media/File:Artist%E2%80%99s_conception_of_a_brown_dwarf_like_2MASSJ22282889-431026.jpg . (*image*)

48. "Brown Dwarf." Wikipedia. Wikimedia Foundation, June 24, 2021. https://en.wikipedia.org/wiki/Brown_dwarf#/media/File:Brown_Dwarf_Comparison_2020.png . *(image)*

49. Tarter, Jill (2014), "Brown is Not a Color: Introduction of the Term 'Brown Dwarf'", in Joergens, Viki (ed.), 50 Years of Brown Dwarfs – From Prediction to Discovery to Forefront of Research, Astrophysics and Space Science Library, 401, Springer, pp. 19–24, doi:10.1007/978-3-319-01162-2_3, ISBN 978-3-319-01162-2

50. Croswell, Ken (1999). Planet Quest: The Epic Discovery of Alien Solar Systems. Oxford University Press. pp. 118–119. ISBN 9780192880833.

51. Boss, Alan (2001-04-03). "Are They Planets or What?". Carnegie Institution of Washington. Archived from the original on 2006-09-28. Retrieved 2006-06-08.

52. Nicholos Wethington (October 6, 2008). "Dense Exoplanet Creates Classification Calamity". Universetoday.com. Retrieved January 30, 2013.

53. Cushing, Michael C. (2014), "Ultracool Objects: L, T, and Y Dwarfs", in Joergens, Viki (ed.), 50 Years of Brown Dwarfs – From Prediction to Discovery to Forefront of Research, Astrophysics and Space Science Library, 401, Springer, pp. 113–140, doi:10.1007/978-3-319-01162-2_7, ISBN 978-3-319-01162-2

54. Hatzes Heike Rauer, Artie P. (2015). "A Definition for Giant Planets Based on the Mass-Density Relationship". The Astrophysical Journal. 810 (2): L25. arXiv:1506.05097. Bibcode:2015ApJ...810L..25H. doi:10.1088/2041-8205/810/2/L25. S2CID 119111221.

55. Exoplanet Criteria for Inclusion in the Archive, NASA Exoplanet Archive.

56. Wright, J. T.; Fakhouri, O.; Marcy, G. W.; Han, E.; Feng, Y.; Johnson, John Asher; Howard, A. W.; Fischer, D. A.; Valenti, J. A.; Anderson, J.; Piskunov, N. (2010). "The Exoplanet Orbit Database". Publications of the Astronomical Society of the Pacific. 123 (902): 412–422. arXiv:1012.5676. Bibcode:2011PASP..123..412W. doi:10.1086/659427. S2CID 51769219.

*All pictures are linked to those refences and are indicated the number in the parentheses below them.

**At the end of the paragraphs, numbers inside parentheses given in order to indicate the source utilized.

Chapter 2

INVESTIGATION OF CHIRONOMIDAE (DIPTERA) FAUNA IN OĞULPAŞA STREAM (EDİRNE/TURKEY)

Nurcan ÖZKAN[1]

1 Nurcan ÖZKAN, Assoc. Prof. Dr., University of Trakya, Faculty of Education, Department of Mathematics and Science Education, nurcanozkan@hotmail.com, ORCID: 0000-0001-5045-6186

1. INTRODUCTION

Limnology and, accordingly, inland fisheries have gained importance in Turkey in recent years and the number of researches on the subject has gradually increased. The aim of these studies is to reveal the natural richness of the investigated biotope. The natural richness of the inland waters depends primarily on the fauna and flora, which are considered to be the fixtures of these places. In order to make the best use of inland water resources, it is inevitable for this living community to be discovered and introduced to the scientific world.

The most important ones among the inland waters fauna are the bottom animals. Among the bottom animals, Chironomidae (Diptera) larvae, which are found in almost every water body, take the first place. Since all Chironomidae spend their winter months in the larval stage, they are abundant in all seasons. Therefore, they are indispensable food animals for fish. Numerous studies reveal that they are consumed with pleasure by fish, contain high levels of important nutrients, especially protein, and are digested quickly and easily by fish. The way they transmit oxygen to the bottom material, especially mud, in the waters they are in, positively affects the oxygenated respiration and, as a result, the mineralization. As a natural result of this, putrification at the bottom is largely prevented, the first materials necessary for photosynthesis are provided and the material cycle is positively affected. This increases the efficiency of water and ensures the continuity of aquatic life (Şahin, 1984).

They have positive functions such as their role in the transition from plant materials to animal protein, the use of their qualitative and quantitative status as an indicator of pollution, and some species also prevent pollution in aquatic environments (Şahin, 1987). Some species also have negative functions such as destroying various aquatic plants (Chernovskii, 1961). In addition, they are one of the most studied organism groups because of their abundance per unit area, showing the productivity of their inland water environment, especially lakes and ponds (Kırgiz, 1988, 1989). Despite their larvae, which can be found in all seasons of the year, especially in winter, and have the above-mentioned characteristics, imagos and adults are only seen between spring and autumn. They have no economic or practical significance.

With this study, the species of Chironomidae fauna, which is so important for inland waters, found in Oğulpaşa Stream were tried to be revealed and introduced to the scientific world.

2. MATERIAL AND METHOD

Oğulpaşa Stream, located within the provincial borders of Edirne, originates near Sarıdanişment village and flows in a north-south direction

for approximately 65-70 km. It follows the villages of Sülecik, Yağcılı, Hacıumur, Oğulpaşa, Abalar, Şerbettar, respectively, and joins the Ergene River in the south of Sazlımalkoç Village, within the provincial borders of Kırklareli (Figure 1).

The stream is used to irrigate the surrounding gardens and fields. In the summer, a large part of it usually dries up. In spring, there are aquatic and semi-aquatic plants in and around the water (*Phragmites australis, Lemna* sp., *Cyperus* sp. and *Lepidium* sp. like), and in winter, these plants dry up.

The study was carried out in monthly periods for 12 months between September 2015 and August 2016 in the Oğulpaşa Stream, a tributary of the Ergene River, which forms a part of the streams of the Meriç-Ergene Basin. 3 stations were determined in Oğulpaşa Stream. The 1st station is 1 km from Abalar Village from above, the 2nd station was chosen from the Şerbettar Village entrance and the 3rd station was selected from the Sazlımalkoç Village exit. Ekman-Birge grab (15x15 cm^2) and hand mud scoop were used to collect mud samples from the stream in the study area. Two samplings were made from each station. Mud samples were washed in sieves with different mesh sizes (0.1-0.5 mm). Organisms collected with fine-tipped forceps were fixed in plastic bottles containing 70% ethyl alcohol. All these collected samples were labelled and transported to the laboratory. All Chironomid larvae were identified by making provisional preparations under binocular and light microscopy.

Identification of Chironomidae species Moller Pillot (1977-1978, 1984), Fittkau and Roback (1983), Şahin (1984, 1991), Boesel (1985), Kırgız (1988) and Özkan (1991, 2003) were used.

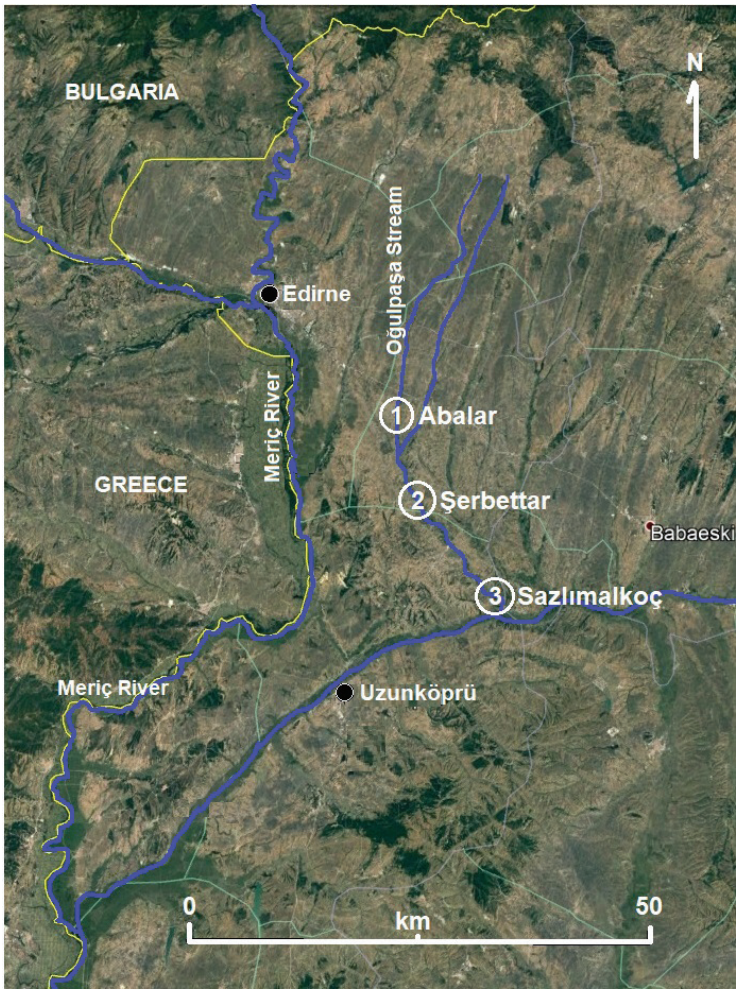

Figure 1. *Oğulpaşa Stream sampling stations: 1. Abalar Village (478818.70 E, 4601035.05 N); 2. Şerbettar Village (480249.32 E, 4591347.00 N); 3. Sazlımalkoç Village (490444.56 E, 4577381.90 N)*

3. RESULTS

As a result of the evaluation of the results of the study that lasted for one year between September 2015 and August 2016 in Oğulpaşa Stream, 1317 larvae consisting of 52 species belonging to 4 subfamilies of Chironomidae family were found. These;

I) Subfamily Tanypodinae: *Tanypus punctipennis*, *T. kraatzi*, *Procladius (Holotanypus)* sp., *Psectrotanypus varius*, *Macropelopia nebulosa*, *Macropelopia goetghebueri*, *Ablabesmyia aequidensi, A. monilis*, *Natarsia punctata*, *Monopelopia tenuicalcar.*

II) Subfamily Prodiamesinae: *Prodiamesa olivacea.*

III) Subfamily Orthocladiinae: *Smittia aquatilis*, *Bryophaenocladius virgo*, *Cricotopus bicinctus*, *C. fuscus*, C. *flavocinctus*, *C. albiforceps*, *C. annulator*, *C. sylvestris*, *Halocladius fucicola*, *Hydrobaenus pilipes*, *Psectrocladius sordidellus*, *Limnophyes pusillus*, *Orthocladius thienemanni*, *Zalutschia megastyla.*

IV. Subfamily Chironominae: Tribus I – Chironomini: *Chironomus halophilus*, *C. reductus*, *C. riparius*, *C. anthracinus*, *C. viridicollis*, *C. plumosus*, *C. tentans*, *Polypedilum nubifer*, *Polypedilum* sp., *P. nubeculosum*, *P. convictum*, *P. exsectum*, *Stictochironomus longipugionis*, *S. yalvacii*, *Cryptochironomus defectus*, *Cladopelma laccophila*, *Endochironomus tendens*, *Einfeldia pagana*, *Dicrotendipes nervosus*, *D. tritomus*, *Harnischia fuscimana*, *Cryptotendipes holsatus*, Tribus II – Tanytarsini: *Cladotanytarsus mancus*, *Paratanytarsus lauterborni*, *Tanytarsus gregarius*, *Virgatanytarsus arduennensis*, *Rheotanytarsus exiquus*.

Species identification key of Chironomidae larvae of Oğulpaşa Stream

1 (24) Glossa and paraglossa are developed and antennae can be retracted into the head (Figure 2).

TANYPODINAE

2 (15) The abdominal segments are broad and have more or less tassel-shaped hairs on the sides (Figure 3). Head capsule is round or oval. Head index is between 0.65-1.00. The mentum is toothed and contains a paralabial plate or a series of chitin teeth arranged in discrete spots. The length of the anal gills is at most twice the width (Figure 3).

3 (8) There are 5 teeth in the glossa.

4 (7) Abdominal segments are very hairy (Figure 3). There are 3 pairs of anal gills. The head index is 1.0, and the apical tooth of the mandible is at most 0.2 of the mandible (Figure 4). Glossa teeth are all the same colour (Figure 5).

Tanypus Meigen, 1803

5 (6) The glossa teeth are the same size and the paraglossa is multi-armed (Figure 5). The mentum has 8 pairs of teeth (Figure 6).

T. punctipennis Meigen, 1818

6 (5) The 3 inner glossa teeth are larger and the same size and the paraglossa has 2 arms (Figure 7). The mentum has 6 pairs of teeth (Figure 8).

T. kraatzi Kieffer, 1912

7 (4) Abdominal segments have sparse hairs and 2 pairs of anal gills. Head index is at most 0.95 (Figure 2). The apical tooth of the mandible is at least 0.25 of the mandible (Figure 9). The tip of the glossa teeth is black (Figure 10).

Procladius Skuse, 1889

P. (*Holotanypus*) sp.

8 (3) There are 4 teeth in the glossa (Figure 11).

9 (12) The ring organ is located in the middle of the maxillary palp or close to the tip.

10 (11) The distal of the mandible is curved and has 5 small lateral teeth (Figure 12).

Psectrotanypus Kieffer, 1909

P. varius Fabricius, 1787

11 (10) The distal mandible is slightly curved. There is a large basal tooth proximally (Figure 13).

12 (9) The ring organ is located close to the base of the maxillary palp (Figure 14).

Macropelopia Thienemann, 1916

13 (14) Dorsomentum has 7 pairs of teeth (Figure 15). The lateral edges of the glossa teeth are curved (Figure 16).

M. goetghebueri (Kieffer, 1918)

14 (13) There are 8 pairs of teeth in the dorsomentum (Figure 17). The lateral edges of the glossa teeth are straight.

M. nebulosa (Meigen, 1804)

15 (2) The abdominal segments are narrow and there are no hair fringes on the sides. The head capsule is long. Head index is between 0.4-0.6. There are no rows of teeth in the mentum. Anal gills are at least three times longer than they are wide.

16 (19) The basal segment of the maxillary palp is two or more segmented (Figure 18).

Ablabesmyia Johannsen, 1905

17 (18) There are 3 short and 1 long joints in the basal segment of the maxillary palp (Figure 18).

A. aequidensi Şahin, 1987

18 (17) There are 4 short and 1 long joints in the basal segment of the maxillary palp (Figure 19).

A. monilis (Linnaeus, 1758)

19 (16) The basal segment of the maxillary palp is single-segmented (Figure 20).

20 (22) One of the hind leg hooks is black and the others are yellow, and the inner edges are notched like a saw (Figure 21). The second antennal joint is brown in colour; the others are light in colour (Figure 22).

21 (23) The row of glossa teeth is deep concave and the median tooth is the smallest (Figure 23).

Monopelopia Fittkau, 1962

M. tenuicalcar (Kieffer, 1918)

22 (20) All of the hind foot hooks are yellow in colour and their inner edges are smooth. All antennal segments are the same colour.

23 (21) The tip of the glossa median teeth is blunt and shorter than the external teeth (Figure 24).

Natarsia Fittkau, 1962

N. punctata (Fabricius, 1804)

24 (1) There is no developed glossa and paraglossa. The antenna cannot be taken inside the head.

25 (28) The third antennal joint has annular lines (Figure 25).

26 (27) Their submental plates are large and smooth, with a beard consisting of long hairs on them (Figure 26).

PRODIAMESINAE

27 (26) There are 2 small teeth in the middle of the mentum plate. The teeth are all the same colour (Figure 26). Only the inner cetae bundle is present in the mandible (Figure 27).

Prodiamesa Kieffer, 1906

P. olivacea (Meigen, 1818)

28 (25) There are no annular lines at the third antennal joint.

29 (51) Submental plaques are generally undeveloped and do not have grooves when developed.

ORTHOCLADIINAE

30 (31) The brush base is large and has beak-shaped projections on its edges (Figure 28). S1 is palm of the hand shaped (Figure 29). There are 2 middle teeth in the middle of the mentum (Figure 30).

Psectrocladius Kieffer, 1906

P. sordidellus (Zetterstedt, 1838)

31 (30) The brush base is not very large, there are no beak-shaped protrusions on the edges. S1 has many bifurcations (Figure 31). There is a single median tooth in the middle of the mentum plate (Figure 32).

Zalutschia Lipina, 1939

Z. megastyla Shilova, 1971

32 (43) There are tassel-shaped bristle on the posterior sides of the abdominal segments (Figure 33).

33 (44) Hair fringes are found in bundles in I-VII or at least one segment, they are not simple hairs.

Cricotopus van der Wulp, 1874

34 (41) The epipharyngeal comb consists of 3 side-by-side setae (Figure 34).

C. (*Cricotopus*) van der Wulp 1874

35 (36) The premandible has a single apical tooth (Figure 35).

C. (*C.*) *annulator* Goetghebuer, 192

36 (35) The premandible has two apical teeth (Figure 36).

C. (*C.*) *fuscus* (Kieffer, 1909)

37 (40) The inner edge of the mandible is not toothed like a saw. All mentum teeth are the same colour.

38 (39) The middle tooth of the mentum is 3 times wider than the first lateral teeth, the lateral teeth are approximately equal to each other (Figure 37).

C. (*C.*) *albiforceps* (Kieffer, 1916)

39 (38) The middle tooth of the mentum is 4 times wider than the first lateral tooth, and the second lateral tooth is smaller than the others (Figure 38).

C. (*C.*) *flavocinctus* (Kieffer, 1924)

40 (37) The inner edge of the mandible is serrated (Figure 39) and the 3 teeth in the middle of the mentum are lighter in colour than the others (Figure 40).

C. (*C.*) *bicinctus* (Meigen, 1818)

41 (34) The epipharyngeal comb consists of a conical plate (Figure 41).

Cricotopus (*Isocladius*) Kieffer, 1909

42 (43) The mentum median tooth is about 1.5 times the length of the first lateral teeth and the tips of the lateral teeth are pointed (Figure 42).

C. (*I.*) *sylvestris* (Fabricius, 1794)

43 (32) The hair fringes consist of simple and single bristles (Figure 43).

Halocladius Hirvenoja, 1973

Halocladius fucicola (Edwards, 1976)

44 (32) The hairs on the posterior sides of the abdominal segments are not in the form of tassels.

45 (46) The middle teeth of the mentum are wider and longer than the lateral teeth (Figure 44).

Hydrobaenus Fries, 1830

Hydrobaenus pilipes (Malloch, 1915)

46 (45) The middle teeth of the mentum are not longer than the first laterals, but wider than them (Figure 45).

Orthocladius van der Wulp, 1874

Orthocladius thienemanni Kieffer, 1906

47 (50) No brush base (Figure 46).

48 (49) The antennae are very short and the first joint is no longer than the others (Fig. 47).

Smittia Holmgren, 1869

Smittia aquatilis Goetghebuer, 1921

49 (48) Antennae are normal (Figure 48).

Bryophaenocladius Thienemann, 1934

Bryophaenocladius virgo Thienemann & Strenzke, 1940

50 (47) There is a brush base (Figure 49).

Limnophyes Eaton, 1875

L. pusillus Eaton, 1875

51 (29) Submental plates are always well developed and grooved.

CHIRONOMINAE

52 (95) Antennae originate from the head capsule or from short antennae bases that are less than their width. The submental plates are broad and fan-shaped, radially grooved.

Tribus 1 CHIRONOMINI

53 (60) There are 2 palps with 2-3 joints in the labrum (Figure 50). The maxillary palp is longer than half of the first antennal joint (Figure 51).

54 (55) The number of teeth in the mentum is even (Figure 52).

Cladopelma Kieffer, 1921

Cladopelma laccophila Kieffer, 1922

55 (54) The number of teeth in the mentum is odd (Figure 53).

56 (57) The premandible 2-armed (Figure 54) and the last 3 pairs of mentum lateral teeth form a separate group (Figure 53).

Cryptotendipes Beck & Beck, 1969

C. holsatus Lenz, 1959

57 (56) The premandible are at least 3-armed (Figure 55) and there are no grouping teeth in the mentum.

58 (59) The epipharynx comb is scale-shaped, the edges are small-toothed (Figure 56). The lateral teeth of the mentum arch anteriorly relative to the middle tooth (Figure 57).

Cryptochironomus Kieffer, 1918

C. defectus (Kieffer, 1913)

59 (58) There are 3 equal arms distal to the epipharyngeal comb. The mentum is normal (Figure 58).

Harnischia Kieffer, 1918

H. fuscimana Kieffer, 1921

60 (53) There is no articulated and long palp in the labrum. The maxillary palp is shorter than half of the first antennal joint.

61 (76) VIII. ventral to the abdominal segment, there are 1-2 pairs of ventral gills.

62 (63) Ventral gills 1 pair (Figure 59).

Einfeldia Kieffer, 1924

E. pagana (Meigen, 1838)

63 (62) Ventral gills 2 pairs (Figure 60).

Chironomus Erichson,1841

64 (67) Ventral gills vestigial in the form of very small projections.

65 (66) In the VII abdominal segment, there are finger-like appendages (Figure 61).

C. reductus (Lenz, 1924)

66 (65) VII. abdominal segment has no extension (Figure 62).

C. halophilus Packard, 1873

67 (64) Ventral gills are normally developed (Figure 60)

68 (71) VII. posterolateral to the abdominal segment are finger-shaped lateral gills (Figure 63).

69 (70) The epipharyngeal comb has 13 teeth (Figure 64).

C. tentans Fabricius, 1805

70 (69) The epipharyngeal comb has 16 teeth (Figure 65).

C. plumosus Linnaeus 1758

71 (68) VII. posterolateral to the abdominal segment, finger-shaped lateral gills are absent.

72 (73) Ventral gills are longer than hind legs (Figure 66).

C. *riparius* Meigen, 1804

73 (72) Ventral gills are shorter than hind legs (Figure 60).

74 (75) The epipharyngeal comb has 12 teeth (Figure 67).

C. anthracinus Zetterstedt, 1860

75 (74) The epipharyngeal comb has 16 teeth (Figure 68).

C. viridicollis van der Wulp, 1859

76 (61) VIII. the ventral gills are absent in the abdominal segment.

77 (87) Antennae 5-jointed, second antennal joint has 2 opposing Lauterborn organs (except *Polypedilum nubifer*).

78 (90) In the mentum, the number of teeth is found in pairs.

Polypedilum Kieffer, 1912

79 (80) The median teeth of the mentum are smaller than the first laterals (Figure 69).

P. exsectum (Kieffer, 1916)

80 (79) The median teeth of the mentum are either greater than or equal to the first lateral teeth.

81 (84) Like those with 6-jointed antennae, one of the Lauterborn organs is alternated at the second and third antennal joint (Figure 70).

82 (83) Mentum has 2 middle teeth (Figure 71).

P. nubifer Skuse, 1889

83 (82) Mentum has 3 middle teeth (Figure 72).

Polypedilum sp.

84 (81) Lauterborn organs are opposite at the second antennal joint (Figure 73).

85 (86) The second and third antennal joints are equal and the mentum teeth are dark brown (Figure 74).

P. nubeculosum (Meigen, 1804)

86 (85) The second antennal joint is smaller than the third joint, the mentum teeth are light brown.

P. convictum (Walker, 1856)

87 (77) Antennae are 6-jointed, there is one Lauterborn organ on the second and third joints (alternate) each (Figure 75).

Stictochironomus Kieffer, 1919

88 (89) The antenna wedge exceeds the antenna tip. Submental plate grooves are prominent (Figure 76). The external tooth of the mandible is equal to the apical tooth (Figure 77).

S. longipugionis (Şahin, 1987)

89 (88) Antenna wedge V. extends to the antenna tip. Submental plate grooves are not prominent (Figure 78). The external mandible tooth is shorter than the apical tooth (Figure 79).

S. yalvacii (Şahin, 1987)

90 (78) The mentum has an odd number of teeth.

91 (92) The first lateral teeth of the mentum are smaller than the second (Figure 80).

Endochironomus Kieffer 1918

E. tendens Fabricius 1775

92 (91) The first lateral teeth of the mentum are larger than the second.

Dicrotendipes Kieffer, 1913

93 (94) The lateral margins of the mentum median tooth are straight, the first laterals are approximately as wide as the median tooth, and the 5 pairs of lateral teeth shrink outwards. The submental plates are narrow and fan-shaped, elongated like a basal stem, with very prominent grooves (Figure 81).

D. nervosus (Staeger, 1839)

94 (93) The mentum median tooth has small notches on the sides. The first and second lateral teeth are adjacent to each other and in forked appearance. There are 6 pairs of lateral teeth, and the submental plates are wide and fan-shaped, the base is not too long, the grooves are very prominent (Figure 82).

D. tritomus (Kieffer, 1916)

95 (52) Antennas come out of antenna bases whose height is greater than their width. Submental plates are narrow and long, and they are grooved (Figure 83).

Tribus 2 TANYTARSINI

96 (99) Premandibles 2-arm (Figure 84).

97 (98) The epipharynx comb is whole, with a maximum of 3-5 teeth (Figure 85).

Paratanytarsus Thienemann & Bause, 1913

P. lauterborni (Kieffer, 1909)

98 (97) Epipharyngeal comb with 3 lobes or segments, with more than 5 teeth on it (Figure 86).

Rheotanytarsus Thienemann & Bause, 1913

R. exiquus (Johannsen, 1905)

99 (96) The premandibles have 3 or more arms (Figure 87).

100 (101) The base of the second antennal joint is narrow, the distal is wide, and it is shorter in length than the third joint, or at most it is as long. Lauterborn organs are broad and stems are short (Figure 88).

Cladotanytarsus Kieffer, 1921

C. mancus (Walker, 1856)

101 (100) The base and distal of the second antennal joint are equal. It is longer in length than the third antennal joint. Lauterborn organs are narrow and their stems are longer than Lauterborn organs (Figure 89).

102 (103) Most of the hindfoot hooks are serrated on the inside (Figure 90). The stems of Lauterborn organs are 1.5 times longer than the last 3 antennal joints (Figure 89).

Virgatanytarsus Pinder, 1982

V. arduennensis (Goetghebuer, 1922)

103 (102) The hindfoot hooks are simple and toothless (Figure 91). The stems of Lauterborn organs are 2.5 times longer than the last 3 antennal joints (Figure 92).

Tanytarsus van der Wulp, 1874

T. gregarius Kieffer 1909

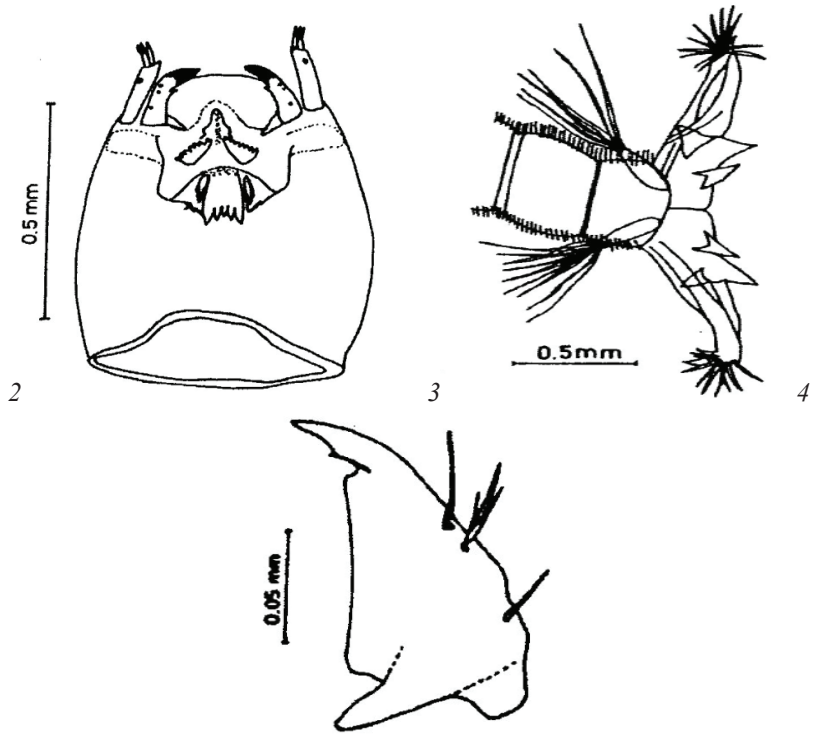

Figure. ***Procladius* (*Holotanypus*) sp.***: 2- head capsule.* ***Tanypus punctipennis*:** *3- last body segments.* ***T. kraatzii*:** *4- mandible.*

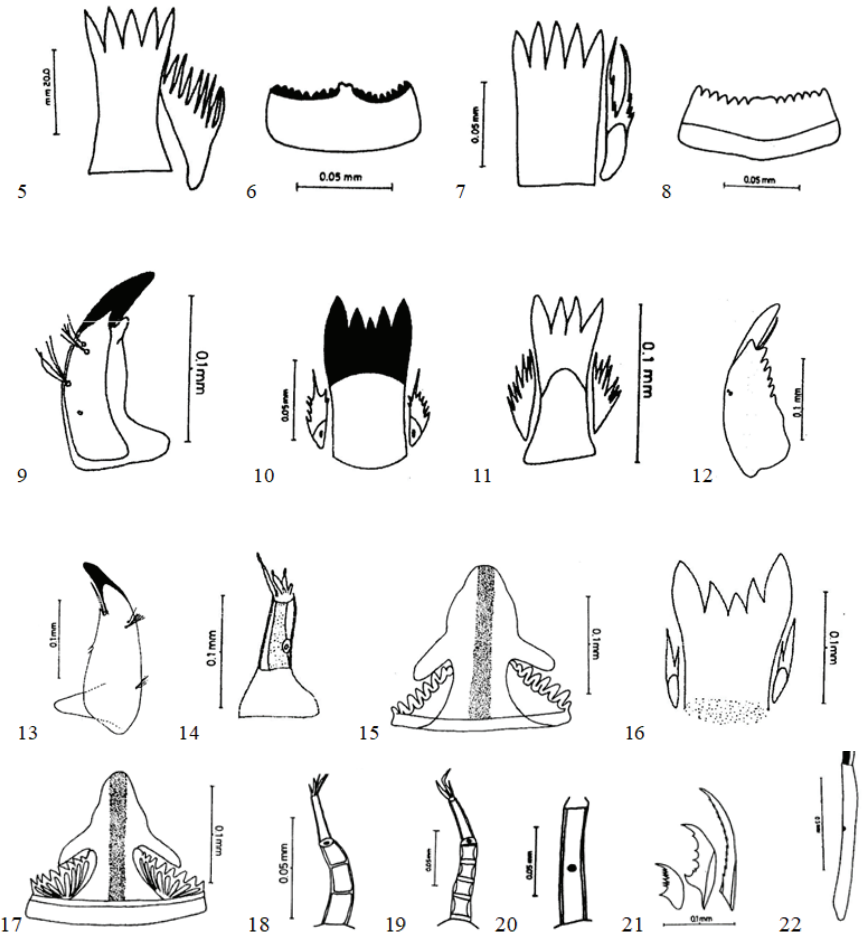

Figure. ***T. punctipennis*****:** *5- glossa and paraglossa; 6- mentum.* ***T. kraatzii*****:** *7- glossa and paraglossa; 8- mentum.* ***Procladius* (*Holotanypus*) sp.:** *9- mandible, 10- glossa and paraglossa;* ***Psectrotanypus varius*****:** *11- glossa and paraglossa, 12- mandible.* ***Macropelopia goetghebueri*****:** *13- mandible, 14- maxillary palpy, 15- mentum, 16- glossa and paraglossa.* ***M. nebulosa:*** *17- mentum.* ***Ablabesmyia aequidensi*****:** *18- maxillary palp.* ***A. monilis*****:** *19- maxillary palp.* ***Monopelopia tenuicalcar*****:** *20- maxillary palp, 21- hind leg hooks, 22- antenna,*

Figure. *23- glossa and paraglossa.* ***Natarsia punctata*****:** *24- glossa and paraglossa.* ***Prodiamesa olivacea*****:** *25- antenna, 26- mentum, 27- mandible.* ***Psectrocladius sordidellus*****:** *28- brush base, 29- S1, 30- mentum.* ***Zalutschia megastyla*****:** *31- S1, 32- mentum.* ***Cricotopus annulator*****:** *33- abdominal segments, 34- epipharyngeal comb, 35- premandible.* ***C. fuscus*****:** *36- premandible.* ***C. albiforceps*****:** *37- mentum.* ***C. flavocinctus*****:** *38- mentum.* ***C. bicinctus*****:** *39- mandible, 40- mentum.* ***C. sylvestris*****:** *41- epipharyngeal comb,*

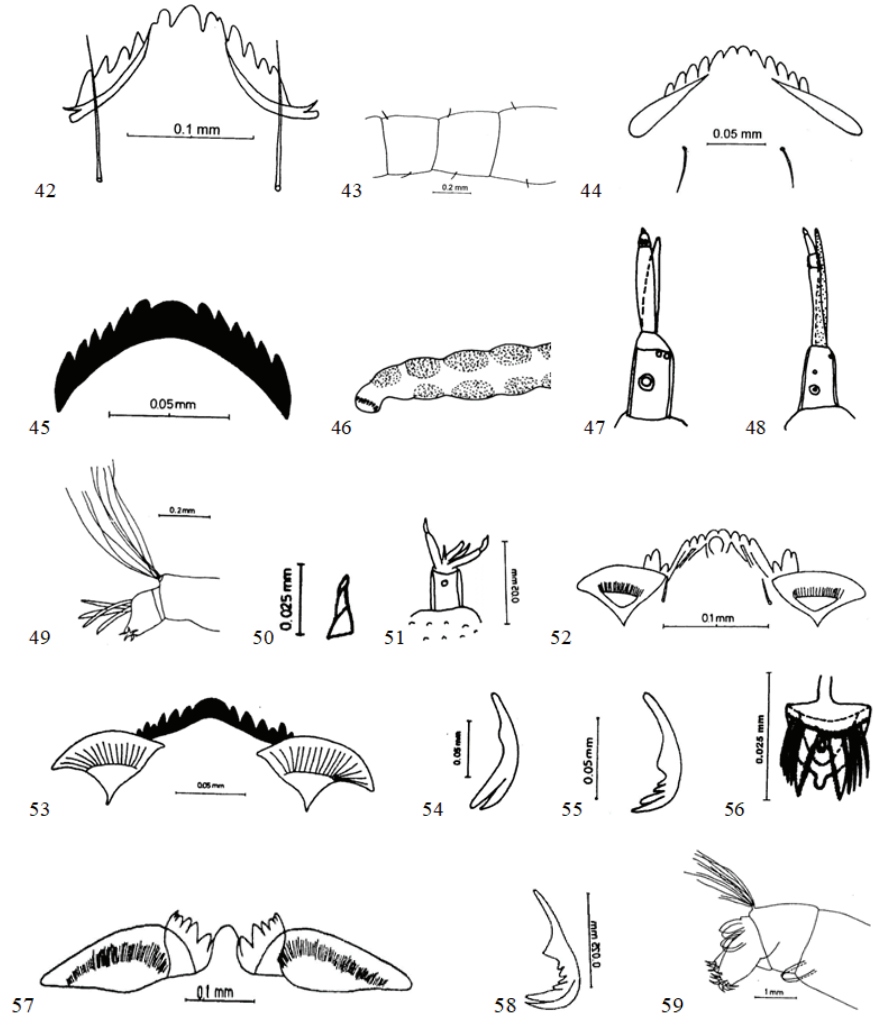

Figure. ***Cricotopus sylvestris*****:** *42- mentum.* ***Halocladius fucicola*****:** *43- fringes of hair.* ***Hydrobaenus pilipes*****:** *44- mentum.* ***Orthocladius thienemanni*****:** *45- mentum.* ***Smittia aquatilis*****:** *46- brush base, 47- antenna.* ***Bryophaenocladius virgo*****:** *48- antenna.* ***Limnophyes pusillus*****:** *49- brush base.* ***Cladopelma laccophila*****:** *50- labrum palp, 51- maxillary palpy, 52- mentum.* ***Cryptotendipes holsatus*****:** *53- mentum, 54- premandible.* ***Cryptochironomus defectus*****:** *55- premandible, 56- epipharyngeal comb, 57- mentum.* ***Harnischia fuscimana*****:** *58- mentum.* ***Einfeldia pagana*****:** *59- ventral gills in the last body segments.*

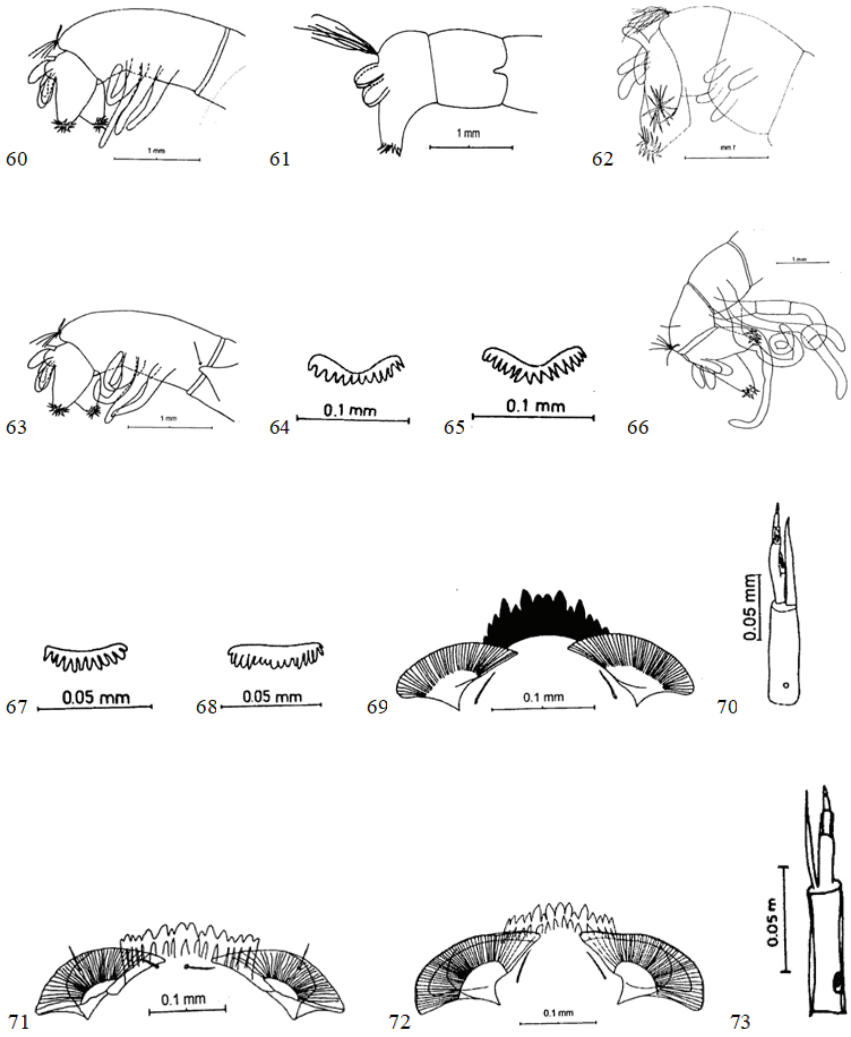

Figure. ***Chironomus anthracinus*****:** *60- ventral gills in the last body segments.* ***C. reductus*****:** *61- last body segments.* ***C. halophilus*****:** *62- last body segments.* ***C. tentans*****:** *63- ventral gills in the last body segments, 64- epipharyngeal comb.* ***C. plumosus*****:** *65- epipharyngeal comb.* ***C. riparius*****:** *66- ventral gills in the last body segments.* ***C. anthracinus*****:** *67- epipharyngeal comb.* ***C. viridicollis*****:** *68- epipharyngeal comb.* ***Polypedilum exsectum*****:** *69- mentum.* ***P. nubifer*****:** *70- antenna, 71- mentum.* ***Polypedilum*** **sp.:** *72- mentum.* ***P. nubeculosum*****:** *73- antenna,*

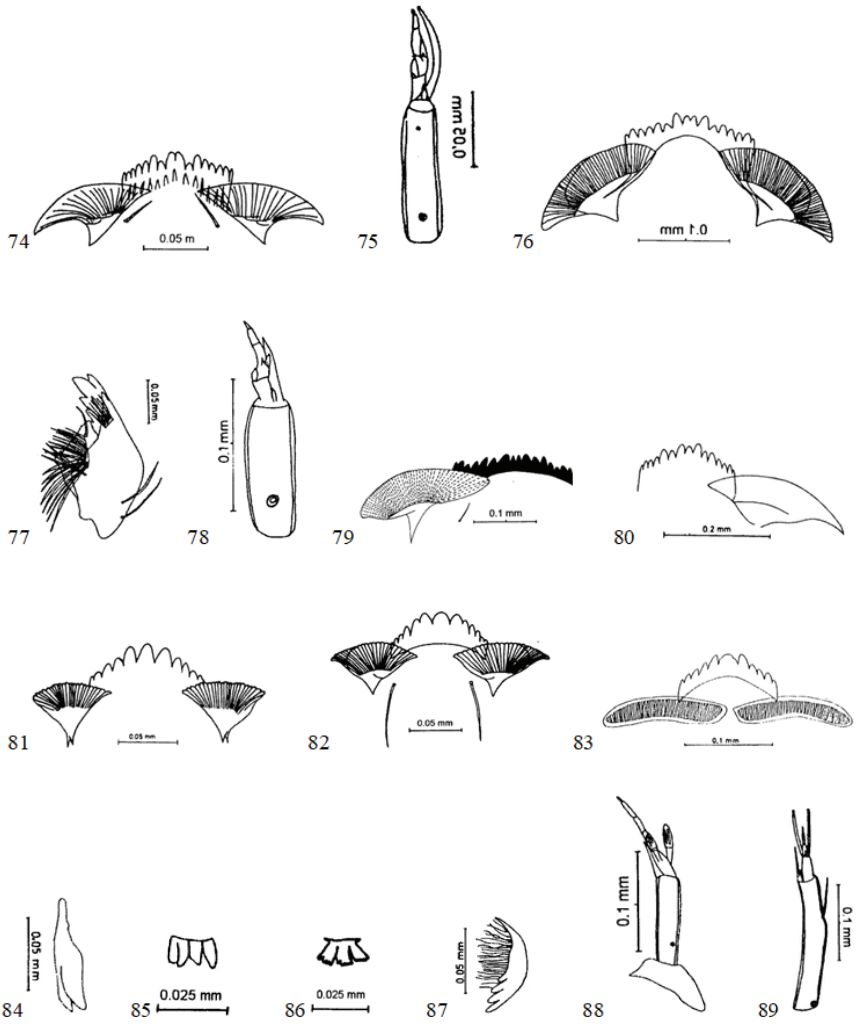

Figure. ***Polypedilum nubeculosum*****:** *74- mentum.* ***Stictochironomus longipugionis*****:** *75- antenna, 76- mentum, 77- mandible.* ***S. yalvacii*****:** *78- mentum, 79- mandible.* ***Endochironomus tendens*****:** *80- mentum.* ***Dicrotendipes nervosus*****:** *81- mentum.* ***D. tritomus*****:** *82- mentum.* ***Pratanytarsus lauterborni*****:** *83- mentum, 84- premandible, 85- epipharyngeal comb.* ***Rheotanytarsus exiquus*****:** *86- epipharyngeal comb.* ***Cladotanytarsus mancus*****:** *88- antenna.* ***Virgatanytarsus arduennensis*****:** *89- antenna,*

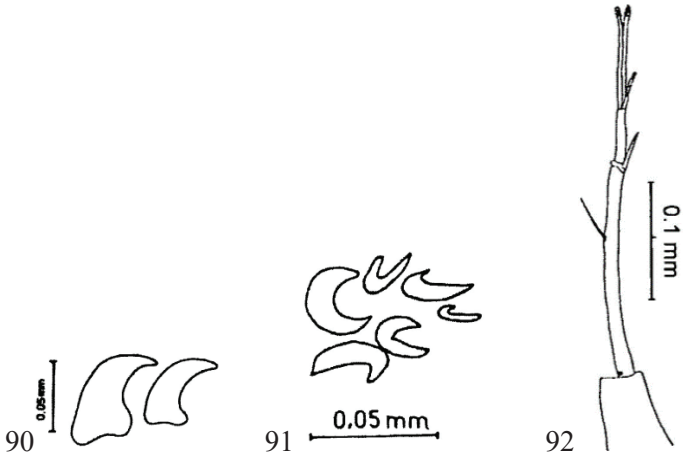

Figure. ***Virgatanytarsus arduennensis*****:** *90- hind leg hooks.* ***Tanytarsus gregarius*****:** *91- hind leg hooks, 92- antenna.*

4. DISCUSSION AND CONCLUSION

In the study, the results of the research conducted between September 20015 and August 2016 on the ground of the Oğulpaşa Stream, which forms a part of the Meriç-Ergene Basin river system, were evaluated. 52 species belonging to 4 subfamilies of Chironomidae were identified. It is distributed as 10 species belonging to Tanypodinae subfamily, 1 belonging to Prodiamesinae subfamily, 14 species belonging to Orthocladiinae subfamily and 27 species belonging to Chironominae subfamily.

Although the number of species is almost the same at the stations studied in the creek, the number of larvae of each species is different. Station 1 is poorer than the other 2 stations. Habitat characteristics cannot be said to be a factor here. The seasonal distribution of the larvae in the stream is in accordance with the general biological characteristics of the larvae of these family members. While it was in high numbers in autumn, it decreased from winter to spring due to the irregularity of the water regime, and in summer, despite the new individuals hatching due to maturation, the number was less than in autumn and winter months. Tanypodinae and Chironominae species were never found among the larvae that emerged in small numbers due to the rapid currents in February, March, and April.

The most common species in Oğulpaşa Stream are *Procladius* (*Holotanypus*) sp., *Chironomus anthracinus*, *C. viridicollis* and *Polypedilum aberrans*. This is in accordance with the bioecological characteristics of the species. *Tanypus, Cricotopus, Polypedilum* and *Chironomus* genera

are cosmopolitan (Polatdemir and Şahin, 1997) and can be found in any aquatic environment. The ratios of their presence in the family are *Tanypus* 9.55%, *Cricotopus* 10.78%, *Chironomus* 25.25%, *Polypedilum* species 32.72%.

Floods in the spring in the creek reduced the number of individuals due to drift. The low incidence of *Tanypus* species from predatory forms can be explained in this way. Also, some of the Tanytarsini members may have been less affected as they were in the tubes they made. However, the fact that *Polypedilum* species from Chironominae are more common is because they are the general preferences of places such as sand and under stones in fast flowing waters.

In addition, Ulfstrand et al (1974) reported that in many countries, aquatic insect larvae and nymphs drift with the current to escape from predators, and their rates in benthos change. Elliot (1971) reported that many aquatic insect adults fly upstream to lay eggs in spring and summer, and their densities in benthic fauna change.

Apart from being consumed by demersal fish in these waters, these numerical or species characteristics that cannot be explained by the physicochemical structure of the water, habitat type and similar factors can be explained by the migration of adults to nearby lakes, ponds and other streams in spring and summer.

REFERENCES

Boesel, M.W. (1985). A brief review of the genus # ,$)! in Ohio, with keys to known stages of species occurring in Northeastern United States (Diptera, Chironomidae). Ohio Academy of Sciences. 80-254.

Chernovskii, A. (1961). Identification of larvae of the midge family Tendipedidae. Fauna USSR, 31, (Trans. from Russian by Natl. Lending Library for Sci. Tech. Boston), 1-279.

Moller Pillot, H.K.M. (1978-1979). De Larven der Nederlandse Chironomidae (Diptera). Leiden, I – 1 – IX. 2. 7.

Moller Pillot, H.K.M. (1984). De Larven der Nederlandse Chironomidae (Diptera) (Orthocla-diinae sensu lato). Leiden. S: 1 – 164.

Fittkau, E.J. & Roback, S.S. (1983). The larvae of Tanypodinae (Diptera: Chironomidae) of the Holarctic Region (keys and diagnoses). Entomology Scandinavian Supplementum. 19, 33 – 110. Lund, Sweden.

Kırgız, T. (1988). Seyhan Baraj Gölü Chironomidae (Diptera) larvaları üzerinde morfolojik ve ekolojik bir çalışma. *Doğa TU Zooloji Dergisi. 12*(3): 245–255.

Kırgız, T. (1989). Gala Gölü bentik faunası. *Anadolu Üniversitesi Fen Edebiyat Fakültesi Dergisi*. *1*(2): 67-87.

Özkan, N. (1991). Edirne Bölgesi Chironomidae (Diptera) limnofaunasının tespiti ve taksonomik incelenmesi. T.Ü. Fen Bilimleri Enstitüsü, Master Thesis. 1 – 80.

Özkan, N. (2003). Trakya Bölgesi (Kırklareli, İstanbul ve Çanakkale) chironomid (Chirono-midae; Diptera) türlerinin tespiti, Trakya Üniversitesi Bilimsel Araştırmalar Projeleri - TÜBAP – 320, 17-65.

Polatdemir, N. & Şahin, Y. (1997). Eskişehir ve Çevresi Durgunsu Sistemleri Chironomidae (Diptera) Larvaları. *Tr. J. of Zoology, 212*: 315-319.

Şahin, Y. (1984). Doğu ve Güneydoğu Anadolu Bölgeleri akarsu ve göllerindeki, Chironomidae (Diptera) larvalarının teşhisi ve dağılışları. Anadolu Üniversitesi Yayınları, No: 57, Fen Edebiyat Fakültesi Yayını, No: 2, Eskişehir.

Şahin, Y. (1987). Burdur, Beyşehir ve Salda gölleri Chironomidae (Diptera) larvaları ve yayılışları. *Doğa TU Biyoloji Dergisi, 11*(2): 59-70.

Şahin, Y. (1991). Türkiye Chironomidae potamofaunası, Tübitak – Proje No: TBAG –869 (and VHAG – 347, TABG – 669, TBAG – 792), 1.

Chapter 3

DETERMINING THE ROLE OF RENEWABLE ENERGY AND ECONOMIC GROWTH IN THE HUMAN DEVELOPMENT PROCESS USING DIFFERENT LINK FUNCTIONS IN FRACTIONAL REGRESSION MODEL

***Haydar KOÇ*[1]**

1 Çankırı Karatekin University, Faculty of Science, Department of Statistics,18100, Çankırı, Turkey. haydarkoc@karatekin.edu.tr, ORCID: 0000-0002-8568-4717

1. Introduction

The Human Development Index (HDI) is a concept created by the United Nations, which is used to measure the human development levels of countries. The HDI determines the human development levels of societies in three main areas: health, education and income. Energy, which is one of the most basic inputs for the socio-economic development of countries, raises the welfare level of societies and is used in almost all areas of daily life. Energy is an important tool to eradicate poverty and sustain human development in job creation, agriculture, transportation, trade and economic development (Karekezi et al. 2012). Increasing energy consumption in the last century has been recognized as a key element in the process of industrialization and economic development (Warr and Ayres, 2010). The continuity and indispensability of the need for energy raises the problem that resources can run out over time. Although the demand/supply of non-renewable energy resources is high, renewable energy resources have become popular in recent years with the determination of economic targets by considering environmental factors. Especially for a sustainable world and sustainable economic growth, renewable energy sources are important for countries. Renewable energy sources have become the focus of clean and inexhaustible energy studies because they are both environmentally friendly and can renew themselves faster than the rate of depletion. Countries are making studies, regulations and investments in this field in order to make progress in renewable energy. In recent years, the number of empirical studies showing that energy consumption, economic growth and human development are interrelated has been increasing. Menyah and Rufael (2010) investigated the causal relationship between CO2 emissions, renewable energy and nuclear energy consumption and real GDP for the USA during the 1960-2007 periods. Steinberger et al. (2012) examined the correlation between carbon emissions and human development and the change over time in the related study. In his study, Doğan (2016) analyzed the relationship between economic growth, renewable and non-renewable energy consumption for Turkey in terms of both short- and long-term estimation and causality. Inal et al. (2017) analyzed the relationship between the annual GDP growth rate and the use of alternative energy sources in Turkey, using annual data for the period 1960-2014. Saricoban et al. (2018) investigated the effects of education expenditures, environmental expenditures and HDI on carbon emissions. Wang et al. (2018) investigated the relationship between renewable energy consumption, economic growth and human development index in Pakistan for 1990-2014 using the Two-Stage Least Squares (2SLS) method. The empirical results revealed that the consumption of renewable energy does not improve the state of the human development process in Pakistan. Rahmani (2019) empirically

investigated the relationship between renewable energy consumption and economic growth in the Turkish economy using time series for the period 1970-2016. Sasmaz et al. (2020) demonstrated the relationship between renewable energy and human development in 28 OECD countries from 1990 to 2017 with panel data analysis and concluded that renewable energy has a positive effect on human development. Abid et al. (2020) examined the relationship between renewable and non-renewable energy consumption, economic growth, environmental sustainability and human development index in Pakistan with a fully modified ordinary least squares approach. Bucak (2021) conducted panel data analysis using the annual data of the Economic Complexity Index, the Human Development Index and per capita carbon emissions (metric tons). As a result of the analysis, it was found that there is a cointegration relationship between the three variables, that is, the series move together in the long term. In this study, we determined the role of renewable energy and economic growth in the human development process in OECD countries with the fractional regression model. In the fractional regression model, the appropriate link function was selected using information criteria and the parameters were estimated using the model. The article is organized as follows. In section 2, the Fractional Regression model is defined. Section 3 presents the employment of fractional regression model. Finally, the results are summarized and discussed.

2.Material and Methods

2.1. Fractional Regression Model

The Fractional Regression model (FRM) was developed by Papke and Wooldridge (1996) in order to deal with limitations on linear and nonlinear econometric models for bounded response variables. In the standard FRM, the data does not require transformation to estimate the conditional expected value of the dependent variable. Furthermore, the semi-maximum likelihood method (QMLE) is used in parameter estimation and it produces fully robust and relatively efficient estimates under general linear model conditions.

Let y_{it}, defined fractional response variable in the range [0,1] for the i-th individual and i=1,…,N, at time t, t=1,…T, and x_{it} denote a k-vector of explanatory variables. The conditional expected value for the standard fractional regression model defined by Papke and Wooldridge (1996) is as follows:

$$E(y_i|x_i)=G(x_i\theta) \quad (1)$$

Here, θ is a vector of the parameters of interest, G (.) is a nonlinear function limited in the range of $0\leq G(.)\leq 1$. The parameters of the model

indicated by equation (1) can be estimated by QML method. Alternatively, nonlinear least squares or maximum likelihood estimation can be used, but it is less efficient than QML estimation. Generally, logit or probit functional form is defined for G (.). Alternative features like loglog, cloglog and cauchit models were defined by Ramalho et al. (2011). Appropriate G(.) link functions for the fractional regression model are given in Table 1.

Table 1. *Link functions for the fractional regression model*

Link	G(xθ)
Logit	$e^{x\theta}/(1+e^{x\theta})$
Probit	$\Phi(x\theta)$
cloglog	$1-e^{-e^{x\theta}}$
loglog	$e^{-e^{x\theta}}$
Cauchit	$1/2+1/\pi(\arctan(x\theta))$

2.2. Performance Measurement

There are many statistical criteria used to evaluate model performance in regression analysis. The criteria used are very important in terms of comparing different regression models. The criteria used in the evaluation of model performance in this study; the coefficient of determination (R2), the mean squared error (MSE), the mean absolute error (MAE), the root mean squared error (RMSE). A high R2 value indicates that the prediction relationship is good. MSE, MAE, RMSE are the average error measure, so low values indicate good performance. The error measures are defined as follows

$$\mathrm{MSE} = \frac{1}{\mathrm{N}}\sum(\mathrm{y_i} - \hat{\mathrm{y}}))$$

$$\mathrm{MAE} = \frac{1}{\mathrm{N}}(\sum|\mathrm{y_i} - \hat{\mathrm{y}}|)$$

$$\mathrm{RMSE} = \sqrt{\frac{1}{\mathrm{N}}\sum(\mathrm{y_i} - \hat{\mathrm{y}})}$$

$$\mathrm{R}^2 = 1 - \frac{\Sigma(\mathrm{y_i}-\hat{\mathrm{y}})^2}{\Sigma(\mathrm{y_i}-\bar{\mathrm{y}})^2}$$

3. Application Part

In the study, data for 2019 of 38 OECD (Organization for Economic Cooperation and Development) countries were used and the data was obtained from (URL-1, 2021). A set of 5 continues variables are used in this paper and described as, dependent variable(Y): Human Development Index (HDI), independent variables: Gross domestic product (GDP-per capita) (x1), CO2 emission (metric tons per capita) (x2), ,Renewable energy (percentage of total primary energy supply) (x3), Urbanization (as the growth rate of urban population) (x4). Analyzes were performed using R software's 3.5.2 version. The role of renewable energy and economic growth in the human development process in OECD countries were determined by the FRM method using "frm" package from the R software. In the fractional regression model, model structures were established by taking logit, probit, cloglog, loglog, cauchit link functions, respectively. Model performance criteria are as given in Table 2.

Table 2. *Performance measurement for Models*

Models	R2	MSE	**MAE**	**RMSE**
FRM1(with logit link)	0.837	0.0003847816	0.01467276	0.01961585
FRM2(with probit link)	0.812	0.0004508721	0.01590308	0.02123375
FRM3 (with cloglog)	0.784	0.0005260815	0.01727863	0.02293647
FRM4 (with loglog link)	0.844	0.0003674295	0.01437777	0.01916845
FRM5 (with cauchit link)	0.919	0.0001868213	0.010108	0.01366826

The model with the highest R2 value and lower error rates than MSE, MAE and RMSE shows the best performance. In Table 2, the model that gives the best performance in parameter estimation is the fractional regression model with cauchit link function (FRM5).

Table 3. *Coefficients for the FRM5 model*

Coefficient	Estimate	Std. Error	t value	Pr(>|t|)
(Intercept)	0.620949	0.207938	2.986	**0.003** ***
x1	0.000062	0.000008	8.256	0.000 ***
x2	0.073498	0.022779	3.227	0.001 ***
x3	-0.115628	0.063544	-1.820	0.069 *
x4	0.005535	0.004131	1.340	0.180

* Significant at the 0.05 probability level

** Significant at the 0.01 probability level

*** Significant at the 0.001 probability level

Table 3 shows the coefficients of fractional regression model where the link function is selected as cauchit. According to the fractional regression model the variables GDP and Renewable energy affect the human development index positively. Besides that, CO2 emission has a negative influence on the human development index.

4. Conclusion

The human development index is a multidimensional concept with economic, social and social dimensions. Human development and the welfare of the society will increase if factors such as improvements in education, health, nutritional conditions, and reduction in crime rates in the society are provided together with economic growth. However, the fact that the economic size of the countries is high does not mean that other factors will increase along with it. When countries use non-renewable energy sources in the production process to increase their economic growth, the amount of carbon released increases, global warming and environmental pollution occur, and welfare decreases. (Dinçer and Karakuş,2020). Renewable energy sources protect the environment by reducing carbon emissions, energy imports are limited or not required if necessary investments are made, thus reducing or eliminating the problem of energy dependence. In the case of non-renewable energy consumption, carbon emissions occur, which creates a major obstacle for countries in the path of development. From this point of view, the scope of the energy used is of great importance for the growth and development of countries.

In this study, fractional regression model was used to determine the role of renewable energy and economic growth in the human development process in OECD countries in 2019. First, five different fractional regression models were created by taking logit, probit, cloglog, loglog, cauchit link functions. When the model performance criteria were examined, it was seen that the fractional regression model created by choosing the cauchit link function with the highest R2=0.919 and the smallest MSE= 0.0001868213 value was the best model. When parameter estimations are made with the fractional regression model by choosing the cauchit link function, a positive effect of GDP, and Renewable energy variables on the human development process, and a negative effect of the CO2 emission variable have been observed. The results are quite consistent with the literature (Manga and Akar, 2020). As CO2 emissions increase, environmental pollution and climate change will be inevitable. Climate change has become an indisputable reality that poses a serious threat to the sustainable growth of society, economy and environment (Wang et al, 2019). Therefore, countries need to implement sustainable environmentally friendly policies.

References

Abid, N., Wu, J., Ahmad, F., Draz, M. U., Chandio, A. A., and Xu, H. (2020). Incorporating environmental pollution and human development in the energy-growth nexus: A novel long run investigation for Pakistan. *International Journal of Environmental Research and Public Health*, *17*(14), 5154.

Bucak, Ç. (2021). Ab15 Ülkelerinde Ve Türkiye'de Ekonomik Karmaşıklık Endeksi, İnsani Gelişme Endeksi Ve Karbon Emisyonu: Panel Veri Analizi. *Ege Stratejik Araştırmalar Dergisi*, *12*(1), 71-88.

Dinçer, H. and Karakuş, H. (2020). Yenilenebilir Enerjinin Sürdürülebilir Ekonomik Kalkınma Üzerindeki Etkisi: Brıcs ve Mınt Ülkeleri Üzerine Karşılaştırmalı Bir Analiz. *Esam Ekonomik Ve Sosyal Araştırmalar Dergisi*, *1*(1), 100-123.

Dogan, E. (2016). Analyzing the linkage between renewable and non-renewable energy consumption and economic growth by considering structural break in time-series data. *Renewable Energy,* 99, 1126-1136.

İnal, V. İnançlı, S. and Çalışkan, M. (2017) alternatif enerjinin ekonomik büyümeye etkisi: Sakli eşbütünleşme testi, Anadolu İnternational Conference Economics, 1-8.

Karekezi, S., McDade, S., Boardman, B. and Kimani, J. (2012). Energy, poverty, and development. *Global Energy Assessment–Toward a Sustainable Future [Johansson, TB, N. Nakicenovic, A. Patwardhan, and L. Gomez-Echeverri (eds.)]. Cambridge University Press, Cambridge, United Kingdom and New York, NY, USA and the International Institute for Applied Systems Analysis, Laxenburg, Austria*, 151-190.

Manga, M. and Akar, P. G. (2020). Ekonomik Büyüme, Karbon Emisyonu ve İnsani Gelişmişlik Arasındaki İlişki: Seçilmiş Akdeniz Ülkeleri. *Kahramanmaraş Sütçü İmam Üniversitesi Sosyal Bilimler Dergisi*, *17*(1), 405-419.

Menyah, K. and Rufael, Y.W. (2010). CO2 emissions, nuclear energy, renewable energy and economic growth in the USA. *Energy Policy,* 38, 2911–2915.

Papke, L. E. and Wooldridge, J. M. (1996). Econometric methods for fractional response variables with an application to 401 (k) plan participation rates. *Journal of applied econometrics*, 11(6), 619-632.

Rahmani, A. (2019). Türkiye ekonomisinde yenilenebilir enerji tüketimi ve ekonomik büyüme ilişkisi: bir zaman serisi analizi (Master's thesis, Namık Kemal Üniversitesi).

Ramalho, E. A., Ramalho, J. J. and Murteira, J. M. (2011). Alternative estimating and testing empirical strategies for fractional regression models. *Journal of Economic Surveys*, *25*(1), 19-68.

Sasmaz, M. U., Sakar, E., Yayla, Y. E. and Akkucuk, U. (2020). The relationship between renewable energy and human development in OECD countries: A panel data analysis. *Sustainability*, *12*(18), 7450.

Sarıçoban, K., Kaplan, F. and Kaplan, Z. (2018). Avrupa Ülkelerinde Karbon Emisyon Miktarına Farklı Bir Bakış. 1. Uluslararası Ekonomi ve İşletme Sempozyumu, 757-764.

Steinberger, J.K., Roberts, J.T. and Peters, G. (2012). National Pathways of Emissions and Human Development: Correcting for Carbon Embodied in Trade. White Rose Research Online. http://eprints.whiterose.ac.uk/76548/14/steinbergerj3pdf.pdf

URL-1. https://data.oecd.org/

Wang, Z. Danish, Zhang, B. and Wang, B. (2018) Renewable energy consumption, economic growth and human development ındex in pakistan: evidence form simultaneous equation model. *Journal of Cleaner Production*, 184, 1081- 1090.

Wang, C. M., Hsueh, H. P., Li, F. and Wu, C. F. (2019). Bootstrap ARDL on health expenditure, CO2 emissions, and GDP growth relationship for 18 OECD countries. *Frontiers in public health*, *7*, 324.

Warr, B.S. and Ayres, R.U. (2010). Evidence of causality between the quantity and quality of energy consumption and economic growth. *Energy* 35, 1688e1693. https:// doi.org/10.1016/j.energy.2009.12.017.

Chapter 4

COMPARING EXTREME LEARNING MACHINE AND MULTILAYER PERCEPTION: TOURISM DATA AS AN EXAMPLE

Pelin AKIN[1]

1 Dr, Çankırı Karatekin Üniversitesi, Fen Fakültesi, İstatistik, Çankırı,Turkey. E-mail: pelinakin@karatekin.edu.tr, ORCID ID: 0000-0003-3798-4827

1. INTRODUCTION

Tourism is one of the largest industries in the world and provides employment opportunities for hundreds of thousands of people every year. The rapidly growing tourism sector encourages the citizens of countries to become producers or consumers of tourism. The economic contribution of tourism to countries can be shown as the reason for these behaviors of countries. The tourism sector, which contributes directly or indirectly to the economy in many countries, is an important economic activity, especially in developing countries. In many developing countries, international tourism is seen as an important source of economic growth (Brohman, 1996). Tourism should not be viewed only to create an economic resource. Tourism is not just a change of geographical location with people moving from one place to another; Simultaneously, it has a direct or indirect effect on many fields such as education, cultural, socio-cultural, economic, sociological, psychological, environmental. Therefore, developed and developing countries give increasing importance to tourism activities. In recent years, the number of studies on estimating the number of foreign tourists has increased. Önder and Hasgül (2009) used artificial neural networks and traditional time series analysis methods to estimate and compare the number of long-term foreign visitors. Chun et al. (2012) used ARIMA models and backpropagation neural network (BPN) methods to estimate the number of tourists coming to Taiwan abroad and stated that the BPN model gave the best results. Karahan (2015) estimated the number of tourists coming to Denizli in the first six months of 2014 with the artificial neural networks (ANN) model. Sel and Numan (2020) estimated the number of foreign tourists and tourism revenues in Turkey for 2020 monthly with ARIMA models. Çuhadar (2020) estimated the domestic tourism demand in Turkey using the Exponential Smoothing and Box-Jenkins methods.

In this study, the data set of the number of citizens coming to Turkey monthly was used between 2012 and 2020, taken from the TUIK database. After applying ELM and MLP algorithms to this data set, model performances were compared. The article is divide as follows: In section 2, MLP and ELM are explained. In section 3 are shown the results of the algorithms. Finally, in section 4, given the conclusion part.

2. MATERIAL AND METHODS

2.1. Extreme Learning Machine (ELM)

The extreme learning machine (ELM) model was proposed by Huang et al. in 2006 (Huang et al., 2006). In the ELM model, unlike the artificial

neural network algorithms, the hidden layer w is determined randomly. In an ELM, let us say X_k is the input and Y_k is the output of the network. The mathematical expression of the ELM model is defined as follows (Suresh et al., 2010)

$$\sum_{i}^{M} \beta_i g(W_i X_k + b_i) = Y_k \quad , k = 1,2 \dots N$$

where β_i the output weight, W_i the input weight matrix, and the b_i the threshold values in the i. neuron.

The ELM algorithm can be summarized in three steps as follows. The first step is, input weight W_i and bias b_i is produced randomly with i =1,..., M. The second step is the output matrix of the hidden layer H calculated. The last step is the calculation of output weights (Liang et al., 2006). Nikolaos Kourentzes et al. have developed a newly introduced R package called nnfor to estimate and forecast ELM algorithms in time series data (Kourentzes, 2019).

2.2. Multilayer Perceptrons (MLP)

In artificial neural network algorithms, the input layer consists of hidden layers and output layers. Multilayer artificial neural networks are preferred for nonlinear problems. In this algorithm, it can have multiple inputs and multiple hidden layers. The neurons of a given layer feed with their outputs the neurons of the next layer. The one-step-ahead forecast $\hat{y}_{t+1}$ is computed using inputs that are lagged observations of the time series or other explanatory variables. The mathematical expression of the MLP model is defined as follows

$$\hat{y}_{t+1} = \beta_0 + \sum_{h=1}^{H} \beta_h g(\gamma_{0i} + \sum_{i=1}^{I} \gamma_{hi} P_i)$$

w(β, γ) are the network weight with β, γ for the output and hidden layers, respectively (Alzahrani et.al., 2020).

In MLP applications for the time series, lags of the series, potentially together with lagged observations of explanatory variables, are used as inputs to the network. The network output is compared to the target, and the resulting error is used to update the network weights.

3. APPLICATIONS

In this study, ELM and MLP methods have been applied to predict the number of tourists in Turkey. Monthly time-series data from 2012 to 2020 of tourist numbers were collected from URL-1. The graph of the change in the number of tourists to Turkey between 2012 and 2019 is given in Figure 1.

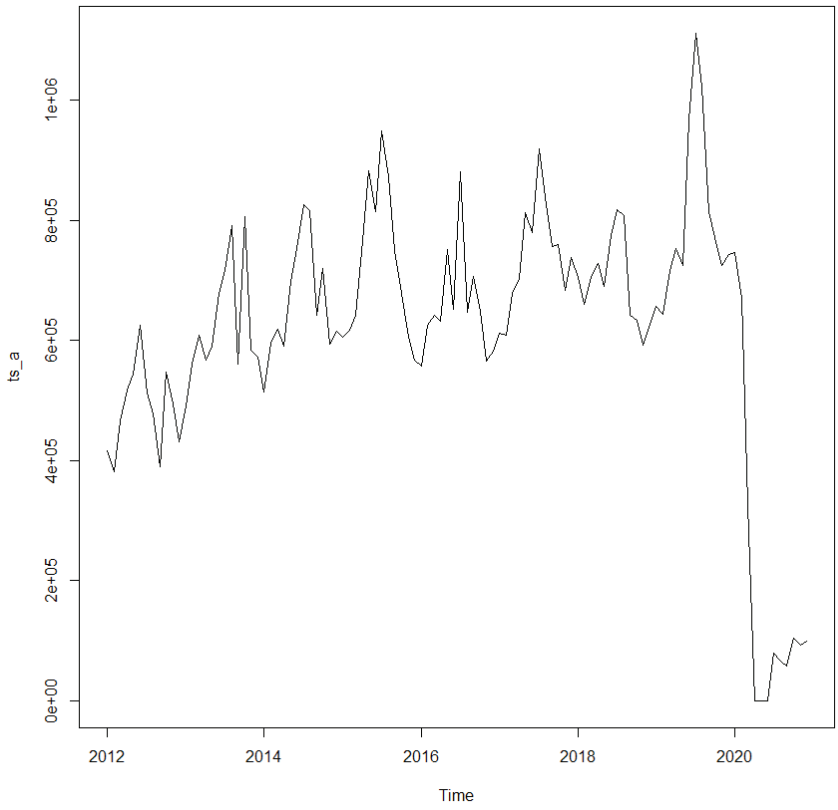

Figure1. Time series plot of the number of tourists in Turkey

While the number of tourists in 2019 found the highest value, the number of tourists decreased in April 2020 due to Covid. After these restrictions were over, they started to rise. The logarithmic transformation has been done to the dataset.

Firstly, The ELM model was applied to the number of tourists. The parameters in Table 1 were obtained as a result of the experiments.

Table 1. Parameters of the ELM learning algorithms

Layer Numbers	Input :4 Hidden Layer:40 Output Layer :1
Activation Functions	Linear
MSE	0.0829

A visual summary of the ELM model was given in Figure 2.

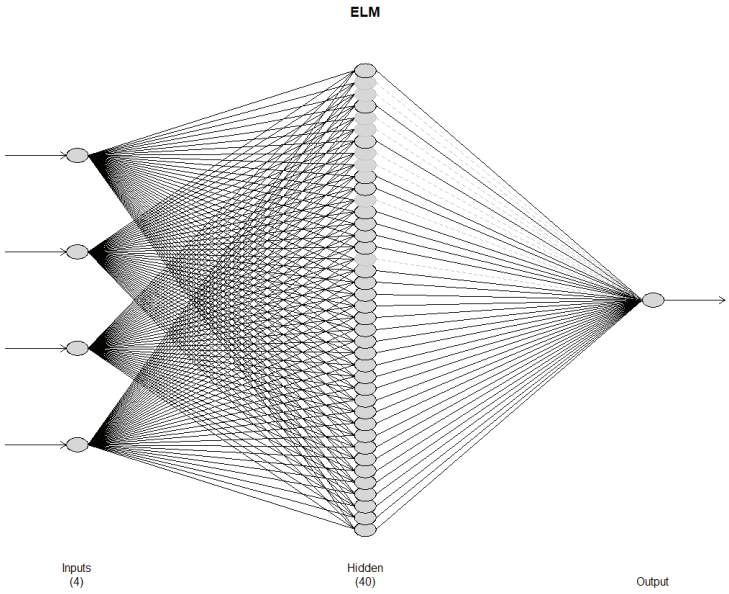

Figure 2. The structure of the ELM model

In Figure 2, the output indicates that the resulting network has 40 hidden nodes, trained 20 times, and the different forecasts were combined using the median operator. Finally, the predicted value obtained from the ELM model and actual values were given in Figure 3.

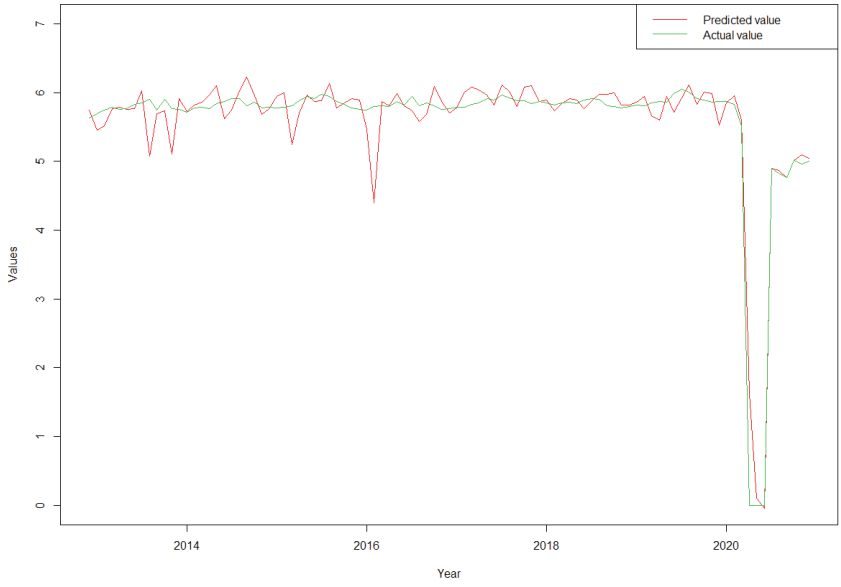

Figure 3. Comparison between the predicted value and actual value for ELM model

It is seen in figure 3 that the predicted values obtained from the ELM model and the actual values are very close. Secondly, the MLP model was applied to tourist data. The parameters in Table 2 were obtained as a result of the experiments.

Table 2. Parameters of the MLP learning algorithms

Layer Numbers	Inputs:35 Hidden Layer:5 Output Layer :1
Activation Functions	Linear
MSE	0.0046

Input

A visual summary of the ELM model was given in Figure 4.

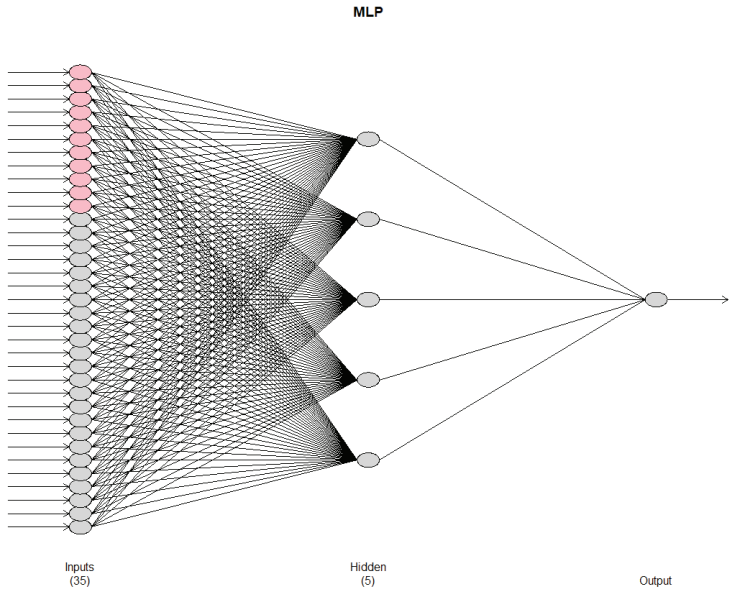

Figure 4. The structure of the MLP model

In Figure 4, the output indicates that the resulting network has five hidden nodes and input nodes, it was trained 20 times, and the different forecasts were combined using the median operator. Finally, the predicted value obtained from the ELM model and actual values were given in Figure 5.

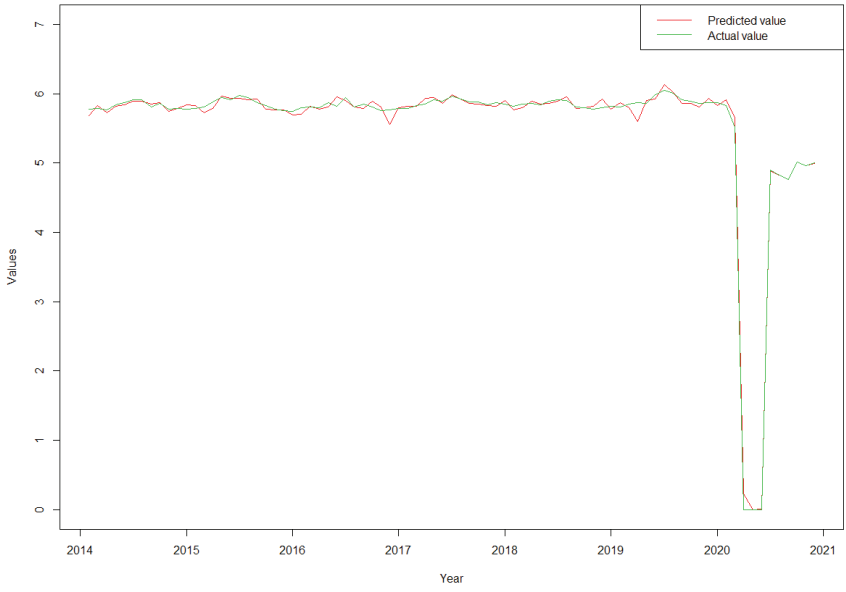

Figure 5. Comparison between the predicted value and actual value for MLP model

It is seen in figure 5 that the predicted values obtained from the MLP model, and the actual values are very close. Predicted values and actual values are very close to each other such as the ELM model.

Table 3. Evaluation Metrics for ELM and MLP models

Model	MSE	RMSE	MAE
ELM	0.0829	0.28479	0.1641
MLP	0.0046	0.068	0.0477

We compared these two models using MSE, RMSE, MAE values. The MLP model outperformed the ELM model with its MSE value of 0.0046, RMSE value of 0.068, and MAE value of 0.0477, which is smaller than the ELM model.

4. CONCLUSION

Many factors affect tourists' visits to a country. Some of them are shaped by the natural and physical conditions of the country. It is shaped depending on the country's natural and physical conditions and political, social, and economic stability. Unusual events such as epidemics, natural disasters, political and economic crises can negatively affect tourism development. The rapid spread of COVID-19 to large areas, the uncertainty of the transmission process and its treatment, and the obligatory travel measures, directly affected tourism and reduced the volume of tourism in the regional sense (Wen et al., 2020). When the tourism data in Turkey and the world are examined, it is seen that there are great decreases in 2020 (URL-2)

In this study, ELM and MLP methods were applied to predict the number of tourists visiting Turkey. First, the optimal result was achieved when four inputs and 40 hidden layer parameters were used in the ELM model to the monthly dataset. The predicted values obtained from the ELM model and the actual values are very close. Secondly, MLP was applied to the monthly dataset. The optimal result was achieved when 35 inputs and five hidden layer parameters were used in the MLP model to the dataset. Similar to the ELM method, the actual and predicted values were close to each other in the MLP method. Afterward, we compared the ELM versus MLP method according to performance criteria. Results show that MLP with one hidden layer overcomes clearly ELM (Vergana et al., 2015). These two models are likely to provide a scientific basis for predicting the number of tourists in the following years.

REFERENCES

Alzahrani, S. I., Aljamaan, I. A., & Al-Fakih, E. A. (2020). Forecasting the spread of the COVID-19 pandemic in Saudi Arabia using ARIMA prediction model under current public health interventions. *Journal of infection and public health*, *13*(7), 914-919.

Brohman, J. (1996). New directions in tourism for third world development. Annals of tourism research, 23(1), 48-70.

Chen, C. F., Lai, M. C., & Yeh, C. C. (2012). Forecasting tourism demand based on empirical mode decomposition and neural network. Knowledge-Based Systems, 26, 281-287.

Çuhadar, M. (2020). Modeling and Forecasting Inbound Tourism Demand to Croatia using Artificial Neural Networks: A Comparative Study. Journal of Tourism and Services, 21 (11), 55-70. Journal of Tourism and Services, 11(21), 55-70.

Huang G-B, Zhu Q-Y, Siew C-K. Extreme learning machine: Theory and applications. Neurocomputing 2006; 70: 489–501.

Karahan, M. (2015). Turizm talebinin yapay sinir ağaları yöntemiyle tahmin edilmesi. Süleyman Demirel Üniversitesi İktisadi ve İdari Bilimler Fakültesi Dergisi, 20(2), 195-209.

Kourentzes, N., Barrow, D. K., & Crone, S. F. (2014). Neural network ensemble operators for time series forecasting. Expert Systems with Applications, 41(9), 4235-4244.

Liang, N. Y., Saratchandran, P., Huang, G. B., & Sundararajan, N. (2006). Classification of mental tasks from EEG signals using extreme learning machine. International journal of neural systems, 16(01), 29-38.

Önder, E., & Hasgül Kuvat, Ö. (2009). Yabancı ziyaretçi sayısının tahmininde box jenkins modeli, winters yöntemi ve yapay sinir ağlarıyla zaman serisi analizi (time series analysis with using box jenkins models and artificial neural network for forecasting number of foreign visitors). Istanbul University, Business Economy Institute Journal of Management, 62, 62-83.

SEL, A. and Zengin, N., (2020) Turizm gelirlerinin mevsimsel arıma modelleri ile tahmini: türkiye örneği., 5. İKSAD uluslararası sosyal bilimler kongresi, 8.

Suresh, S., Saraswathi, S., & Sundararajan, N. (2010). Performance enhancement of extreme learning machine for multi-category sparse data classification problems. Engineering Applications of Artificial Intelligence, 23(7), 1149-1157.

URL1. https://data.tuik.gov.tr/

URL2. https://www.tursab.org.tr/dunya-turizm-istatistikleri

Vergara, G., Cózar, J., Romero-González, C., Gámez, J. A., & Soria-Olivas, E. (2015, June). Comparing elm against mlp for electrical power prediction in buildings. In International Work-Conference on the Interplay Between Natural and Artificial Computation (pp. 409-418). Springer, Cham.

Chapter 5

VITAMIN D AND ITS IMPORTANCE IN METABOLISM

Ebru ÇOTELI[1]

1 Assist. Prof. Ebru COTELI, Ph.D. Kırşehir Ahi Evran University, Health Services Vocational College, Departments of Medical Services and Techniques, Kırşehir, Turkey, e-mail address: e.coteli@ahievran.edu.tr, ORCID IDs: 0000-0002-9473-0914

1. INTRODUCTION

Substances which are necessary for biochemical tasks in the metabolism, synthesized by the organism or not synthesized by the organism and taken externally through the nutrients are called vitamins. Especially green plants are among the most important sources of vitamins (Munzuroğlu et al., 2000). Vitamins are involved in the regulation of biochemical events in metabolism with their presence in the structure of enzymes and proteins that function in metabolism. Vitamins are classified into two groups, fat-soluble and water-soluble. One of the fat-soluble vitamins is vitamin D. Vitamin D is a type of sterol which is a hormone and has hormone precursors, and is produced in tissues and released to the bloodstream, acting in other tissues.(Holick, 1994; Champe et al., 2007).

Vitamin D is also called the sunshine vitamin. This vitamin is crystalline in structure, white in color. It is also resistant to heat and oxidation (Holick, 2005). Vitamin D is also referred to as calciferol. Two types, called metabolism cholecalciferol (vitamin D3) and ergocalciferol (vitamin D2), are very common (Öngen et al., 2008). Since vitamins D2 and D3 are metabolized via similar pathways, they are called vitamin D (Hatun et al., 2003; Göçoğlu, 2010). While most of the cholecalciferol form is synthesized in the skin by ultraviolet-B (UVB) rays, very little is taken via diet. The D2 form is obtained from plant-based foods (Gil et al., 2018; Uitterlinden et al., 2004).

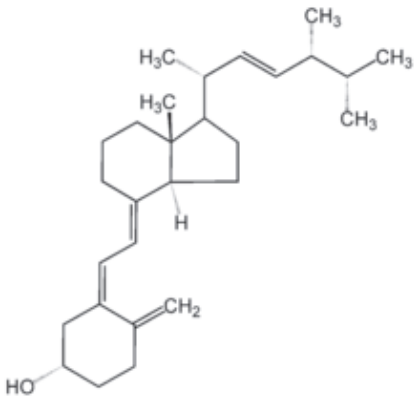

Figure 1. *Ergocalciferol (D2)*

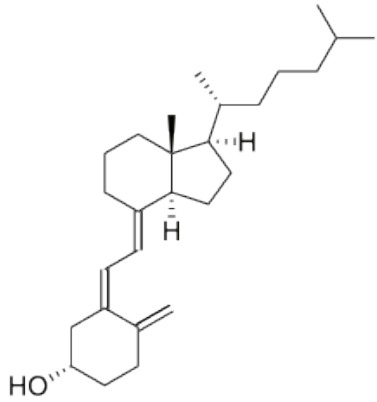

Figure 2. *Cholecalciferol (D3)*

2. SOURCES OF VITAMIN D

Vitamin D is obtained in three ways. It is taken by the metabolism through nutrients, the exposure of vitamin D-containing substances

to ultraviolet light, and the direct exposure of the skin to sunlight (Gözükara, 2011). Vitamin D has two forms; the form of cholecalciferol (Vitamin D3), which is synthesized in the skin by ultraviolet rays, and the form of ergocalciferol (Vitamin D2), which is taken via nutrients (fish, dairy products and eggs, etc.). Cholecalciferol (D3) is synthesized from 7-dehydrocholesterol in the skin under the influence of ultraviolet rays (UV) (Glerup et al., 2000; Holick, 2005). Vitamin D taken into the body is converted to 25(OH)D by the 25 hydroxylase enzyme in the liver (Lerchbaum & Obermayer-Pietsch, 2012). In addition to its synthesis in the body, vitamin D can also be taken into the body with foods (Öngen et al., 2008). Dietary intake of vitamin D is limited. Especially mackerel, salmon and tuna, egg yolk, butter, milk, liver, oats, broccoli, potatoes, parsley, seaweed, and mushrooms are among the foods rich in vitamin D (Ataş et al., 2008; Holick, 2006). Studies indicate that cod liver oil is rich in vitamin D. Sources of vitamin D are shown in Figure 3 (Akşit, 2012).

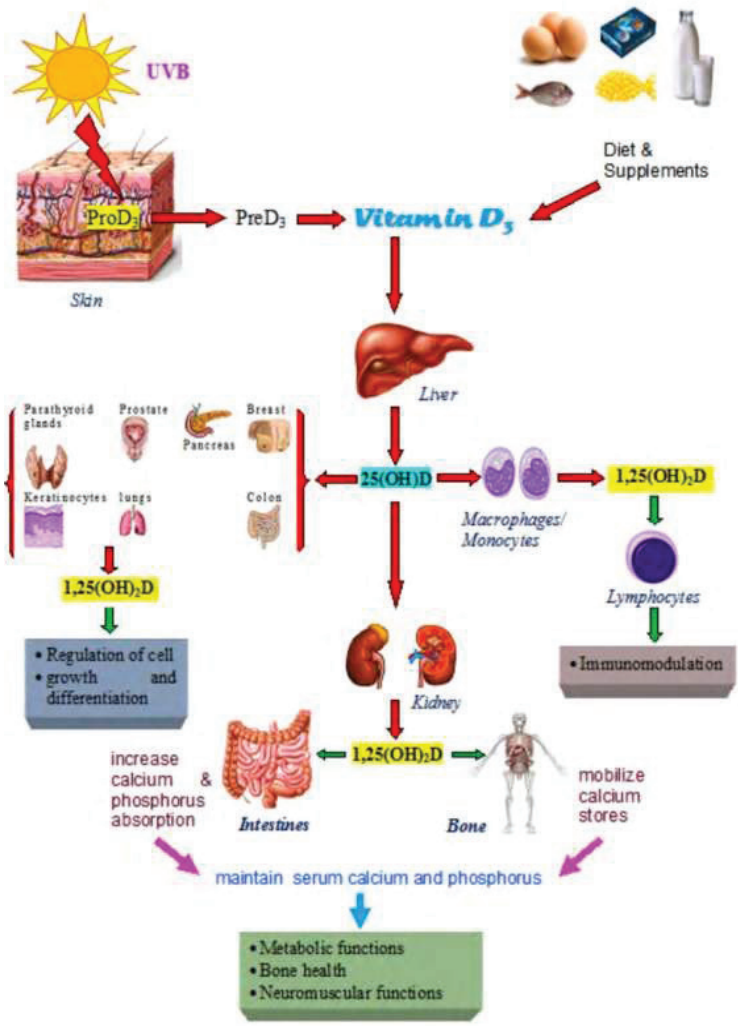

Figure 3. *Sources of Vitamin D*

However, none of these nutrients can meet the daily requirement of vitamin D (Fletcher et al., 2002; Ataş et al., 2008). The largest source of this vitamin is the D3 form produced with sunlight (Glerup et al., 2000). Studies have shown that the biological activity of vitamin D3 is higher than that of vitamin D2 (Armas et al., 2004; Bikle, 2007). The two forms of vitamin D are chemically similar, but they are biologically quite different. The ways of obtaining the two forms of this vitamin are different. While cholecalciferol is synthesized in the skin through sunlight, ergocalciferol is plant-based. Ergocalciferol is produced by exposing the ergosterol in yeast and fungi to ultraviolet rays (Müller & Volmer, 2015).

3. VITAMIN D METABOLISM

Vitamin D forms in metabolism are absorbed in the intestines. Later, it is mixed into the bloodstream via vitamin D binding proteins. The metabolisms of D group vitamins are similar. Fat-soluble D group vitamins are present in many structures such as the liver, adipose tissue, intestines, and skin (Gürdöl & Ademoğlu, 2010). These vitamins, which are transported to the liver especially by binding proteins, are converted to 25(OH)D to 25-hydroxy vitamin D via the 25-hydroxylase enzyme (Murray et al., 2004; Öngen et al., 2008). The enzyme involved in the synthesis of vitamin D is 25-hydroxylase. Steps of vitamin D synthesis are presented in Figure 4. (Wacker & Holick, 2013; Bringhurst et al, 2005).

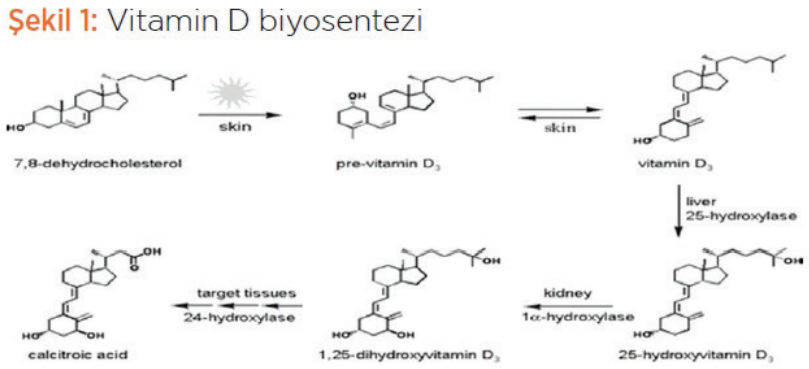

Figure 4. *Biosynthesis of Vitamin D*

The first step in the synthesis of vitamin D is the conversion of Provitamin D (7-dehydrocholesterol) in the skin to Previtamin D3 with the help of UVB rays with a wavelength between 290-315 nm. Previtamin D3 is then converted to vitamin D3 (cholecalciferol). Vitamin D (cholecalciferol or ergocalciferol) in metabolism is converted to 25-hydroxycholecalciferol [25(OH)D, calcidiol] by the 25-hydroxylase enzyme in the liver. Then, the resulting 25(OH)D is converted to 1,25-dihydroxycholecalciferol [1,25(OH)2D3], which is an active vitamin D product, by the 1α-hydroxylase enzyme in the kidneys and other tissues. Eighty-five percent of vitamin D is transported by binding to vitamin D-binding protein (DBP) and 14.6% by binding to albumin (Bouillon, 2011).

Moreover, 25-hydroxy vitamin D gives information about the level of vitamin D in the body (Özkan & Döneray, 2011). Many studies have been conducted on blood 25(OH)D levels to specify vitamin D deficiency and excess in the human body. The results of these studies are shown in Table 1 below (Wacker & Holick, 2013; Holick et al, 2011; Lavie et al., 2011).

Table 1. *Blood serum 25(OH)D Level (ng/mL)*

Serum 25(OH)D Level (ng/mL)	**Diagnosis**
>10 ng/mL	Severe deficiency
<20 ng/mL	Deficiency
21-29 ng/mL	Insufficiency (Moderate deficiency)
>30 ng/mL	Sufficient (optimum range 40-60 ng/mL)
40-50 ng/mL	Ideal
>150 ng/mL	Intoxication (Toxic)

4. FUNCTIONS OF VITAMIN D IN METABOLISM

Important effects of vitamin D, which is an important nutrient for metabolism, on health has recently been discovered. It is known that vitamin D affects important biochemical events such as calcium metabolism and absorption. Studies show that vitamin D deficiency is associated with increases in tuberculosis, sclerosis, type 1 diabetes, cardiovascular diseases, rheumatoid arthritis, hypertension and many types of cancer, etc. (Grant & Holick, 2005; McLaren, 2006).

The most important function of this vitamin in metabolism is calcium and phosphorus metabolism and mineralization of bones (Champe et al., 2007; Fariba et al., 2013). Vitamin D especially regulates phosphorus and calcium metabolism in the body. It is an important hormone playing a role in the body's growth, development, and formation of a healthy skeletal structure (Ataş et al., 2008; Kulie et al., 2009). Furthermore, together with parathormone, vitamin D ensures calcium and phosphorus absorption in the body. In this way, it ensures the equilibrium of these elements (Ca and P) in the body. Calcium metal is extremely important for human and animal metabolisms. The need for calcium metal in the body leads to the secretion of parathormone in the metabolism. For this reason, parathormone has a very important role in the regulation of vitamin D metabolism (Hatun et al., 2003). 1,25 dihydroxy vitamin D3 (1,25(OH)2D) is an active metabolite of this vitamin. This metabolite functions in maintaining the plasma calcium level. 1,25 dihydroxy vitamin D3 helps increase Ca absorption in the duodenum and P absorption in the ileum in the body. Moreover, 1,25 dihydroxy vitamin D3 metabolite decreases parathormone synthesis and increases the production of insulin hormone (Öngen et al., 2008).

Recent studies have been conducted on the effects of this vitamin on reproductive health and infertility (Colonese et al., 2015). In particular, it has been reported that vitamin D has different functions in cell proliferation, differentiation, neurotransmission, and neuroplasticity in the nervous system in the body (Eyles et al., 2012).

Vitamin D has been found to have a protective role against many types of cancer (Dadalı, 2010). It has also been proven by studies that it protects the body against significant diseases such as hyperparathyroidism, coronary artery disease, and tuberculosis (Wilkinson et al., 2000; Wang et al., 2008; Talapatra & Tymms, 2010).

5. VITAMIN D DEFICIENCY AND RELATED DISEASES

Vitamin D deficiency in the metabolism has many causes. These are age, indoor environments, covered clothing, genetic factors, kidney and liver diseases, smoking, air pollution, use of sunscreen, physical inactivity, and use of drugs that affect vitamin D metabolism.

Increases were observed in Type I diabetes, multiple sclerosis, rheumatoid arthritis, osteoarthritis, Crohn's disease, various cardiovascular diseases, and many types of cancer associated with the deficiency of this vitamin (Mutlu & Hatun, 2011). It was stated that vitamin D and Ca deficiency led to osteoporosis, in which there was a high probability of weakening and fracture of bones (Fletcher et al., 2002).

It was revealed by studies that the deficiency of this vitamin affected the endocrine functions and inhibited insulin secretion in the rat pancreas (Norman et al., 1980). In another study conducted with rats, it was concluded that the deficiency of this vitamin negatively affected the reproductive capacity of rats (Halloran & Deluca, 1980). It was reported that the deficiency of this vitamin caused rickets in children and osteomalacia in adults (Lane, 2009). It was also concluded that the deficiency of this vitamin leds to high plasma triglycerides and VLDL levels and impaired insulin metabolism in the body (Whayne, 2011).

It is known that vitamin D deficiency in high-risk areas leads to various types of cancer (breast, ovarian, colon, esophageal, and prostate cancer). There is also evidence that the deficiency of this vitamin leads to heart failure. A relationship was determined between vitamin D deficiency and rheumatoid arthritis development (Holick, 2005). Studies have shown that low levels of this vitamin cause an increase in daytime sleepiness in the body (McCarty et al., 2012).

Besides, it was determined that there was an increase in the cases of depression and schizophrenia as the amount of vitamin D in the body decreased. An increase was determined in the cases of both schizophrenia and bipolar disorder in children born in autumn-winter periods, during which the exposure to sunlight in pregnancy was less (McGrath et al., 2002).

6. VITAMIN D EXCESS AND RELATED DISEASES

High amounts of vitamin D intake has a toxic effect. An excess amount of vitamin D leads to an increase especially in serum calcium and phosphate levels. As a result, calcium accumulates in the kidneys and blood vessels. Disorders such as weakness in the muscles, gastrointestinal disorders, and renal dysfunction occur in the body (Ası, 1999). Furthermore, high amounts of vitamin D cause calcification in the joints and soft tissues. A high level of 25 (OH) vitamin D in blood serum leads to increased calcium absorption and severe hypercalcemia. In addition, the symptoms observed as a result of excess vitamin D are related to the effect of hypercalcemia. Studies have reported that calcium causes symptoms such as hypotonia, polyuria, fatigue, polydipsia, restlessness, arrhythmia, nausea, and vomiting, as well as its effects on the heart, kidneys, nerves, digestion, and muscles (Kara et al., 2012; Hatun et al., 2003).

7. METHODS OF QUANTIFYING VITAMIN D AMOUNT

To quantify serum vitamin D levels, 25(OH)D levels are used. This is because the half-life of 25(OH)D metabolite was reported as 2-3 weeks. The 1.25(OH)2D metabolite, which is the biologically active form of vitamin D, is not suitable for quantifying vitamin D levels. This is because the half-life of this metabolite is as short as 4-6 hours. Additionally, it has 1000 times lower activity than the 25(OH)D metabolite (Aksoy, 2000). There are many methods to quantify the 25-OH Vit D metabolite amount in the metabolism. These methods are as follows:

1. Enzyme immunoassay,

2. Competitive protein binding method,

3. Chemiluminescence immunoassay (CLIA),

4. Radioimmunoassay,

5. High performance liquid chromatography (HPLC),

6. Liquid chromatography-tandem mass spectrometry (LC-MS/MS) (Burtis et al., 2012).

Today, LC-MS/MS method is more preferred. The reason this method is more preferred is that it produces more accurate and error-free results with fewer samples. Moreover, with the LC-MS/MS method, the extraction of 25(OH)D2 and 25(OH)D3 vitamins from serum or plasma can be performed and quantitatively measured (Horst & Hollis, 1999; Burtis et al., 2012).

REFERENCES

Aksoy, M. (2000). *Nutritional Biochemistry*. Hatiboğlu Publishing House (3rdEdition), Ankara.

Akşit, S. (2012). *New recommendations for vitamin D deficiency and its prevention*. II. National Social Pediatrics Congress, 7-11 November, Istanbul.

Armas, L. A., Hollis, B. W., & Heaney, R. P. (2004). Vitamin D2 is much less effective than vitamin D3 in humans. *The Journal of Clinical Endocrinology and Metabolism*, *89*, 5387-5391. doi: 10.1210/jc.2004-0360

Ası, T. (1999). *Biochemistry with Tables I-II*, Nobel Medical Bookstore, Ankara.

Ataş, A., Çakmak, A., & Soran M.D. (2008). Vitamin D metabolism and Rickets disease. *Bakirkoy Journal of Medicine*, *4*, 1-7.

Bringhurst, F. R., Demay, M. B., Krane, S. M., & Kronenberg, H. M. (2005). *Bone and Mineral Metabolism in Health and Disease. In: Kasper DL, Braunwald E, Fauci AS, Hauser SL, Longo DL, Jameson JL, editors. Harrison's Principles of Internal Medicine*. 16th edition. New York:MCGraw-Hill Companies, 2238-86.

Bikle, D. D. (2007). What's new in vitamin-D: 2006-2007. *Current Opinion Rheumatology*, *19*(4), 383-388. doi: 10.1097/BOR.0b013e32818e9d58

Bouillon, R. (2011). The vitamin D binding protein DBP. In: Feldman D, Pike JW, Adams JS, editors. *Vitamin D*. 3rd ed. Academic Press; London: p. 57–72.

Burtis, C. A. (2012). Ashwood ER, Bruns DE.*Tietz Textbook of Clinical Chemistry and Molecular Diagnostics (5 thed)*, Saunders Elsevier, USA.

Champe, P.C., Harvey, R.A., & Ferrier, D.R. (2007). *Biochemistry*. Translation Editor:Ulukaya E. Lippincott's Illustrated Review Series 3rd Edition, Nobel Medical Bookstores.

Colonese, F., Laganà, A. S., Colonese, E., Sofo, V., Salmeri, F. M., Granese, R., & Triolo, O. (2015). The pleiotropic effects of vitamin D in gynaecological and obstetric diseases: an overview on a hot topic. *Biomed Res Int., 2015*, 986281. doi: 10.1155/2015/986281

Dadalı, M. (2010). The significance of Vit- D, Lycopen and dietary fat in the prevention of prostate cancer. *Turk Urology Seminars*, *1*,177-182.

Eyles, D. W., Burne, T. H., & McGrath, J. J. (2012). Vitamin D, effects on brain development, adult brain function and the links between low levels of vitamin D and neuropsychiatric disease. *Front Neuroendocrinol, 34*, 47-64. doi: 10.1016/j.yfrne.2012.07.001

Fariba, A., Tharsiya, N., Ronksley, P. E., Suzanne, C., Maeve, O., & Doreen, M. R. (2013). Association between maternal serum 25-hydroxyvitamin D level and pregnancy and neonatal outcomes: systematic review and meta-

analysis of observational studies. *BMJ 26,* 346:f1169. doi: 10.1136/bmj.f1169

Fletcher, R. H., & Fairfield, K. M. (2002). Vitamins for chronic disease prevention in adults: clinical applications. *The Journal of the American Medical Association, 287*(23), 3127-3129. doi: 10.1001/jama.287.23.3127

Glerup, H., Mikkelsen, K., Poulsen, L., Hass, E., Overbeck, S., Thomsen, J., Charles, P., & Eriksen F. (2000). Commonly recommended daily intake of vitamin D is not sufficient if sunlight exposure is limited. *Journal of Internal Medicine*, *247*, 260-268. doi: 10.1046/j.1365-2796.2000.00595.x

Gil, A., Plaza-Diaz, J., & Mesa, M. D. (2018). Vitamin D: Classic and Novel Actions. *Ann Nutr Metab*., *72*(2), 87–95. doi: 10.1159/000486536

Grant, W. B., & Holick, M. F. (2005). Benefits and requirements of vitamin D for optimal health: A review. *Alternative Medicine Review, 10*(2), 94-111.

Göçoğlu, Ş. E. (2010). *Vitamins and Their Effects on Tooth Development*. Ege University Faculty of Dentistry, Department of Pedodontics, Dissertation, İzmir.

Gözükara, E. M. (2011). *Biochemistry*. Fifth Edition, Nobel Medical Bookstores Ltd. Inc., İstanbul.

Gürdöl F., & Ademoğlu E. (2010). Biochemistry. Second edition. Nobel Medical Bookstores Ltd. Inc., İstanbul.

Halloran, B. P., & Deluca, H. F. (1980). Effect of vitamin D deficiency of fertility and reproductive capacity in the female rat. *Journal of Nutrition*, *110*, 1573-1580. doi: 10.1093/jn/110.8.1573

Hatun, Ş., Bereket, A., Çalıkoğlu, A.S., & Özkan, B. (2003). Vitamin D deficiency and rickets today. *Journal of Pediatrics*, *46*, 224-241.

Holick, M. F. (1994). McCollum Award Lecture, 1994: vitamin D--new horizons for the 21st century. *Am J Clin Nutr*., *60*, 619-630. doi: 10.1093/ajcn/60.4.619

Holick, M.F. (2005). The vitamin D epidemic and its health consequences. *The American Journal of Clinical Nutrition, 22*, 2739-2747.

Holick, M. F. (2005). Vitamin D: Important for Prevention of Osteoporosis, Cardiovascular Heart Disease,Type 1 Diabetes,Autoimmune Diseases, and Some Cancers. *South Med J., 98*(10), 1024-1027. doi: 10.1097/01.SMJ.0000140865.32054.DB

Holick, M. F. (2006). High Prevalence of Vitamin D Inadequacy and Implications for Health. *Mayo Clin Proc*., *81*, 353-373. doi: 10.4065/81.3.353

Holick, M. F., Binkley, N. C., Bischoff-Ferrari, H. A., Gordon, M. C., Hanley, D. A., Heaney, R.P., Hassan Murad, M., & Weaver, C. M. (2011). Evaluation, Treatment, and Prevention of Vitamin D Deficiency: an Endocrine Society Clinical Practice Guideline. *J Clin Endocrinol Metab*., *96*, 1911-30. doi: 10.1210/jc.2011-0385

Horst, R. L., & Hollis, B. W. (1999). *Vitamin D assays and their clinical utility*. In: Holick MF, ed. Physiology, Molecular Biology, and Clinical Applications. Totowa, NJ: Humana Press Inc. 239-271.

Kara, S., Yıldırım Baş, F., & Öngel, K.D. (2012). Hypervitaminosis: A case report. *The Journal of Turkish Family Physician*., *16*(2), 93-95. doi:10.2399/tahd.12.093

Kulie, T., Groff, A., Redmer, J., Hounshell, J., & Sch-rager, S. (2009). Vitamin D: an evidence-based review. *J Am Board Fam Med*., *22*, 698-706. doi: 10.3122/jabfm.2009.06.090037

Lane, N. E. (2009). *Metabolic Bone Disease*. In: Firestein GS, Budd RC, Harris ED, Mclnnes IB, Ruddy S, Sergent JS, editors. Textbook of Rheumatoogy Kelley's, Saunders Elsevier; p.1579-1599.

Lavie, C. J., Lee, J. H., & Milani, R. V. (2011). Vitamin D and Cardiovascular Disease Will It Live Up to its Hype? *Journal of the American College of Cardiology*, *58*, 1547-56. doi: 10.1016/j.jacc.2011.07.008

Lerchbaum, E., & Obermayer-Pietsch, B. (2012). Vitamin D and fertility: A systematic review. *Eur J Endocrinol, 166*, 765-78. doi: 10.1530/EJE-11-0984

McCarty, D. E., Reddy, A., Keigley, Q., Kim, P. Y., & Marino, A. A. (2012). Vitamin D, race, and excessive daytime sleepiness. *J Clin Sleep Med*., *8*, 693-697. doi: 10.5664/jcsm.2266

McGrath, J., Selten, J. P., & Chant, D. (2002). Long-term trends in sunshine duration and its association with schizophrenia birth rates and age at first registration data from Australia and the Netherlands. *Schizophr Res*., *54*(3), 199-212. doi: 10.1016/s0920-9964(01)00259-6

McLaren, D. S. (2006). Vitamin D deficiency disorders (VDDD): A global threat to health. *Sight and Life Magazine 3,* 6-15.

Munzuroğlu, Ö., Karataş, F., & Gür, N. (2000). Investigation of A, E, and C vitamins and selenium levels in rhubarb (Rheum ribes L.) plant. *Turkish Journal of Biology*, *24*, 397-404.

Murray, R. K., Granner, D. K., Mayes, P. A., & Rodwell, V. W. (2004). *Harper's Illustrated Biochemistry*. Nobel Medical Bookstores, 25th Edition.

Mutlu, Y. G., & Hatun, Ş. (2011). Perinatal Vitamin D Deficiency. *Journal of Pediatrics*, *54*, 87-98.

Müller, M. J., & Volmer, D. A. (2015). Mass Spectrometric Profiling of Vitamin D Metabolites beyond 25-Hydroxyvitamin D. *Clin Chem*., *61*(8), 1033-1048. doi: 10.1373/clinchem.2015.241430

Norman, A.W., Frankel, J. B., Heldt, A. M., & Grodsky, G. M. (1980). Vitamin D deficiency inhibits pancreatic secretion of insulin. *Science*, *209*, 823-825. doi: 10.1126/science.6250216

Öngen, B., Kabaroğlu, C., & Parıldar, Z. (2008). Biochemical and laboratory evaluation of vitamin D. *Turkish Journal of Clinical Biochemistry*, *6*, 23-31.

Özkan, B., & Döneray, H. (2011). Extraskeletal effects of vitamin D. *Journal of Pediatrics*, *54*, 99-119.

Talapatra, I., & Tymms, D. J. (2010). A case of proximal myopathy resulting from multiple causes. *Europan Journal of General Medicine*, *7*(4), 429-432.

Uitterlinden, A. G., Fang, Y., Van Meurs, J. B. J., Pols, H. A.P., & Van Leeuwen, J. P. T.M. (2004). Genetics and biology of vitamin D receptor polymorphisms. *Gene*, *338*, 143–156. doi:10.1016/j.gene.2004.05.014

Wacker, M., & Holick, M. F. (2013). Vitamin D-Effects on Skeletal and Extraskeletal Health and the Need for Supplementation. *Nutrients*, *5*(1), 111-148. doi.org/10.3390/nu5010111

Wang, T. J., Pencina, M. J., Booth, S. L., Jacques, P. F., Ingelsson, E., Lanier, K., Benjamin, E. J., D'Agostino, R. B., Wolf, M., & Vasan, R. S. (2008). Vitamin D deficiency and risk of cardiovascular disease. *Circulation*, *117*, 503-511. doi: 10.1161/CIRCULATIONAHA.107.706127

Whayne, T. F. (2011). Vitamin D: Popular Cardiovascular Supplement But Benefit Must Be Evaluated. *International Journal of Angiology*, *20* (2), 63-72. doi: 10.1055/s-0031-1279679

Wilkinson, R. J., Llewelyn, M., Toossi, Z., Patel, P., Pasvol, G., Lalvani, A., & Wright, D. (2000). Influence of vitamin D deficiency and vitamin D receptor polymorphisms on tuberculosis among Gujarati Asians in west London: a case-control study. *The Lancet*, *355*, 618-621. doi: 10.1016/S0140-6736(99)02301-6

Chapter 6

BIOACTIVE COMPONENTS AND BIOLOGICAL ACTIVITIES OF THE CARDAMOM (*Elettaria cardamomum* L.) PLANT

Handan SARAC[1]

1 Assistant Professor Handan Sarac, Department of Plant and Animal Production, Sivas Technical Sciences Vocational School, Sivas Cumhuriyet University, Sivas, Turkey. ORCID ID: 0000-0001-7481-7978

1. The Importance of Medicinal and Aromatic Plants

Plants have been used by humans since the existence of humanity to meet many basic needs such as nutrition, shelter, heating, treatment of diseases and still continue to be used with increasing interest (Bayram et al., 2010; Faydaoglu and Surucuoglu, 2011; Sevindik et al., 2017; Mohammed et al., 2018; Goktas and Gidik, 2019). Medicinal and aromatic plants, which do not yet have a standard classification among the plants, but represent an important group in terms of health, are used to prevent or treat diseases, to ensure the continuity of health, and to give a pleasant smell, aroma or flavor (Bayram et al., 2010; Pehlivan et al., 2018; Mohammed et al., 2019a). Today, medicinal and aromatic plants, which have a wide range of uses, are utilized in many areas such as food, cosmetics, paint, textile, medicine and agriculture. The demand, interest and usage rate of these plants varies according to the development level of the countries (Acibuca and Budak, 2018; Goktas and Gidik, 2019). Traditional, complementary and alternative medicine, in which medicinal and aromatic plants are used, is preferred more in developing countries than in developed countries. However, it is seen that the interest in medicinal and aromatic plants and the use rate of herbal origin drugs have increased in developed countries in recent years (Besen and Beji, 2014; Bayram et al., 2010; Acibuca and Budak, 2018; Mohammed et al., 2019b; Akgül et al., 2020). Compared to the 1930s and 1940s, when the production and use of synthetic drugs worldwide peaked, the increase in demand for natural products in developed countries towards the end of the 20th century led to the fact that both herbal medicines and medicinal and aromatic plants became important (Bayram et al., 2010; Mohammed et al., 2020). In this case, it can be said that the demand for medicinal and aromatic plants in the world market has increased (Bayram et al., 2010; Goktas and Gidik, 2019). As a matter of fact, it is estimated that the medicinal and aromatic plants market has reached an annual figure of approximately 100 billion dollars (Acibuca and Budak, 2018; Mohammed et al., 2021).

Today, it has become necessary to discover natural bioactive compounds and to create natural and alternative treatment opportunities from these compounds, due to reasons such as the fact that synthetic drugs and various treatment methods used in the treatment of human-specific diseases cause serious side effects and are costly (Akgül et al., 2017; Korkmaz et al., 2018; Bal et al., 2019; Goktas and Gidik, 2019; Sarac et al., 2019; Ashokkumar et al., 2020). The raw material of the developed herbal drugs is usually obtained from medicinal plants (Faydaoglu and Surucuoglu, 2011). Medicinal plants have a large number of components with different bioactivities that can affect animal metabolism or physiology. Therefore, medicinal plants are an important resource for the discovery of

new alternatives and bioactive molecules in drug development studies for various diseases (Sarac et al., 2018). In a study conducted by the World Health Organization (WHO) on 91 countries, it was reported that the medicinal plants used for treatment are around 20,000 in total, and about 500 of them are cultivated and produced (Benli and Yiğit, 2005; Bayram et al., 2010; Faydaoglu and Surucuoglu, 2011; Sarac et al., 2018).

In the studies carried out so far, it has been determined that many medicinal plants, especially the plants used traditionally among the people, and the extracts obtained from these plants have beneficial biological activities and therapeutic effects (Khalaf et al., 2008; Yucel et al., 2012; Sarac et al., 2019).

2. General Characteristics of Cardamom (*Elettaria cardamomum* L.) Plant

Elettaria cardamomum L., which originates from South Asia, is a perennial, rhizomatous herbaceous plant species belongs to the Zingiberaceae family that can grow up to 2-5 m (Akgul, 1993; El Malti et al., 2007; Rajan et al., 2017; Ashokkumar et al., 2020). The leaves, which are lanceolate, green or dark green and glabrous, are about 30-35 cm long and 7-10 cm wide. Its flowers are white. Approximately 120 days after flowering, triangular, oval, capsule type fruits are formed. Initially green, the fruit turns a golden yellow or brownish color when ripe. Each capsule contains about 12 to 32 seeds, depending on the genotype. It is commonly known by the names small, green or true cardamom (Akgul, 1993; Agaoglu et al., 2006; Rajan et al., 2017; Ashokkumar et al., 2020).

Figure 1. *Capsule fruits and seeds of E. cardamomum plant*

It is cultivated mostly in southern India, Sri Lanka, Tanzania, Nepal, Indonesia, Malaysia, Costa Rica, Mexico and Guatemala (El Malti et al., 2007; Ashokkumar et al., 2020; Souissi et al., 2020). It is also known in Morocco as the producer of cardamom used in cooking (El Malti et al., 2007; Singh et al., 2008). In southern India, where its cultivation is most intense, it is cultivated at an altitude of 900 to 1400 m and there are Cardamom Hill Reserves for cardamom cultivation, covering an area of 1050 square kilometers (Ashokkumar et al., 2020).

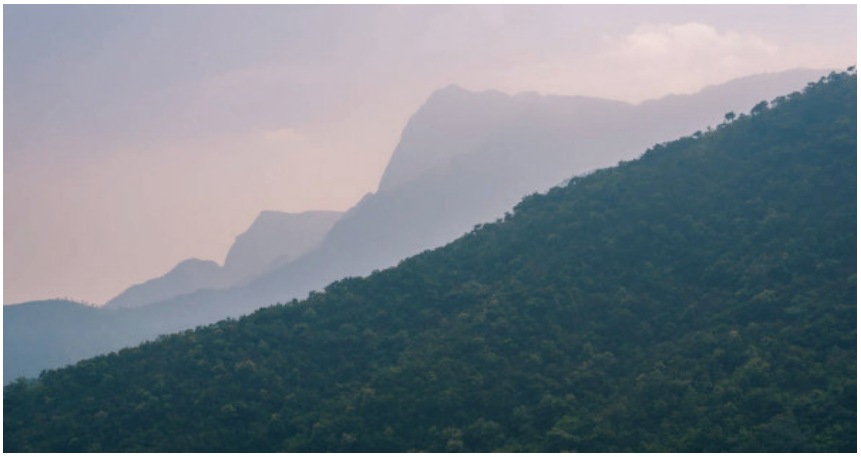

Figure 2. *An image of Cardamom Hills in India*

The use of the cardamom plant by humans dates back to the fourth century BC and is still used for various purposes today (Korikanthimathm et al., 2000). Commonly used parts of the plant are the capsule fruits and seeds. Its seeds, which are ground into powder, are used as a spice in various dishes, especially meat dishes, in many countries. It is one of the most widely used spices in Moroccan cuisine, especially to flavor Moroccan tajines. In addition, in India, which is known as the world's largest producer, consumer and exporter of spices, cardamom spice has

been used frequently since ancient times and is known as the “Queen of all Spices” (Korikanthimathm et al., 2000; El Malti et al., 2007). It is the third most expensive spice after saffron and vanilla (Paniagua-Zambrana et al., 2020). Due to its distinctive sharp aroma and pleasant flavor, there is also a cardamom coffee variety among the flavored coffee varieties (Karaca et al., 2005). Cardamom coffee, which is called “gawah” in Arab culture, is a popular coffee variety because it reduces the caffeine content in coffee and is good for headaches and stress (Ashokkumar et al., 2020).

The essential oil obtained from its seeds has a wide range of uses. It is used in products such as alcoholic and non-alcoholic beverages, frozen desserts, bakery products, puddings, sauces, etc. in the food sector, and in perfumes, lotions, soaps, detergents and massage oils due to its strong aphrodisiac and antiseptic effect (Ravindran, 2002; El Malti et al., 2007; Singh et al., 2008; Ashokkumar et al., 2020).

It is known that the cardamom plant is used traditionally in the treatment of various diseases, as well as the use of flavor and aroma. It is used in traditional Chinese and Indian medicine to relieve intestinal gas problems and various digestive problems (Ravindran, 2002; El Malti et al., 2007). In fact, it is stated in the literature that it has positive effects on fertility as it plays a role in genital system secretion (Besen and Beji, 2014). Capsule type fruits are traditionally used in the treatment of diseases such as asthma, gum infections, cataracts, heart and kidney diseases, diarrhea and constipation. In addition, it is known that the drink made from cardamom powder is an antidote for snake and scorpion venom, its capsules have an effect on inflammation and headache, and it is also used in the treatment of epilepsy. It has a high potential for use as pharmaceutical and nutraceutical thanks to various bioactive substances found in its fruits, seeds and especially its essential oil (Karaca et al., 2005; Ashokkumar et al., 2020). Phytochemical analyzes showed that cardamom plant has important components such as carbohydrates, proteins, lipids, minerals, essential oils, flavonoids, terpenoids, alkaloids, tannins, anthocyanins and carotenoids in its chemical composition (Khatri et al., 2017; Noumi et al., 2018; Souissi et al., 2020; Ashokkumar et al., 2020). Although the essential oil content of the plant, which is widely used, varies depending on environmental factors such as soil conditions, climate difference and altitude, it contains mainly monoterpene group components (Singh et al., 2008; Savan and Kucukbay, 2013; Ashokkumar et al., 2019; Jena et al., 2021).

Table 1. *The major components in E. cardamomum plant*

Compound	Composition	Part of Plant	References
Carbohydrates (%)	68.2	Fruits	Sontakke et al. (2018); Ashokkumar et al. (2020)
Protein (%)	10.6	Fruits	Sontakke et al. (2018); Ashokkumar et al. (2020)
Lipid (%)	2.4	Fruits	Sontakke et al. (2018); Ashokkumar et al. (2020)
Ash (%)	6.72	Seeds	Abera et al. (2019)
Oleoresin (%)	10.025	Seeds	Abera et al. (2019)
Essential oil (%)	8.01	Seeds	Abera et al. (2019)
Total Flavanoids (µg/g)	314.0	Fruits	Ashokkumar et al. (2019)
Minerals (mg/100g)			
Calcium (Ca)	109.87	Seeds	Abera et al. (2019)
Potassium (K)	843.28	Seeds	Abera et al. (2019)
Phosphorus (P)	151.29	Seeds	Abera et al. (2019)
Iron (Fe)	11.66	Seeds	Abera et al. (2019)
Magnesium (Mg)	102.76	Seeds	Abera et al. (2019)
Manganese (Mn)	29.32	Seeds	Abera et al. (2019)
Zinc (Zn)	1.57	Seeds	Abera et al. (2019)
Sulfur (S)	37.14	Seeds	Abera et al. (2019)

Table 2. *The main components in the essential oil of E. cardamomum plant*

Compound	Composition (%)	References
α-terpinyl acetate	44.3-40.7	Singh et al. (2008); Savan and Kucukbay (2013)
1,8-cineole	10.7-30.4	Singh et al. (2008); Savan and Kucukbay (2013); Chegini and Abbasipour (2017)
α-terpineol	9.8-14.89	Singh et al. (2008); Ashokkumar et al. (2019)
linalool	8.6- 6.4	Singh et al. (2008); Savan and Kucukbay (2013)
sabinene	2.1-13.50	Savan and Kucukbay (2013); Ashokkumar et al. (2019)
α-pinene	1.15-2.42	Ashokkumar et al. (2019)
nerol	3.69-6.10	Ashokkumar et al. (2019)

3. Biological Activity and Therapeutic Effects of Cardamom (*E. cardamomum* L.) Plant

Various bioactivity properties of cardamom plant, which is rich in bioactive components, have been studied to reveal its medicinal effects and the traditional use of the plant has been scientifically supported. The biological activity studies of the cardamom plant have mostly been on the determination of the antioxidant, antimicrobial, antiinflammatory, antidiabetic and anticancer effects of the plant. Among these, it is seen that there are more studies on antimicrobial activity in the literature.

3.1. **Antimicrobial Activity**

Compounds with antimicrobial effects are mostly found in the essential oil of plants (Faydaoglu and Surucuoglu, 2013). For this reason, studies investigating the antimicrobial effect of the cardamom plant were generally carried out using the essential oil extract of the plant or various extracts of the fruit and seeds with high essential oil content. It has been shown by various in vitro studies that most of these extracts inhibit some important pathogenic microorganisms such as *Escherichia coli, Staphylococcus aureus, Bacillus cereus* and have antimicrobial effects (Kubo et al. 1991; Singh et al., 2008; Ozkan et al., 2018). In one of these studies, cardamom essential oil was tested on a variety of pathogenic and multi-antibiotic resistant bacteria, and the essential oil extract of the plant was found to be very effective in inhibiting the growth in the majority of the pathogenic strains (El Malti et al., 2007). In another study in which the antibacterial effect of extracts obtained from the fruit and seeds of the cardamom plant was determined, it was reported that both fruit and seed extracts were effective against *Aggregatibacter actinomycetemcomitans, Fusobacterium nucleatum, Porphyromonas gingivalis*, and *Prevotella intermedia* microorganisms (Souissi et al., 2020). In a different study investigating the antibacterial effect as well as the antifungal effect of the cardamom plant, it was determined that 3000 ppm doses the essential oil of and methanol, ethanol, chloroform and diethyl ether oleoresins of the plant had a wide spectrum of antimicrobial activity against *Aspergillus terreus* (MTCC 3374), *Fusarium graminearum* (MTCC 2088), *Penicillium purpurogenum* (MTCC 1786) and *Penicillium madriti* (MTCC 3003) fungi strains and various gram positive (*S. aureus* (MTCC 3103) and *B. cereus* (MTCC 430)) and negative (*E. coli* (MTCC 1672) and *Salmonella typhi* (MTCC 733)) bacterial strains (Singh et al., 2008). In a similar study, the antimicrobial effect of water, ethanol, methanol, ethyl acetate and hexane extracts of the dried fruits of the cardamom plant was studied by a total of six gram positive and gram negative bacterial strains (*E. coli* MTCC-739, *S. typhi* MTCC-531, *B. cereus* MTCC-430, *Bacillus subtilis* MTCC-736, *Streptococcus pyogenes* MTCC-442, and *S. aureus* MTCC-740). As a result of the study, it was determined that water and ethanol extract had an inhibitory effect on all tested bacteria, but the activity in the water extract was higher. In addition, it was determined that ethyl acetate extract was effective against all microflora except *S. typhi* strain, methanol extract was effective only against *S. aureus* and *E. coli*, and hexane extract was completely ineffective against all test microorganisms (Kaushik et al., 2010). In another study conducted in previous years, some pathogens that cause food poisoning and various diseases in humans and strains that cause food spoilage were selected as test microorganisms, and it was found that

the diethyl ether extract obtained from cardamom seeds showed different levels of inhibitory activity on *Mycobacterium smegmatis, Klebsiella pneumoniae, S. aureus, E. coli, Enterococcus faecalis, Micrococcus luteus* and *Candida albicans,* except for *Pseudomonas aeruginosa.* In addition, it was detected that the most sensitive strain to cardamom seed extract was *S. aureus* (Agaoglu et al., 2006). Due to the traditional use of cardamom in the treatment of dental diseases, researchers have focused on investigating the effect of cardamom extracts against various microorganisms that cause dental caries or periodontal diseases. In most studies conducted for this purpose, it has been concluded that cardamom extracts can be a potential source of new antimicrobial agents in the treatment of microbial-induced dental problems (Aneja and Joshi, 2009; Souissi et al., 2020). As a result of these studies, it is clear that the essential oil extract and different extracts of the cardamom plant have a strong antimicrobial effect on both gram negative or gram positive bacteria and fungi strains. Considering that plants with antimicrobial activity are used for therapeutic purposes, as well as as food preservatives, anthelmintic and antifungal against plant pests (Faydaoglu and Surucuoglu, 2011), the importance of the cardamom plant, which has a strong antimicrobial effect emerges. It is estimated that the broad-spectrum antimicrobial activity of the cardamom plant may provide an important resource for new antimicrobial treatments and potentially be used in the treatment of many diseases caused by microorganisms showing antibiotic resistance.

3.2. Antioxidant Activity

Antioxidants are systems that destroy the negative effects of free radicals (Faydaoglu and Surucuoglu, 2011; Sevindik et al., 2016; Bal et al., 2017; Celik and Ayran, 2020). The antioxidant potential of a plant depends on the presence of components such as ascorbic acid, carotenoid, anthocyanin and tocopherol, primarily phenolic compounds such as flavonoids and phenolic acids (Khalaf et al., 2008; Sarac et al., 2018; Sarac et al., 2021). Many biological activity properties such as antimutagenic, anticarcinogenic, antiaging, antimicrobial, antiviral, antiallergic are also based on antioxidant compounds (Sarac et al., 2018; Sevindik et al., 2018; Mohammed et al., 2020; Sarac et al., 2021). Cardamom fruits or seeds are very rich in antioxidant substance content that neutralizes free radicals and prevents oxidation at the initial stage. In a study, it was determined that the cardamom essential oil extract and methanol, ethanol, chloroform and diethyl ether oleoresins have significant antioxidant capacity (Singh et al., 2008). In another study investigating the antioxidant activity of methanol extract of some important plants, including *E. cardamomum*, it was determined that the cardamom plant showed a moderate antioxidant activity (Khalaf et al., 2008). In a study investigating both antioxidant and

antidiabetic properties of methanol and water extracts of cardamom fruits, it was determined that water and methanol extract of the plant exhibited in vitro antidiabetic and antioxidant activities. In addition, it was detected that the water extract exhibited better activity among the extracts (Ahmed et al., 2017). In a similar study with water extract of cardamom fruits, it was determined that the plant exhibits antioxidant, antiobesity and antidiabetic activities (Al-Yousef et al., 2021). Furthermore, studies on diabetic rats have found that various cardamom extracts improve impaired hippocampal functions such as learning and memory, and have the potential to lower blood sugar and cholesterol (Winarsi et al., 2014; Gomaa et al., 2019). Among the purposes of use of antioxidant-based drugs are the prevention or treatment of important diseases such as Alzheimer's, stroke and diabetes, which can develop due to oxidative or cellular damage caused by free radicals (Khalaf et al., 2008; Ahmed et al., 2017). Due to the thought that synthetic antioxidants used today are not reliable, important studies are carried out on obtaining natural antioxidants from medicinal and aromatic plants (Faydaoglu and Surucuoglu, 2011; Celik and Ayran, 2020). In this respect, it is predicted that it is possible to develop new and natural antioxidative drug formulations from the cardamom plant, which has a high antioxidant potential, as an alternative to synthetic antioxidants for the future.

3.3. **Anti-inflammatory Activity**

In the literature review, various studies have been found to reveal the anti-inflammatory activity of the cardamom plant. In a study investigating the anti-inflammatory activity of cardamom essential oil on rats, it was determined that cardamom essential oil extract showed anti-inflammatory activity in a model of acute right paw inflammation induced by lambda-carrageenan in rats. In addition, it was determined that the anti-inflammatory effect of cardamom essential oil at a dose of 0.10 mL/kg was close to indomethacin, which was determined as the reference drug in the study (Karaca et al., 2005). In a similar study, it has been reported that 1,8-cineole found in the essential oil of the cardamom plant has an anti-inflammatory potential against inflammatory airway diseases such as asthma and chronic obstructive pulmonary disease (Juergens, 2014). In other studies, it is thought that the anti-inflammatory effect of cardamom plant is largely due to this component. Furthermore, α-pinene, one of the major components of cardamom essential oil, has been reported in some studies to have a gastric protective effect and therefore the cardamom plant has gastro-protective activity. (Polo et al., 2012; Ashokkumar et al., 2019).

3.4. Anticancer Activity

There have been several studies showing that cardamom extracts significantly increase the cytotoxic activity of natural killer cells and have a strong cytotoxic activity in cancer cells. One of these studies predicted that the cardamom plant has a potential anticancer effect and can be used as a potential therapeutic means to prevent or weaken carcinogenesis (Majdalawieh and Carr, 2010). In another study, it was found that nanoparticles synthesized from cardamom plant have a high cytotoxic effect on Human Cervical Carcinoma (HeLa) cell line (Rajan et al., 2017). In a similar study, it was determined that silver nanoparticles synthesized from cardamom seed extract exhibited significant anticarcinogenic activity on Human Larynx Carcinoma (Hep-2) cancer cells (Krishnan et al., 2015). In a different study investigating the chemoprotective effect of cardamom, results supporting the the chemopreventive anticancer effect of cardamom were obtained. The study revealed that cardamom extract can serve as an apoptotic stimulating agent, offer a new and potentially curative effect for cancer therapy, and have fewer side effects than commercially used anticancer drugs (Elguindy et al., 2016). Today, 63% of cancer drugs are derived from plants, and studies show that herbal drugs have few side effects and a high success rate in treatment (Sarac et al., 2018). Therefore, researching plants with the potential for anticancerogen effects such as cardamom will lead to promising important developments in cancer treatment.

3.5. Insecticidal Activity

Although it is known that cardamom essential oil has insecticidal activity in addition to many bioactivity properties, very few studies have been carried out on this subject. One of these studies found that cardamom essential oil has a toxic effect against tomato leaf miner, *Tuta absoluta* insect pests, one of the most important pests of the Solanaceae family in the World (Chegini and Abbasipour, 2017). The use of cardamom essential oil as a natural insecticide that is not harmful to health and does not cause pollution by accumulating in the soil will provide an important advantage for both the environment, health and farmers (Ashokkumar et al., 2020).

4. Conclusion

In this review, general information about the bioactive components, biological activity and therapeutic effects of Cardamom (*E. cardamomum*) plant and scientific studies on this subject are presented. Today, due to health problems and concerns caused by synthetic products, people have started to look for the remedy in natural products. Assuming that we live in a world where everything that is natural is preferred, natural methods and products should be used in such matters as prevention or treatment of

diseases. In this respect, it is important to investigate and scientifically support the causes of traditional use of medicinal plants, which constitute a resource rich in bioactive compounds in nature, to identify their active ingredients and to develop drugs for the future from these substances. (Sarac et al., 2019). Cardamom, one of these plants, has been used by humans for centuries both as a functional food with its smell, flavor and nutritional quality, and in the treatment of various diseases due to its medicinal effects. Many scientific studies have shown that bioactive phytochemicals found in the structure of the cardamom plant have antioxidant, antimicrobial, antidiabetic, anticancer, gastro-protective and insecticidal activities. In these studies, it is noted that biological activities of the plant, especially in the extract of essential oil and water, are high. However, it is seen in the literature that the toxicity data and in vivo studies of the cardamom plant are inadequate. With the contribution of such scientific studies, it is thought that cardamom plant can benefit significantly in the fields of medicine, pharmacy and agriculture.

References

Abera, S., Gezahegn, B. and Hirko, B. (2019). Nutritional composition of Cardamom (*Elettaria cardamomum)* seed cultivated in Ethiopia. *International Journal of Modern Pharmaceutical Research, 3*(5), 50-53.

Acibuca, V. and Budak, D. B. (2018). Place and importance of medicinal and aromatic plants in the world and Turkey. *Çukurova Journal of Agricultural and Food Sciences, 33*(1), 37-44.

Agaoglu, S., Dostbil, N. and Alemdar, S. (2006). Antimicrobial effect of seed extract of cardamom (*Elettaria cardamomum* Maton). *YÜ Vet Fak Derg*, *16*(2), 99-101.

Ahmed, A. S., Ahmed, Q. U., Saxena, A. K. and Jamal, P. (2017). Evaluation of in vitro antidiabetic and antioxidant characterizations of *Elettaria cardamomum* (L.) Maton (Zingiberaceae), *Piper cubeba* L. f.(Piperaceae), and *Plumeria rubra* L.(Apocynaceae). *Pakistan Journal of Pharmaceutical Sciences*, *30*(1), 113-126.

Akgul A. (1993). *Baharat Bilimi & Teknolojisi (1st ed.)*. Ankara: Gıda Teknolojisi Derneği Yayınları.

Akgul, H., Korkmaz, N., Dayangaç, A. and Sevindik, M. (2020). Antioxidant potential of endemic *Salvia absconditiflora. Turkish Journal of Agriculture-Food Science and Technology, 8*(10), 2222-2224.

Akgul, H., Sevindik, M., Coban, C., Alli, H. and Selamoglu, Z. (2017). New approaches in traditional and complementary alternative medicine practices: *Auricularia auricula* and *Trametes versicolor*. *J Tradit Med Clin Natur, 6*(2), 239.

Akgül, H., Nur, A. D., Sevindik, M., & Doğan, M. (2016). *Tricholoma terreum* ve *Coprinus micaceus*' un bazı biyolojik aktivitelerinin belirlenmesi. *Artvin Çoruh Üniversitesi Orman Fakültesi Dergisi, 17*(2), 158-162.

Al-Yousef, H. M., Alqahtani, A. S., Hassan, W. H., Alzoubi, A. and Abdelaziz, S. (2021). Chemical profile, in vitro antioxidant, pancreatic lipase, and alpha-amylase inhibition assays of the aqueous extract of *Elettaria cardamomum* L. fruits. *Journal of Chemistry*. https://doi.org/10.1155/2021/5583001.

Aneja, K. R. and Joshi, R. (2009). Antimicrobial activity of *Amomum subulatum* and *Elettaria cardamomum* against dental caries causing microorganisms. *Ethnobotanical Leaflets, 13,* 840-49.

Ashokkumar, K., Murugan, M., Dhanya, M.K., Surya, R. and Kamaraj, D. (2019). Phytochemical variations among four distinct varieties of Indian cardamom *Elettaria cardamomum* (L.) Maton. *Natural Product Research, 34*(13), 1919-1922.

Ashokkumar, K., Murugan, M., Dhanya, M. K. and Warkentin, T. D. (2020). Botany, traditional uses, phytochemistry and biological activities of

cardamom [*Elettaria cardamomum* (L.) Maton]–A critical review. *Journal of Ethnopharmacology*, *246*, 112244.

Bal, C., Sevindik, M., Akgul, H. and Selamoglu, Z. (2019). Oxidative stress index and antioxidant capacity of *Lepista nuda* collected from Gaziantep/ Turkey. *Sigma, 37*(1), 1-5.

Bal, C., Akgul, H., Sevindik, M., Akata, I. and Yumrutas, O. (2017). Determination of the anti-oxidative activities of six mushrooms. *Fresenius Envir Bull, 26*(10), 6246-6252.

Bayram, E., Kirici, S., Tansi, S., Yilmaz, G., Kizil, O. A. S. and Telci, İ. (2010). Tibbi ve aromatik bitkiler üretiminin arttirilmasi olanaklari. *TMMOB Ziraat Mühendisleri Odasi, Ziraat Mühendisligi VII. Teknik Kongresi*, 11-15.

Benli, M. and Yigit, N. (2005). Ülkemizde yaygın kullanımı olan Kekik (*Thymus vulgaris*) bitkisinin antimikrobiyal aktivitesi. *Orlab On-Line Mikrobiyoloji Dergisi*, *3*(8), 1-8.

Besen, Ö. G. M. A. and Beji, N. K. (2014). Fertilite ve bitkiler. *Andrology Bulletin*, *59*, 286-289.

Celik, S. A. and Ayran, I. (2020). Some medicinal and aromatic plants as antioxidant sources. *Turkish Journal of Scientific Reviews*, *13*(2), 115-125.

Chegini, S. G. and Abbasipour, H. (2017). Chemical composition and insecticidal effects of the essential oil of cardamom, *Elettaria cardamomum* on the tomato leaf miner, *Tuta absoluta*. *Toxin reviews*, *36*(1), 12-17.

Elguindy, N. M., Yacout, G. A., El Azab, E. F. and Maghraby, H. K. (2016). Chemoprotective effect of *Elettaria cardamomum* against chemically induced hepatocellular carcinoma in rats by inhibiting NF-κB, oxidative stress, and activity of ornithine decarboxylase. *South African journal of botany*, *105*, 251-258.

El Malti, J., Mountassif, D. and Amarouch, H. (2007). Antimicrobial activity of *Elettaria cardamomum*: Toxicity, biochemical and histological studies. *Food chemistry*, *104*(4), 1560-1568.

Faydaoglu, E. and Surucuoglu, M. S. (2011). History of the use of medical and aromatic plants and their economic importance. *Kastamonu University Journal of Forestry Faculty*, *11*(1), 52-67.

Faydaoglu, E. and Surucuoglu, M. S. (2013). Medical and aromatic plants' antimicrobial, antioxidant activities and use opportunities. *Erzincan University Journal of Science and Technology, 6*(2), 233-265.

Goktas, Ö. and Gidik, B. (2019). Uses of medicinal and aromatic plants. *Bayburt University Journal of Science*, *2*(1), 145-151.

Gomaa, A. A., Makboul, R. M., El-Mokhtar, M. A., Abdel-Rahman, E. A., Ahmed, I. A. and Nicola, M. A. (2019). Terpenoid-rich *Elettaria cardamomum* extract prevents Alzheimer-like alterations induced in diabetic rats via

inhibition of GSK3β activity, oxidative stress and pro-inflammatory cytokines. *Cytokine*, *113*, 405-416.

Jena, S., Ray, A., Sahoo, A., Champati, B. B., Padhiari, B. M., Dash, B., ... Panda, P. C. (2021). Chemical composition and antioxidant activities of essential oil from leaf and stem of *Elettaria cardamomum* from Eastern India. *Journal of Essential Oil Bearing Plants*, 1-9.

Juergens, U. R. (2014). Anti-inflammatory properties of the monoterpene 1.8-cineole: current evidence for co-medication in inflammatory airway diseases. *Drug research*, *64*(12), 638-646.

Karaca, M., Tutuncu, M., Aydin, H. İ. M., Akkan, H. A. and Ozbek, H. (2005). Antiinflammatuar effect of *Eletteria cardamom* L. essential oil extract in rats. *The Journal of The Faculty of Veterinary Medicine University of Yuzuncu Yil*, *16*(2), 27-30.

Kaushik, P., Goyal, P., Chauhan, A. and Chauhan, G. (2010). In vitro evaluation of antibacterial potential of dry fruit extracts of *Elettaria cardamomum* Maton (Chhoti Elaichi). *Iranian journal of pharmaceutical research: IJPR*, *9*(3), 287.

Khalaf, N. A., Shakya, A. K., Al-Othman, A., El-Agbar, Z. and Farah, H. (2008). Antioxidant activity of some common plants. *Turkish Journal of Biology*, *32*(1), 51-55.

Khatri, P., Rana, J. S., Jamdagni, P. and Sindhu, A. (2017). Phytochemical screening, GC-MS and FT-IR analysis of methanolic extract leaves of *Elettaria cardamomum*. *International Journal of Research-Granthaalayah*, *5*(2), 213-224.

Korikanthimathm, V. S., Prasath, D. and Rao, G. (2000). Medicinal properties of cardamom *Elettaria cardamomum*. *Journal of Medicinal and Aromatic Plant Sciences*, *22*, 683-685.

Korkmaz, A. I., Akgul, H., Sevindik, M. and Selamoglu, Z. (2018). Study on determination of bioactive potentials of certain lichens. *Acta Alimentaria, 47*(1), 80-87.

Krishnan, V., Kalyanaraman, R., Fathima, G., Sheriff, K., Illiyas, M., Rather, H. A., ... Krishnan, T. (2015). Green biosynthesis of silver nanoparticles from *Elettaria cardamomum* (Seed) and its in vitro cytotoxic activity. *World Journal of Pharmacy and Pharmaceutical Sciences, 4*(4), 723-733.

Kubo, I., Himejima, M. and Muroi, H. (1991). Antimicrobial activity of flavor components of cardamom *Elettaria cardamomum* (Zingiberaceae) seed. *Journal of agricultural and food chemistry*, *39*(11), 1984-1986.

Majdalawieh, A. F. and Carr, R. I. (2010). In vitro investigation of the potential immunomodulatory and anti-cancer activities of black pepper (*Piper nigrum*) and cardamom (*Elettaria cardamomum*). *Journal of Medicinal Food*, *13*(2), 371-381.

Mohammed, F. S., Sabik, A. E., Sevindik, E., Pehlivan, M. and Sevindik, M. (2020). Determination of antioxidant and oxidant potentials of *Thymbra spicata* collected from Duhok-Iraq. *Turkish Journal of Agriculture-Food Science and Technology, 8*(5), 1171-1173.

Mohammed, F. S., Akgul, H., Sevindik, M. and Khaled, B. M. T. (2018). Phenolic content and biological activities of *Rhus coriaria* var. zebaria. *Fresenius Environmental Bulletin, 27*(8), 5694-5702.

Mohammed, F. S., Karakaş, M., Akgül, H. and Sevindik, M. (2019a). Medicinal properties of *Allium calocephalum* collected from Gara Mountain (Iraq). *Fresen Environ Bull, 28*(10), 7419-7426.

Mohammed, F. S., Sevindik, M., Bal, C., Akgül, H. and Selamoglu, Z. (2019b). Biological Activities of *Adiantum capillus-veneris* Collected from Duhok Province (Iraq). *Communications Faculty of Sciences University of Ankara Series C Biology, 28*(2), 128-142.

Mohammed, F. S., Pehlivan, M., Sevindik, E., Akgul, H., Sevindik, M., Bozgeyik, I. and Yumrutas, O. (2021). Pharmacological properties of edible Asparagus acutifolius and Asparagus officinalis collected from North Iraq and Turkey (Hatay). *Acta Alimentaria, 50*(1), 136-143.

Mohammed, F. S., Günal, S., Pehlivan, M., Doğan, M., Sevindik, M. and Akgül, H. (2020). Phenolic content, antioxidant and antimicrobial potential of endemic *Ferulago platycarpa. Gazi University Journal of Science, 33*(4), 670-677.

Noumi, E., Snoussi, M., Alreshidi, M. M., Rekha, P. D., Saptami, K., Caputo, L., ... De Feo, V. (2018). Chemical and biological evaluation of essential oils from cardamom species. *Molecules*, *23*(11), 2818.

Ozkan, O. E., Olgun, C., Guney, B., Mahmut, G., Guney, K. and Ateş, S. (2018). Chemical composition and antimicrobial activity of Myristica fragrans & Elettaria cardamomum essential oil. *Kastamonu University Journal of Forestry Faculty*, *18*(2), 225-229.

Paniagua-Zambrana, N. Y., Bussmann, R. W. and Romero, C. (2020). *Elatteria cardamomum* (L.) Maton Zingiberaceae. *Ethnobotany of the Andes*, 1-3.

Pehlivan, M., Mohammed, F. S., Sevindik, M. and Akgul, H. (2018). Antioxidant and oxidant potential of *Rosa canina*. *Eurasian Journal of Forest Science, 6*(4), 22-25.

Polo, C. M., Moraes, T. M., Pellizzon, C. H., Marques, M. O., Rocha, L. R. M. and Hiruma-Lima, C. A. (2012). Gastric ulcers in middle-aged rats: The healing effect of essential oil from *Citrus aurantium* L.(Rutaceae). *Evidence-Based Complementary and Alternative Medicine*, *2012*. *doi:10.1155/2012/509451*.

Rajan, A., Rajan, A. R. and Philip, D. (2017). *Elettaria cardamomum* seed mediated rapid synthesis of gold nanoparticles and its biological activities. *OpenNano, 2*, 1-8.

Ravindran, M. K. (Ed.). (2002). Cardamom: the genus *Elettaria*. New York: Taylor and Francis.

Sarac, H., Dastan, T., Demirbas, A., Dastan, S. D., Karakoy, T. and Durukan, H. (2018). Nutrient composition and in vitro anti-carcinogenic activity of Knotweed (*Polygonum cognatum* Meissn.) plant extracts. *Ziraat Fakültesi Dergisi, 1st International Congress on Agricultural Structures and Irrigarion Special Print*, 340-347.

Sarac, H., Demirbas, A., Dastan, S. D., Atas, M., Çevik, Ö. and Eruygur, N. (2019). Evaluation of nutrients and biological activities of Kenger (*Gundellia tournefortii* L.) seeds cultivated in Sivas province. *Turkish Journal of Agriculture-Food Science and Technology*, *7*(sp2), 52-58.

Sarac, H., Durukan, H. and Demirbas, A. (2021). Nutrient Concentrations and Antioxidant Activity of *Achillea millefolium* L. (Yarrow), One of the Important Medicinal Plants. *Turkish Journal of Agriculture-Food Science and Technology*, *9*(3), 590-594.

Savan, E. K. and Kucukbay, F. Z. (2013). Essential oil composition of *Elettaria cardamomum* Maton. *Journal of Applied Biological Sciences*, *7*(3), 42-45.

Sevindik, M., Akgul, H., Dogan, M., Akata, I. and Selamoglu, Z. 2018. Determination of antioxidant, antimicrobial, DNA protective activity and heavy metals content of *Laetiporus sulphureus*. *Fresenius Environmental Bulletin, 27*(3), 1946-1952.

Sevindik, M., Akgul, H., Pehlivan, M. and Selamoglu, Z. (2017). Determination of therapeutic potential of *Mentha longifolia* ssp. *longifolia*. *Fresen Environ Bull, 26*(7), 4757-4763.

Sevindik, M., Akgul, H., Selamoglu, Z., & Braidy, N. (2020). Antioxidant and antigenotoxic potential of *Infundibulicybe geotropa* mushroom collected from Northwestern Turkey. *Oxidative medicine and cellular longevity, 2020. doi:10.1155/2020/5620484*.

Sevindik, M., Akgül, H., Akata, I., Altuntaş, D., Bal, C. and Doğan, M. (2016). *Macrolepiota procera* (Scop.) Singer. Mantarının Ağır Metal İçeriklerinin ve Oksidatif Stres Durumunun Belirlenmesi. *Süleyman Demirel Üniversitesi Fen Bilimleri Enstitüsü Dergisi, 20*(3), 504-508.

Singh, G., Kiran, S., Marimuthu, P., Isidorov, V. and Vinogorova, V. (2008). Antioxidant and antimicrobial activities of essential oil and various oleoresins of *Elettaria cardamomum* (seeds and pods). *Journal of the Science of Food and Agriculture*, *88*(2), 280-289.

Sontakke, M.D., Syed, H.M. and Sawate, A.R. (2018). Studies on extraction of essential oils from spices (Cardamom and Cinnamon). *International Journal of Chemical Studies, 6*, 2787–2789.

Souissi, M., Azelmat, J., Chaieb, K. and Grenier, D. (2020). Antibacterial and anti-inflammatory activities of cardamom (*Elettaria cardamomum*) extracts:

Potential therapeutic benefits for periodontal infections. *Anaerobe*, *61*, 102089.

Winarsi, H., Sasongko, N. D., Purwanto, A. and Nuraeni, I. (2014). Effect of cardamom leaves extract as antidiabetic, weight lost and hypocholesterolemic to alloxan-induced Sprague Dawley diabetic rats. *International Food Research Journal*, *21*(6), 2253.

Yucel, E., Yucel, S. I. and Coban, Z. (2012). The wild plants consumed as a food in Afyonkarahisar/Turkey and consumption forms of these plants. *Biological Diversity and Conservation, 5*(2), 95-105.

Chapter 7

THE STABILITY ANALYSIS OF AUTONOMOUS INCOMMENSURATE FRACTIONAL-ORDER SYSTEM AND ITS SOME CONCLUSIONS

Bahatdin DAŞBAŞI[1]

1 Corresponding Author: Assoc. Prof. Dr. Bahatdin DAŞBAŞI, Orcid ID: 0000-0001-8201-7495, Kayseri University, Faculty of Engineering, Architecture and Design, Department of Engineering Basic Sciences, 38280, Kayseri/Turkey, Email : bdasbasi@kayseri.edu.tr and dasbasi_bahatdin@hotmail.com

1. INTRODUCTION

Mathematical models of processes and systems in real-world problems are generally expressed in terms of difference or differential equations. In this context, mathematical modeling is widely used in natural sciences such as physics, chemistry, biology, earth science, meteorology, engineering disciplines such as computer science, artificial intelligence, medicine, as well as in social sciences such as economics, management, finance, economics, psychology, sociology and political science. In these modeling processes by differential equations, besides ordinary differential equations (ODEs) [1-7], impulsive differential equations (IDEs) [8-10], fractional-order differential equations (FODEs) [11-12] and piecewise differential equations (PDE) [13-14] are frequently used in the literature.

With regard to the qualitative theory of FOSs, stability analysis is one of the most important research topics. The basic results regarding the stability properties of fractional order systems have been recently reviewed in [15].

In here, an n-dimensional autonomous IFOS with Caputo derivatives is introduced. Then, some definitions and theorems about LAS conditions of the equilibrium point are given for both commensurate FOS (CFOS) and IFOS. In addition, the some extracted results related to stability analysis are given.

2. PRELIMINARIES AND DEFINITIONS

Definition 2.1. The Riemann-Liouville form derivative of order $\alpha > 0$ of a function f fractional integral operator with order $\alpha > 0$ for the function $f: (0, +\infty) \to \mathbb{R}$ is described as the following:

$$ {}^{RL}D_t^{\alpha}\big(f(t)\big) = \frac{1}{\Gamma(n-\alpha)}\Big(\frac{d}{dt}\Big)^n \int_a^t (t-x)^{n-\alpha-1} f(x)dx \,, n-1 < \alpha \le n, \quad (1) $$

where $\Gamma(.)$ is the Gamma function, which is defined by

$$ \Gamma(x) = \int_0^{\infty} t^{x-1}e^{-t}dt \quad (2) $$

[16-18].

Definition 2.2. Taking into account the definition of Caputo sense, the fractional derivative of the function $f(t)$ is identified as

$$ {}^{C}D_{t}^{\alpha}\big(f(t)\big) = \frac{1}{\Gamma(n-\alpha)}\Big(\frac{d}{dt}\Big)^{n}\int_{a}^{t}(t-x)^{n-\alpha-1}\Big(\frac{d}{dx}\Big)^{n} f(x)dx\,, n-1<\alpha\leq n, \quad (3) $$

where f: $(0,+\infty)\rightarrow\mathbb{R}$ and $\alpha>0$ [19-21].

The Caputo sense was used in this study.

Remark 2.1. Let us consider the nonlinear FOS given as

$$ \frac{d^{\bar{\alpha}}X(t)}{dt^{\bar{\alpha}}} = F\big(t,X(t)\big), \quad (4) $$

with suitable initial conditions $X(0)=X_0$, where
$X(t)=[x_1(t),x_2(t),\dots,x_n(t)]^T\in\mathbb{R}^n$ is the state vectors of Eqs (4),
$F=[f_1,f_2,\dots,f_n]^T\in\mathbb{R}^n$, f_i: $[0,+\infty)\mathrm{x}\mathbb{R}^n\rightarrow\mathbb{R}$, $(i=1,2,\dots,n)$,
$\bar{\alpha}=[\alpha_1,\alpha_2,\dots,\alpha_n]^T$ is the multi-order of Eqs (5),
$\frac{d^{\bar{\alpha}}X(t)}{dt^{\bar{\alpha}}}=\Big[\frac{d^{\alpha_1}x_1(t)}{dt^{\alpha_1}},\frac{d^{\alpha_2}x_2(t)}{dt^{\alpha_2}},\dots,\frac{d^{\alpha_n}x_n(t)}{dt^{\alpha_n}}\Big]^T$ [18,19,22,23].

In the remainder of the paper, it is assumed that α_i is a rational number in the interval $(0,1]$.

Definition 2.3. Let us consider that $\alpha_1=\alpha_2=\cdots=\alpha_n=\alpha$. In this case, Eqs. (4) can be rewritten as

$$ \frac{d^{\alpha}X(t)}{dt^{\alpha}} = F\big(t,X(t)\big), \quad (5) $$

namely CFOS. Otherwise, Eqs (4) is called as IFOS [15,24].

Definition 2.4. The autonomous IFOS in the equations (4) can be represented as

$$ \frac{d^{\bar{\alpha}}X(t)}{dt^{\bar{\alpha}}} = F\big(X(t)\big), \quad (6) $$

with initial conditions $X(0) = X_0$. In addition, the fixed point (or equilibrium point) of the equations (6) is the point $\bar{X} = (\overline{x_1}, \overline{x_2}, \dots, \overline{x_n})$ calculated from

$$F(\bar{X}) = 0. \quad (7)$$

[25].

Lemma 2.1. Considering CFOS in (5), it is

$$\begin{cases} \dfrac{d^\alpha x_1}{dt^\alpha} = f_1(x_1, x_2, \dots, x_n) \\ \dfrac{d^\alpha x_2}{dt^\alpha} = f_2(x_1, x_2, \dots, x_n) \\ \vdots \\ \dfrac{d^\alpha x_n}{dt^\alpha} = f_n(x_1, x_2, \dots, x_n) \end{cases} \quad (8)$$

with the initial values $x_1(0) = x_{1_0}, x_2(0) = x_{2_0} \dots x_n(0) = x_{n_0}$. The fixed point (or equilibrium point) is point $\bar{X} = (\overline{x_1}, \overline{x_2}, \dots, \overline{x_n})$ found by the equations $f_i(x_1, x_2, \dots, x_n) = 0$ for $i = 1,2, \dots, n$. By $J = \begin{bmatrix} \frac{\partial f_1}{\partial y_1} & \frac{\partial f_1}{\partial y_2} & \cdots & \frac{\partial f_1}{\partial y_n} \\ \frac{\partial f_2}{\partial y_1} & \frac{\partial f_2}{\partial y_2} & \cdots & \frac{\partial f_2}{\partial y_n} \\ \vdots & \vdots & \ddots & \vdots \\ \frac{\partial f_n}{\partial y_1} & \frac{\partial f_n}{\partial y_2} & \cdots & \frac{\partial f_n}{\partial y_n} \end{bmatrix}$, the Jacobian matrix for evaluate the locally asymptotic stability (LAS) of equilibrium points is used. Let λ_i for $i = 1,2, \dots, n$ be the roots of the characteristic polynomial obtained from the equation $Det\left(J_{(y_1, y_2, \dots, y_n) = (y_1^{eq}, y_2^{eq}, \dots, y_n^{eq})} - \lambda I_n\right) = 0$, where I_n is the unit matrix. If these eigenvalues satisfy Routh-Hurwitz stability criteria or the conditions

$$\left(|arg(\lambda_i)| > \frac{\alpha\pi}{2}\right), \quad (9)$$

then, the equilibrium point is LAS for system (8) [26].

Theorem 2.1. (Routh-Hurwitz Criteria)**:** Let be real constants the coefficients a_i for $i = 1, \dots, n$ are, the charasteristic polynomial is

$$P(\lambda) = \lambda^n + a_1\lambda^{n-1} + \dots + a_{n-1}\lambda + a_n. \quad (10)$$

the n Hurwitz matrices by the coefficients a_i of upper polynomial are $H_1 = (a_1)$, $H_2 = \begin{pmatrix} a_1 & 1 \\ a_3 & a_2 \end{pmatrix}$, $H_3 = \begin{pmatrix} a_1 & 1 & 0 \\ a_3 & a_2 & a_1 \\ a_5 & a_4 & a_3 \end{pmatrix}$, …, $H_n = \begin{pmatrix} a_1 & 1 & 0 & 0 & . & . & . & 0 \\ a_3 & a_2 & a_1 & 1 & . & . & . & 0 \\ a_5 & a_4 & a_3 & a_1 & . & . & . & 0 \\ . & . & . & . & . & & & . \\ . & . & . & . & & . & & . \\ . & . & . & . & & & . & . \\ 0 & 0 & 0 & 0 & . & . & . & a_n \end{pmatrix}$ where $a_j = 0$ if $j > n$. The roots of polynomial $P(\lambda)$ are negative or have negative real parts, iff the determinants of all Hurwitz matrices are positive: $Det\, H_j > 0$, $j = 1,2,\dots,n$. In terms of convenience, the criteria for equations of degree $n = 2,\ 3,\ 4$ and 5 can be given as

$$\begin{cases} n = 2: a_1, a_2 > 0, \\ n = 3: a_1, a_3 > 0 \text{ and } a_1 a_2 > a_3, \\ n = 4: a_1, a_3, a_4 > 0 \text{ and } a_1 a_2 a_3 > {a_3}^2 + {a_1}^2 a_4, \\ n = 5: a_1, a_2, a_3, a_4, a_5 > 0, a_1 a_2 a_3 > {a_3}^2 + {a_1}^2 a_4 \text{ and} \\ \qquad (a_1 a_4 - a_5)(a_1 a_2 a_3 - {a_3}^2 - {a_1}^2 a_4) > a_5 (a_1 a_2 - a_3)^2 + a_1 {a_5}^2. \end{cases}$$

This criteria has given necessary and sufficient conditions for the roots of the characteristic polynomial (with real coefficients) to lie in the left half of the complex plane [27].

Thus we have following figure:

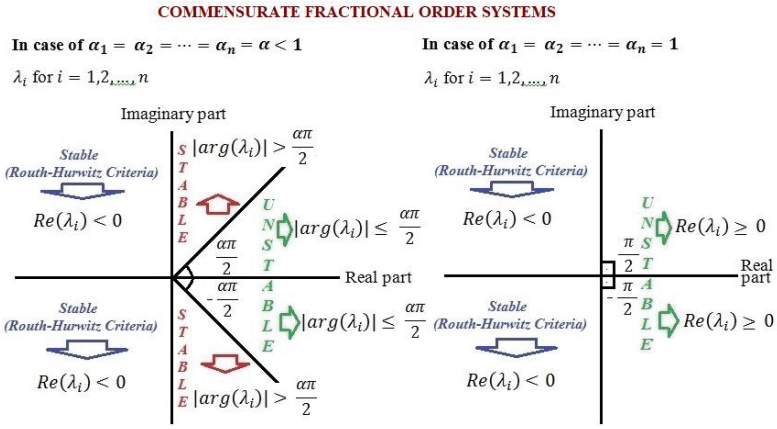

Figure 1. Regions of stability and instability of the equilibrium point in terms of the roots of the characteristic equation of the system (8).

Lemma 2.2. Eigenvalues λ_i for $i = 1,2,\dots,m(\alpha_1 + \alpha_2 + \cdots + \alpha_n)$ of system (6) are obtained from the charasteristic polinom are obtained from

$$det\big(diag(\lambda^{m\alpha_1}, \lambda^{m\alpha_2}, \dots, \lambda^{m\alpha_n}) - J(\bar{X})\big) = 0 \quad (8)$$

where m is the smallest of the common multiples of the denominators of rational numbers $\alpha_1, \alpha_2, \dots, \alpha_n$ and $J(\bar{X}) = \frac{\partial F}{\partial X}\Big|_{X=\bar{X}}$. If all eigenvalues λ_i obtained from Eq. (8) satisfy

$$|arg(\lambda_i)| > \frac{\pi}{2m}, \quad (9)$$

then $\bar{X}$ is LAS for IFOS in Eqs (6) [21].

As a result, Figure 2. can be given.

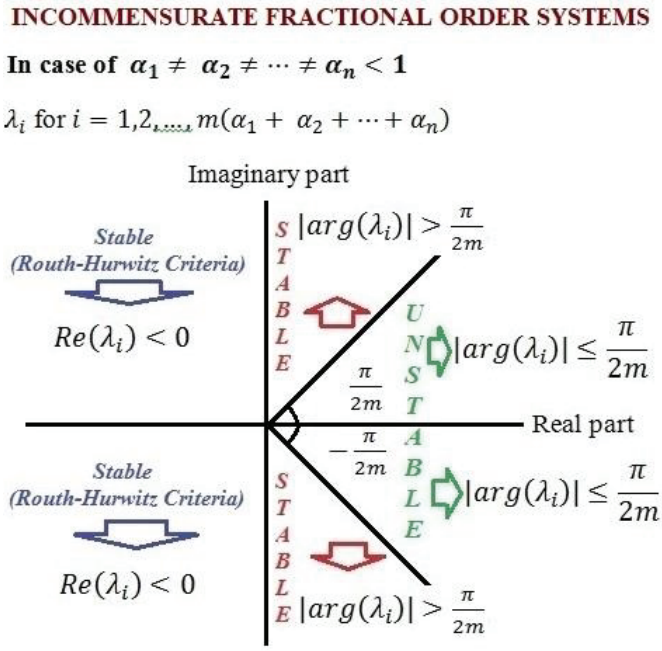

Figure 2. Regions of stability and instability of the equilibrium point in terms of the roots of the characteristic equation of the system (6) [28].

Corollary 2.1. Let us consider IFOS $(0 \leq \bar{\alpha} < 1)$ in Equations (4) and CFOS $(0 \leq \alpha < 1)$ Equations (5). Moreover, let $\bar{X} = (\overline{x_1}, \overline{x_2}, \dots, \overline{x_n})$ be the equilibrium point. If the characteristic equation satisfies the Routh-

Hurwitz stability criterion, then this point is LAS. But the reverse of this situation is not true. That is, if this criterion is not met, we cannot say that the point is unstable.

Corollary 2.2. Considering CFOS ($\alpha = 1$) in equations (5), this system is said as ODES (Ordinary Differential Equations System). Let $\bar{X} = (\overline{x_1}, \overline{x_2}, \dots, \overline{x_n})$ be the equilibrium point. This point is LAS, if and only if the characteristic equation satisfies the Routh-Hurwitz stability conditions.

Theorem 2.1. (Descartes's Rule of Signs)[29] Let $p(x) = a_0 x^{b_0} + a_1 x^{b_1} + \cdots + a_n x^{b_n}$ denote a polynomial with nonzero real coefficients a_i , where the b_i are integers satisfying $0 \le b_0 < b_1 < b_2 < \cdots < b_n$. The number of positive real roots of $p(x) = 0$ is either equal to the number of variations in the sign in the sequence of coefficients $a_0, \dots, a_n$, or less than that by an even whole number. The number of negative real roots of $p(x) = 0$ is either equal to the number of variations in sign in the sequence of the coefficients of $p(-x)$ or less than that by an even whole number.

Lemma 2.3. Considering Eqs. (6), let $n \ge 2$ and the equilibrium point $\bar{X} = (\overline{x_1}, \overline{x_2}, \dots, \overline{x_n})$. Also, it is assumed $\alpha_1 > \alpha_2 > \cdots > \alpha_n$, otherwise It can be arranged by changing the order of the equations in system (6). By partial derivatives, the determinant of the charasteristic equation of (8) is

$$\begin{vmatrix} \left(\lambda^{m\alpha_1} - \left.\frac{\partial f_1}{\partial x_1}\right|_{X=\bar{X}}\right) & -\left.\frac{\partial f_1}{\partial x_2}\right|_{X=\bar{X}} & \dots & -\left.\frac{\partial f_1}{\partial x_n}\right|_{X=\bar{X}} \\ -\left.\frac{\partial f_2}{\partial x_1}\right|_{X=\bar{X}} & \left(\lambda^{m\alpha_2} - \left.\frac{\partial f_2}{\partial x_2}\right|_{X=\bar{X}}\right) & \dots & -\left.\frac{\partial f_2}{\partial x_n}\right|_{X=\bar{X}} \\ \vdots & \vdots & \ddots & \vdots \\ -\left.\frac{\partial f_n}{\partial x_1}\right|_{X=\bar{X}} & -\left.\frac{\partial f_n}{\partial x_2}\right|_{X=\bar{X}} & \dots & \left(\lambda^{m\alpha_n} - \left.\frac{\partial f_n}{\partial x_n}\right|_{X=\bar{X}}\right) \end{vmatrix} = 0. \quad (10)$$

The characteristic polynomial obtained from (10), which involves most 2^n terms, can be write follows:

For $n = 2$, it is

$$\lambda^{m(\alpha_1+\alpha_2)} + \left(-\frac{\partial f_2}{\partial x_2}\Big|_{X=\bar{X}}\right)\lambda^{m\alpha_1} + \left(-\frac{\partial f_1}{\partial x_1}\Big|_{X=\bar{X}}\right)\lambda^{m\alpha_2} + \left(\frac{\partial f_1}{\partial x_1}\Big|_{X=\bar{X}}\frac{\partial f_2}{\partial x_2}\Big|_{X=\bar{X}} - \frac{\partial f_1}{\partial x_2}\Big|_{X=\bar{X}}\frac{\partial f_2}{\partial x_1}\Big|_{X=\bar{X}}\right) = 0.$$

For $n = 3$, it is

$$\lambda^{m(\alpha_1+\alpha_2+\alpha_3)} - \lambda^{m(\alpha_1+\alpha_2)}\frac{\partial f_3}{\partial x_3}\Big|_{X=\bar{X}} - \lambda^{m(\alpha_1+\alpha_3)}\frac{\partial f_2}{\partial x_2}\Big|_{X=\bar{X}} - \lambda^{m(\alpha_2+\alpha_3)}\frac{\partial f_1}{\partial x_1}\Big|_{X=\bar{X}} + \lambda^{m\alpha_1}\left(\frac{\partial f_2}{\partial x_2}\Big|_{X=\bar{X}}\frac{\partial f_3}{\partial x_3}\Big|_{X=\bar{X}} - \frac{\partial f_2}{\partial x_3}\Big|_{X=\bar{X}}\frac{\partial f_3}{\partial x_2}\Big|_{X=\bar{X}}\right) + \lambda^{m\alpha_2}\left(\frac{\partial f_1}{\partial x_1}\Big|_{X=\bar{X}}\frac{\partial f_3}{\partial x_3}\Big|_{X=\bar{X}} - \frac{\partial f_1}{\partial x_3}\Big|_{X=\bar{X}}\frac{\partial f_3}{\partial x_1}\Big|_{X=\bar{X}}\right) + \lambda^{m\alpha_3}\left(\frac{\partial f_2}{\partial x_2}\Big|_{X=\bar{X}}\frac{\partial f_1}{\partial x_1}\Big|_{X=\bar{X}} - \frac{\partial f_1}{\partial x_2}\Big|_{X=\bar{X}}\frac{\partial f_2}{\partial x_1}\Big|_{X=\bar{X}}\right) + \left(\frac{\partial f_1}{\partial x_1}\Big|_{X=\bar{X}}\frac{\partial f_2}{\partial x_3}\Big|_{X=\bar{X}}\frac{\partial f_3}{\partial x_2}\Big|_{X=\bar{X}} - \frac{\partial f_3}{\partial x_3}\Big|_{X=\bar{X}}\frac{\partial f_2}{\partial x_2}\Big|_{X=\bar{X}}\frac{\partial f_1}{\partial x_1}\Big|_{X=\bar{X}} + \frac{\partial f_1}{\partial x_2}\Big|_{X=\bar{X}}\frac{\partial f_2}{\partial x_1}\Big|_{X=\bar{X}}\frac{\partial f_3}{\partial x_3}\Big|_{X=\bar{X}} - \frac{\partial f_1}{\partial x_2}\Big|_{X=\bar{X}}\frac{\partial f_2}{\partial x_3}\Big|_{X=\bar{X}}\frac{\partial f_3}{\partial x_1}\Big|_{X=\bar{X}} - \frac{\partial f_1}{\partial x_3}\Big|_{X=\bar{X}}\frac{\partial f_2}{\partial x_1}\Big|_{X=\bar{X}}\frac{\partial f_3}{\partial x_2}\Big|_{X=\bar{X}} + \frac{\partial f_2}{\partial x_2}\Big|_{X=\bar{X}}\frac{\partial f_1}{\partial x_3}\Big|_{X=\bar{X}}\frac{\partial f_3}{\partial x_1}\Big|_{X=\bar{X}}\right).$$

…

For n, it is

$$\lambda^{m(\alpha_1+\alpha_2+\cdots.+\alpha_n)} - \lambda^{m(\alpha_1+\alpha_2+\cdots.+\alpha_{n-1})}\frac{\partial f_n}{\partial x_n}\Big|_{X=\bar{X}} - \lambda^{m(\alpha_1+\alpha_2+\cdots.+\alpha_{n-2}+\alpha_n)}\frac{\partial f_{n-1}}{\partial x_{n-1}}\Big|_{X=\bar{X}} \ldots = 0. \quad (11)$$

Corollary 2.3. Consider the characteristic equation in (11), where $m(\alpha_1 + \alpha_2 + \cdots.+\alpha_n)$-degree. With respect to to the Descartes's Rule of Signs, let P be the number of sign changes of the terms of this polynomial. If P is an odd number, then $\bar{X}$ is unstable point.

Corollary 2.4. Taking into consideration the determinant in (10). Suppose the characteristic equation can be written as the multiplication of the some elements on the principal diagonal of this determinant. For example, we have

$$\left(\lambda^{m\alpha_1}-\frac{\partial f_1}{\partial x_1}\Big|_{X=\bar{X}}\right)\left(\lambda^{m(\alpha_2+\alpha_3+\cdots.+\alpha_n)}-\lambda^{m(\alpha_2+\alpha_3+\cdots.+\alpha_{n-1})}\frac{\partial f_n}{\partial x_n}\Big|_{X=\bar{X}}-\lambda^{m(\alpha_2+\alpha_3+\cdots.+\alpha_{n-2}+\alpha_n)}\frac{\partial f_{n-1}}{\partial x_{n-1}}\Big|_{X=\bar{X}}\ldots\right)=0,$$

and so,

$$\lambda^{m\alpha_1}-\frac{\partial f_1}{\partial x_1}\Big|_{X=\bar{X}}=0 \qquad (12-a)$$

$$\lambda^{m(\alpha_2+\alpha_3+\cdots.+\alpha_n)}-\lambda^{m(\alpha_2+\alpha_3+\cdots.+\alpha_{n-1})}\frac{\partial f_n}{\partial x_n}\Big|_{X=\bar{X}}-\lambda^{m(\alpha_2+\alpha_3+\cdots.+\alpha_{n-2}+\alpha_n)}\frac{\partial f_{n-1}}{\partial x_{n-1}}\Big|_{X=\bar{X}}\ldots=0 \qquad (12-b)$$

Consider the equation in (12-a). In here, it is

$$\lambda^{m\alpha_1}=\frac{\partial f_1}{\partial x_1}\Big|_{X=\bar{X}}. \qquad (13)$$

i. Let $\frac{\partial f_1}{\partial x_1}\Big|_{X=\bar{X}}>0$. Since $m\alpha_1$ is a positive integer, one eigenvalue λ_i is a positive real number for $i=1,2,\ldots,m\alpha_1$. As seen Figure 2, the eigenvalues do not satisfy the stability condition of the equilibrium point. Thus the point is unstable.
Note: If the Descartes's Rule of Signs is taken into account, then the sign change number of terms of equation (12-a) is found to be 1. In this case, it is concluded that one of the eigenvalues is a positive real number.

ii. Let $\frac{\partial f_1}{\partial x_1}\Big|_{X=\bar{X}}<0$. By De-Moivre formulas, we have $\lambda^{m\alpha_1}=\overbrace{-\frac{\partial f_1}{\partial x_1}\Big|_{X=\bar{X}}}^{>0}cis\pi$, and so, $\lambda_k=\left[-\frac{\partial f_1}{\partial x_1}\Big|_{X=\bar{X}}\right]^{\frac{1}{m\alpha_1}}cis\left(\frac{\pi+2k\pi}{m\alpha_1}\right)$ for $k=0,1,2,\ldots,(m\alpha_1-1)$, such that $cis\pi=\cos\pi+i\sin\pi$, $i=\sqrt{-1}$. Also, it is

$$\begin{aligned}|arg(\lambda_0)|&=\frac{\pi}{m\alpha_1}\\ |arg(\lambda_1)|&=\frac{3\pi}{m\alpha_1}\\ &\vdots\\ \left|arg\left(\lambda_{(m\alpha_2-1)}\right)\right|&=\frac{(2m\alpha_2-1)\pi}{m\alpha_1}.\end{aligned} \qquad (14)$$

Considering the condition $|arg(\lambda)|>\frac{\pi}{2m}$ for stability the equilibrium point, the stability condition is $\frac{\pi}{m\alpha_1},\frac{3\pi}{m\alpha_1},\ldots,\frac{(2m\alpha_1-1)\pi}{m\alpha_1}>\frac{\pi}{2m}$, and so,

$$\begin{aligned} &\alpha_1 < 2 \\ &\alpha_1 < 6 \\ &\qquad \vdots \\ &\alpha_1 < 2(2m\alpha_2 - 1). \end{aligned} \qquad (15)$$

Inequalities in (15) has been always provided since the inequaties $0 < \alpha_1, \alpha_2, \dots, \alpha_n \leq 1$ in Remark 2.1 is already satisfied. Thus, the multiplier in (12-a) satisfies the stability condition of the equilibrium point. In this case, it will be sufficient to examine only equation (12-b).

REFERENCES

[1] L. Esteva, E. I. Mondragon ve J. R. Leyton, «Un modelo matemático sobre bacterias sensibles y resistentes a antibióticos,» *Matemáticas: Ensenanza Universitaria,* cilt 19, no. 2, pp. 55-73, 2011.

[2] E. Ibargüen-Mondragón, M. C. Gómez ve E. M. Burbano-Rosero, «Assessing the role of bacterial plasmid replication in a competition model of sensitive and resistant bacteria to antibiotics,» *AIMS Mathematics,* cilt 6, no. 9, pp. 9446-9467, 2021.

[3] E. Ibargüen-Mondragón, J. Romero-Leiton, L. Esteva, M. C. Gómez ve S. P. Hidalgo-Bonilla, «Stability and periodic solutions for a model of bacterial resistance to antibiotics caused by mutations and plasmids,» *Applied mathematical modelling,* 276, pp. 238-251, 2019.

[4] M. B. Koç, I. Boztosun ve D. Boztosun, «On the Numerical Solution of Black-Scholes Equation,» *International Workshop on MeshFree Methods*, 2003.

[5] N. H. AlShamrani, «Stability of an HTLV-HIV coinfection model with multiple delays and CTL-mediated immunity,» *Adv. Differ. Equ.,* cilt 270, no. https://doi.org/10.1186/s13662-021-03416-7, 2021.

[6] B. Daşbaşı, D. Boztosun ve E. Baraz, «Matematiksel Modelleme ile Nüfus ve Yapay Sinir Ağlari Yardimiyla Kişi Başina Düşen Milli Gelir Tahmini: Türkiye Örneği,» *Journal Of Social & Humanities Sciences Research,* cilt 4, no. 5, pp. 841-850, 2017.

[7] E. I. Mondragón, S. Mosquera, M. Cerón, E. M. Burbano-Rosero, S. P. Hidalgo-Bonilla, L. Esteva ve J. P. Romero-Leitón, «Mathematical modeling on bacterial resistance to multiple antibiotics caused by spontaneous mutations,» *BioSystems,* cilt 117, p. 60–67, 2014.

[8] P. Feketa ve N. Bajcinca, «Stability of nonlinear impulsive differential equations with non-fixed moments of jumps,» *2018 European Control Conference (ECC)*, 2018.

[9] Y. Ding, D. O'Regan ve J. Wang, «Stability Analysis for Conformable Non-instantaneous Impulsive Differential Equations,» *Bull. Iran. Math. Soc.,* https://doi.org/10.1007/s41980-021-00595-7, 2021.

[10] J. P. Ndenda, J. B. H. Njagarah ve S. Shaw, «Role of immunotherapy in tumor-immune interaction: Perspectives from fractional-order modelling and sensitivity analysis,» *Chaos, Solitons & Fractals,* cilt 148, no. 111036, 2021.

[11] C. Balzotti, M. D'Ovidio, A. C. Lai ve P. Loreti, «Effects of Fractional Derivatives with Different Orders in SIS Epidemic Models.,» *Computation,*

cilt 9, no. 8, p. 89, 2021.

[12] A. S. Alshomrani, M. Z. Ullah ve D. Baleanu, «Caputo SIR model for COVID-19 under optimized fractional order,» *Advances in Difference Equations,* cilt 1, pp. 1-17, 2021.

[13] H. Zhou ve P. A. Zegeling, «Stability and Convergence Analysis of a Class of Continuous Piecewise Polynomial Approximations for Time-Fractional Differential Equations.,» *J. Sci. Comput.,* cilt 77, no. https://doi.org/10.1007/s10915-018-0704-z, pp. 225-262, 2018.

[14] A. Platonov, «Stability analysis for a class of mechanical systems with piecewise constant coefficients,» Journal of Physics: Conference Series, doi:10.1088/1742-6596/1959/1/012037, pp. 1959, 2021.

[15] O. Brandibur ve E. Kaslik, «Exact stability and instability regions for two-dimensional linear autonomous multi-order systems of fractional-order differential equations,» *Fractional Calculus and Applied Analysis,* cilt 24, no. 1, pp. 225-253, 2021.

[16] M. Caputo ve M. Fabrizio, «A new definition of fractional derivative without singular kernel,» *Progr. Fract. Differ. Appl.,* cilt 1, pp. 73-85, 2015.

[17] A. K. Golmankhaneh ve D. Baleanu, «On nonlinear fractional Klein-Gordon equation,» *Signal Processing,* cilt 91, pp. 446-451, 2011.

[18] I. Podlubny, Fractional Differential Equations, Academic Press, 1999.

[19] A. A. Kilbas, H. M. Srivastava ve J. J. Trujillo, Theory and applications of fractional differential equations, cilt 204, Elsevier, 2006.

[20] I. Podlubny, «Geometric and physical interpretation of fractional integration and fractional differentiation,» *Fractional Calculus and Applied Analysis,* cilt 5, p. 367–386, 2002.

[21] I. Koca, «NUMERICAL ANALYSIS OF COUPLED FRACTIONAL DIFFERENTIAL EQUATIONS WITH ATANGANA-BALEANU FRACTIONAL DERIVATIVE,» *DISCRETE AND CONTINUOUS DYNAMICAL SYSTEMS SERIES S,* cilt 12, no. 3, pp. 475-486, 2019.

[22] B. Daşbaşı ve D. Boztosun, «Çoklu Kesirli Mertebeden Diferansiyel Denklemler ile Palomba Ekonomi Modelinin Kararlılık Analizi,» *Journal of International Social Research,* cilt 11, no. 59, pp. 901-907, 2018.

[23] B. Daşbaşı ve T. Daşbaşı, «Mathematical Analysis of Lengyel-Epstein Chemical Reaction Model by Fractional-Order Differential Equation's System with Multi-Orders,» *International Journal of Science and Engineering Investigations,* cilt 6, no. 70, pp. 78-83, 2017.

[24] Z. M. Odibat, «Analytic study on linear systems of fractional differential equations,» *Computers and Mathematics with Applications,* cilt 59, no. 3, pp. 1171-1183, 2010.

[25] Y. Ji, J. Lu ve J. Qiu, «Stability of equilibrium points for incommensurate fractional-order nonlinear systems,» *35th Chinese Control Conference (CCC)*, 2016.

[26] B. Daşbaşı, «Mycobacterium Tuberculosis için Genelleştirilmiş Kesirsel Mertebeden Matematiksel Modelin Kararlılık Analizi Üzerine,» *Journal of the Institute of Science and Technology,* cilt 9, no. 1, pp. 272-287, 2019.

[27] L. J. S. Allen, An Introduction to Mathematical Biology, 2007.

[28] B. Daşbaşı, «Stability analysis of the hiv model through incommensurate fractional-order nonlinear system,» *Chaos, Solitons & Fractals,* cilt 137, no. 109870, 2020.

[29] XiaoshenWang, «A Simple Proof of Descartes's Rule of Signs,» *American Mathematical Monthly,* cilt 111, no. 6, pp. 525-526, 2004.

Chapter 8

ANOMALOUS PHOTO-SENSITIVITY OF AL/$CH_3NH_3PBI_{3-X}CL_X$/SI/AL VERTICAL JUNCTION DIODES; PHOTODIODE- AND SOLAR CELL-LIKE

Ali BALTAKESMEZ[1]

1 Assoc. Prof. Dr. Ali Baltakesmez, Department of Electricity and Energy, Technical Science Vocational School, Ardahan University, 75000, Ardahan, Turkey, https://orcid.org/0000-0003-2175-1180

Organic-inorganic hybrid perovskite semiconductors (HPS) have recently tended to be one of the effective and important semiconductors to applications in optoelectronic devices. The HPS group is described as AMX_3 formula, with A being an organic cation surrounded by a metal halide in an octahedral structure [1]. The HPSs having direct band gap with high absorption coefficient [2], low exciton binding energy with low recombination [3] and high carrier mobility with large carrier diffusion length [4] properties play a crucial role in obtaining optoelectronic devices with relatively high efficiency. Therefore, the HPSs as active layer are used in various efficient optoelectronic device such as solar cell (SC) [5], light emitting diode (LED) [6], photodiode (PD) [7] and laser diode (LD) [8].

On the other hand, metal-semiconductor Schottky interfaces (MSIs), which are essential components of almost all semi-conductor based (opto) electronic devices, have an important role in process- and cost-effective device fabrication thanks to their simple structure. Also, the MSIs have also never lost their attractiveness for understanding photoelectric responses and supporting developments in the related technological field thanks to very fast switching and low forward voltage [9]. Schottky barrier diodes (SBDs) are based on MSIs. Additionally, electrical parameters of SBDs depend especially on the ideality factor (n), zero-bias-barrier height (Φ_{B0}), series resistance (R_s), interfacial layer and density of interface states [10]. Recently, the main electrical parameters have also been investigated as function of light intensity while the analysis of electrical parameters typically have been carried out in dark condition. Furthermore, various SBDs applications, especially having interface layer, have been performed in optoelectronic devices such as solar cell and photodiode [11-15].

Typically, the light harvesting devices such as solar cells and photodiodes absorb photons at their active layer and then photo-current is generated. Therefore, circular or liner channel space, grid-line, transparent window and semi-transparent metal contact in the vertical or planar SBD configurations should be preferred [16-19], which allows photons to reach the active layer. For example, Cifci et al. have been investigated Al/perovskite/p-Si Schottky barrier photodiode with ultra-thin metal cathode (10 nm Al) [20]. The reverse-bias current has increased by light illumination from 4.91×10^{-11} A to 1.48×10^{-7} A in the presence of perovskite interlayer (from 2.05×10^{-8} to 1.61×10^{-7} for the Al/Si Schottky junction). Moreover, Ravi et al. have reported that the photo-current has dramatically decreased and the photo-response has dropped more than a fourfold due to increasing metal contact thickness from 15 nm to 300 nm in the Au/Si Schottky junction [21]. This result has been attributed to the need for the metal contact to be thin enough for the photons to pass through it and

to reach the interface. However, in the many reported studies, the vertical SBD formed with opaque rectifier contact has showed significant photo-response and thus a reflection of the optoelectronic device characteristic in the current-voltage (I-V) curve. For example, Torkhov et al. have studied the effect of rectifier contact area and shape in the SBD (Au/n-GaAs:Sn) in dark and illumination conditions in detail [22]. In this case, the reverse-bias I-V characteristics have showed that the reverse-bias current can be increased by three orders of magnitude under illumination. It has been attributed to a significant decrease in the effective barrier height due to light absorption. Furthermore, Li et al. have reported anomalous photo-current in $Fe/Zn_{0.96}Fe_{0.04}S$ Shottky barrier contact [23]. In the report, in which decay behaviors with changing temperature were investigated, the anomalous photo-current has been attributed to photoionization of the acceptor-like interface states.

In this study, the $CH_3NH_3PbI_{3-x}Cl_x$ perovskite thin film was coated on the n- and p-type Si substrates using spin coating process. Additionally, the rectifier Al contact (~120 nm) having different contact area (diode area) was deposited by thermal evaporation, $7.85x10^{-3}$ cm^2 (S: small) and $3.14x10^{-2}$ cm^2 (L: large). The fabricated diodes have been named as Sn-Si ($Al/CH_3NH_3PbI_{3-x}Cl_x$/n-Si/Al), Ln-Si ($Al/CH_3NH_3PbI_{3-x}Cl_x$/n-Si/Al), Sp-Si ($Al/CH_3NH_3PbI_{3-x}Cl_x$/p-Si/Al) and Lp-Si ($Al/CH_3NH_3PbI_{3-x}Cl_x$/p-Si/Al), which indicate different contact areas and substrates. The current density-voltage (J-V) characteristics of the $Al/CH_3NH_3PbI_{3-x}Cl_x$/Si/Al SBDs were investigated in dark and under solar light to reveal out photo-response mechanism.

Result and Discussion

Solution-based coating method is one of the most used and straightforward process to grow thin films. However, there are several drawbacks to obtain suitable perovskite thin film by precursor solution containing organic and inorganic salts due to different crystallization rates, wettability of substrate surface (surface energy), ambient condition (solvent vapor pressure) and solution/coating parameters [25]. Additionally, these parameters have profound effect on chemistry of the material and the resulting film characteristics. Therefore, the perovskite thin film deposited by solution-based method should be analyzed carefully in aspect of morphology, structure and optic before device fabrication stage.

The SEM surface images recorded at 10 μm scale given in Fig. 1(a, b) were recorded to analyze of surface morphology of perovskite thin films coated onto the n- and p-type Si substrates. As seen in Fig. 1(a) and (b), the perovskite films have same surface morphology with good covering Si surface, and also the SEM images produced from randomly chosen

locations indicate smooth and uniform morphology. Furthermore, the films have grown in densely compact way without common morphological defect such as pinholes, cracks, pitfalls and voids. On the other hand, an attentive observation of the top surface reveals that surface of the films has a cluster-like nano-grains. These features are suitable to effective light absorption, charge separation, carrier transportation, and carrier collection, and thus high photo-response [26]. Fig. 1(c-f) shows 3D (c, d) and 2D (e, f) AFM images. The cluster-like nano-grains and morphology without the defects are also observed in AFM images. Although the surface roughness of the film coated on the n-Si substrate is lower, the surface roughness value of the films is close each other; (root mean-square) R_{RMS}: 27.33 nm and R_{RMS}: 32.29 nm, as seen in Fig. 1(e, f). The AFM images show a similar tendency in agreement with the SEM results. Thus, it can be concluded that the Si substrates have same surface features and the electrical conductivity type does not play a critical role in the formation of perovskite thin film.

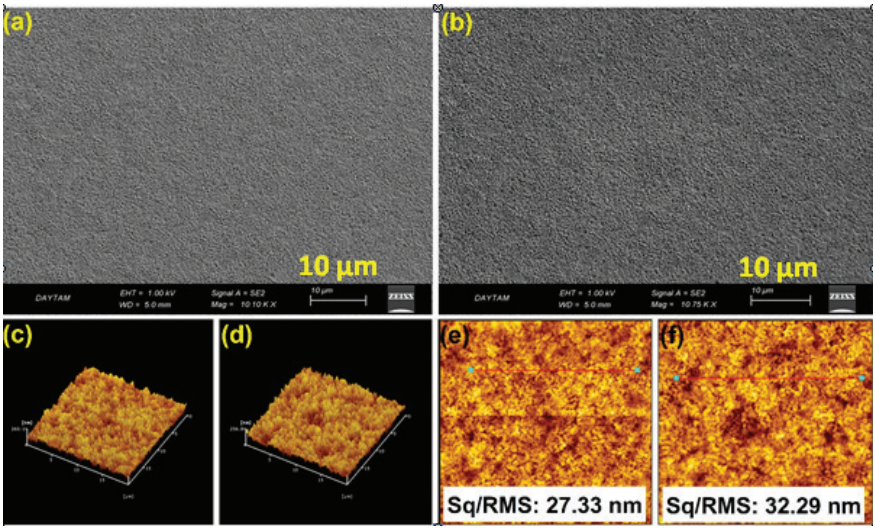

Figure 1. *SEM and AFM images of perovskite thin films deposited onto the n-type (a, c, e) and p-type (b, d, f) Si substrates.*

The structural analyze was carried out using the perovskite thin film coated onto the n-Si substrate. Figure 2(a) shows the XRD patterns of the perovskite film with inset figure corresponding $K_{\alpha 1}$ and $K_{\alpha 2}$ diffraction peaks of the Si in range of 2θ:68° and 70°. The diffraction pattern includes dominant characteristic peaks located at 14.42° and 28.67° and weak peaks at 22.83°, 32.50°, 43.87° and 59.40°. The dominant characteristic peaks located at 14.42° and 28.67° are assigned to (110) and (220) crystal planes, which oriented parallel to the substrate [27], and (211), (310), (314) and (400) crystal planes indicate reflection positions inconsistent with cubic

symmetry of cluster-like nano-grains [28]. The crystal growth in the two dominant characteristic planes is attributed to tetragonal crystal structure [29], represented in Fig. 2(b). Furthermore, the values of full width at half maximum (FWHM) of the peaks located at 14.42° and 28.67° were determined as to be 0.143° and 0.101° and these small values mean phase purity [30]. The structural analyze (XRD) is consistent with the morphological results (SEM). The optical absorption spectrum of the perovskite film coated onto the PEDOT:PSS/ITO substrate is given in Fig. 2(c). The optical absorbance spectrum clearly shows that the perovskite film has absorption onset at around 790 nm and then good absorbance feature in range of visible light region. Additionally, the $(\alpha h\nu)^2$ versus hν plot and band gap energy obtained from following equations:

$$T = \frac{(1-R)^2 \exp(-\alpha t)}{1 - R^2 \exp(-2\alpha t)} = \exp(-A) \quad (1)$$

$$\alpha h\nu = K(h\nu - E_g)^{1/2} \quad (2)$$

where T, R, α, t, hν and K indicate transmittance, reflectance, absorption coefficient, film thickness (~190 nm), energy of incident photon and a constant. The energy band gap (E_g) is found out to be 1.59 eV. The calculated E_g value is compared with values for the $CH_3NH_3PbI_{3-x}Cl_x$ perovskite films reported [31]. On the other hand, as similar to the absence of diffraction peak of PbI_2 impurity in the XRD pattern, the absorbance spectral curve has also exhibited no PbI_2 shoulder peak around 500 nm [32]. Briefly, the morphological, structural and optical analyses have verified the presence of suitable perovskite interlayer film which can serve as a high photo-sensitive layer.

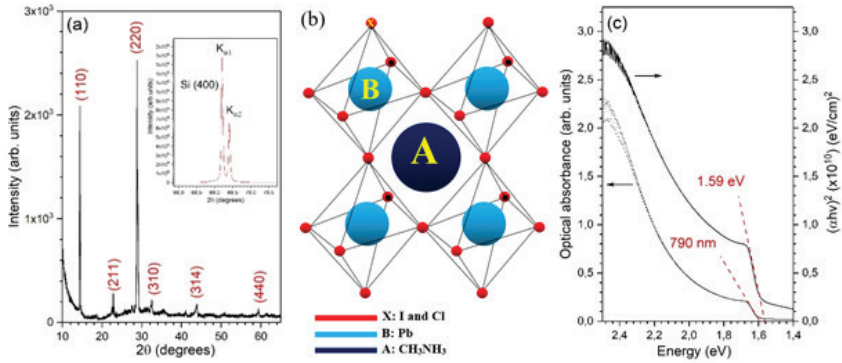

Figure 2. *XRD pattern (a), cell structure (b) and UV-vis absorbance spectrum (c) of $CH_3NH_3PbI_{3-x}Cl_x$ thin film.*

In the theory, interdependence of current and voltage for ideal SBD with dominant parameters consisting of the current flow through the metal–semiconductor junction (I), saturation current (I_o), voltage drop across the junction (V), electronic charge (q), Boltzmann constant (k), absolute temperature (T), ideality factor (n) determines by the thermionic emission theory (TE) given by following Eq. (3).

$$I = I_o \exp\left(\frac{qV}{nkT}\right)\left[1 - \exp\left(-\frac{qV}{kT}\right)\right] \quad (3)$$

The I_o given by

$$I_o = AA^*T^2 \exp\left(-\frac{q\Phi_{B0}}{kT}\right) \quad (4)$$

where A is the active diode area (rectifier contact area), A^* is the effective Richardson constant as 112 $A.cm^{-2}K^{-2}$ for n-type Si and 32 $A.cm^{-2}K^{-2}$ for p-type Si, Φ_{B0} is the zero bias barrier height. Fig. 3(a) shows the semi-logarithmic current density-voltage (log(J)-V) plots of samples dependent on prepared opaque rectifier contact area and substrate conductivity type. As seen in the figure, the n-Si based diodes have high rectifier behavior at forward bias with low saturation current at reverse-bias region. Additionally, the threshold voltage of Sn-Si diode has shifted towards positive voltage region at around 0.2 V. On the other hand, the p-Si based diodes have a similar rectifier behavior at forward bias region while the saturation current at reverse-bias region is relatively lower for the Sp-Si. The rectifier performances of Ln-Si, Sn-Si, Sp-Si and Lp-Si are given inset figure in Fig. 3(a). These different behaviors and values evidence that the substrate conductivity type and rectifier contact area (active area) designate electrical properties of the SBDs. The energy band structures of diodes based on n- and p-type Si are illustrated in Fig. 3(b). This energy band structure models have been consisted of using band energy values and fermi levels reported literature [33, 35]. As show in the energy band structure models, Koller et al. have reported the anomalous contribution to the photo-current phenomena and explained it as assuming the formation of double junctions inside the single device [36]. The anomalous contribution to the photo-current phenomena has attributed to superiority between the normal and anomalous current of the two junctions [36, 37]. Similarly, the SBDs having $CH_3NH_3PbI_{3-x}Cl_x$ perovskite interlayer may be have two junctions and then two depletion regions, as seen in Fig. 3(b). The Junction-1 has formed perovskite semiconductor layer at the equilibrium condition while the Junction-2 at the perovskite/Si interface has a depletion region as-like p-n, p^+-p or n^+-n junctions. Therefore, the band structures of

diodes show that the perovskite/p-Si interface generates a potential barrier to both electrons and holes, and thus this barrier may be cause of low rectifier performance of the p-Si based diodes rather than n-Si based.

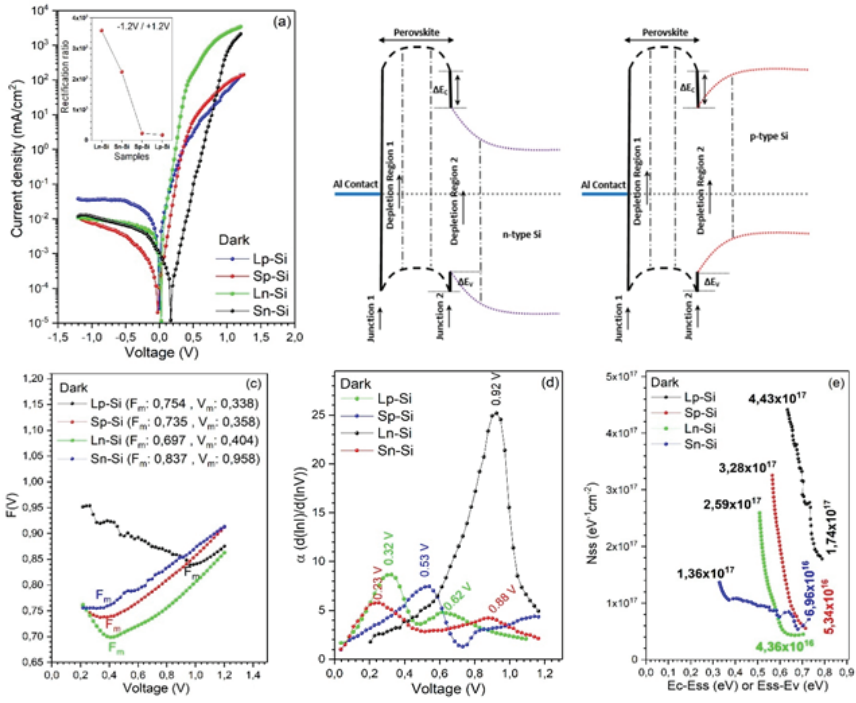

Figure 3. *(a) J-V curves of the diodes with inset figure shows rectification ratio, (b) schematic energy band diagrams of n- and p-Si based diodes after contact, (c) F(V)-V curves based Norde method of the diodes, (d) α-V curves based Mikhelashvili model of the diodes and (e) N_{ss}-(E_c-E_{ss} or E_{ss}-E_v) curves of the diodes.*

To determine barrier height and ideality factor, from Eq. 3-based the TE method [38], the zero bias barrier height (Φ_{B0}) and ideality factor (n) can be rewritten as Eq. (5) and (6).

$$\Phi_{B0} = \frac{kT}{q} ln(\frac{AA^* T^2}{I_o}) \tag{5}$$

$$n = \frac{q}{kT}(\frac{dV}{dlnI}) \tag{6}$$

As seen in Table 1, the barrier height of the diodes has varied from 0.766 eV to 0.935 eV. Interestingly, in the both Si substrates, the barrier

height of diode having small rectifier contact area is lower than that the diode having large contact area. However, the more ideal diode having the n value close to unit has been obtained by large contact area in the diode based on n-Si while the diode based on p-Si has a higher ideality factor value than the others. For the comparing, the Norde model as an alternative method can be used to determine the series resistance (R_s) and Φ_{B0} value. The Rs and Φ_{B0} values are determined using plot of F(V) versus V and the Norde function is given by Eq. (7).

$$F(V) = \frac{V}{\gamma} - \frac{kT}{q} \ln\left(\frac{I(V)}{AA^*T^2}\right) \tag{7}$$

where I(V) is current obtained from the log(J)–V plot. As seen in Fig. 4(c), from the plots of F(V) versus V, the Φ_{B0} value can be calculated by Eq. (8).

$$\Phi_B = F(V_{min}) + \frac{V_{min}}{\gamma} - \frac{kT}{q} \tag{8}$$

where $F(V_{min})$ is the minimum value of F(V) and V_{min} is the corresponding voltage. The Y is a constant which is an arbitrary integer greater than ideality factor. For real contacts (n> 1), the Rs value can be obtained by Eq. (9).

$$R_s = \frac{kT(\gamma - n)}{qI_{min}} \tag{9}$$

where I_{min} is the value of the forward current at the voltage V_{min}. As given in Table 1, the Φ_{B0} values are compatible with the values obtained by the TE method and the Rs values showed a considerable change from 0.624 kΩ to 5.084 kΩ. Furthermore, n and Φ_{B0} values were also calculated by using the Mikhelashvili model [39], which also includes the series resistance region of log(J)-V curve. The power exponent parameter α is descripted as given Eq. (10).

$$\alpha(V) = \frac{d(lnI)}{d(lnV)} \tag{10}$$

The n and Φ_{B0} values were calculated from Eq. (11) and (12) using α(V) versus V plot given in Fig. 3(d).

$$n = \frac{qV_{max}(\alpha_{max} - 1)}{kT\alpha_{max}^2} \tag{11}$$

$$\Phi_b = \frac{kT}{q}\left[\alpha_{max} + 1 - ln\left(\frac{I_{max}}{AA^*T^2}\right)\right] \tag{12}$$

where α_{max} and V_{max} are x and y coordinate points of maximum peak level in the plot of α(V)-V. As given in Table 1, n and Φ_{B0} values are compatible with the values obtained by TE and Norde methods. The high n value can be largely attributed to increasing series resistance, interface defects and inhomogeneity of Schottky barrier height [40, 41]. Therefore, the interface state density (N_{ss}) distribution was calculated using Card and Rhoderick's function [42] related to energy of the E_C-E_{SS} and E_{SS}-E_V. The E_C-E_{SS} and E_{SS}-E_V. are energy gaps between the interface states energy (E_{ss}) and bottom of the conduction band for the n-Si, and the top of valance band for p-Si, respectively.

$$E_C - E_{SS} = q(\Phi_e - V) \tag{10}$$

$$E_{SS} - E_V = -q(\Phi_e - V) \tag{11}$$

As seen in Fig. 3(e), the Nss values have decreased from conduction band to mid-gap with increasing E_C-E_{SS} and increased from mid-gap to valance band with decreasing E_{SS}-E_V. On the other hand, the Sn-Si diode has a broad distribution that meaning the states act as deep and shallow donor type while the state distribution in the Lp-Si diode has located at higher energy gap (around 0.65 eV) with a sharp decrease which indicates dominantly deep acceptor states. Furthermore, the energy distribution profiles of the both diodes based on p-Si suggest that the states are dominantly deep acceptor type. It can be attributed to existence of the perovskite/Si interface caused the deep acceptor type states. Similarly, the localized deep acceptor/donor type state distribution has reported by Gökçen et al. for Au/poly(propylene glycol)-b-polystyrene($HAuCl_4$ dispersed)/n-Si diode [43].

Table 1. *Ideality factor, Schottky barrier height and series resistance values of the diodes.*

	TE Method (I-V)		Norde Method (F(V)-V)		Mikhelashvili Method (α-V)	
	n	Φ_B (eV)	Φ_B (eV)	R_s (kΩ)	**n**	**Φ_B (eV)**
Sn-Si	2.077	0.935	0.966	3.133	1.869	0.982
Sp-Si	1.424	0.830	0.796	1.628	1.312	0.767
Ln-Si	1.335	0.802	0.784	0.624	1.248	0.867
Lp-Si	2.337	0.766	0.778	5.084	2.244	0.745

Fig. 4(a-d) shows log(J)-V plots of the diodes in dark, and under AM1.5 50 mW/cm^2 and 100 mW/cm^2 light intensity (0.5 Sun and one Sun), respectively. As seen in Fig. 4(a) and (b), the Sn-Si diode has showed high response in reverse bias region with dramatically increasing reverse saturation current value as in a photodiode, while the photo- response of solar cell log(J)-V curve-like has originated with increased contact area in the Ln-Si diode. Interestingly, the p-Si based diodes nearly has not been affected from the sole light, except for a weak photo-response starting from 0.5 V at the reverse-bias current of the Lp-Si diode. Furthermore, to analyze detail of the charge transport in the diodes, the log(J)-log(V) plots are given in Fig. 5(a-d), Sn-Si, Ln-Si, Sp-Si and Lp-Si, respectively. Typically, the forward-bias characteristic of the SBDs has three distinct charge transport mechanisms having different slopes (n), namely ohmic conduction, trap-filling regime (TFL) and quadratic trap-free space charge-limited current (Child's) mechanisms. While the ohmic conduction occurs dominantly by the mobile charge-carriers which its mobility depends on electric field, the Child's regime dominantly occurs by charge carriers injected from the contacts. In the TFL region, the charge-carriers movement at both energetic and positional distribution originate from the trapping and de-trapping processes and the presence of large TFL region suggests that the electrons or holes trapped at rather deep energy levels [44]. The deep traps as observed in the N_{ss} distribution profile related to large TFL region, especially in Sp-Si and Lp-Si diodes at around 0.1-1 V, has proven itself as very weak photo-response.

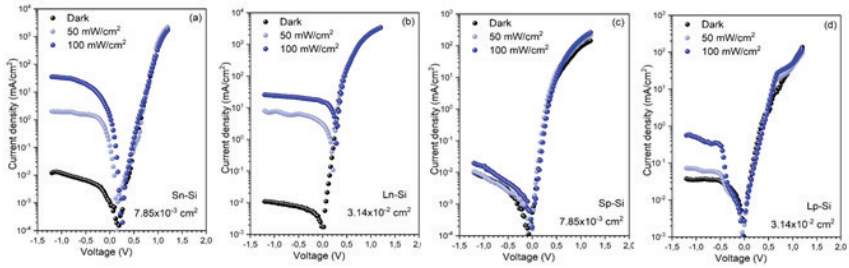

Figure 4. *J-V plots of Al/$CH_3NH_3PbI_{3-x}Cl_x$/n-Si/Al and Al/$CH_3NH_3PbI_{3-x}Cl_x$/p-Si/Al diodes in dark and under different light intensity, respectively.*

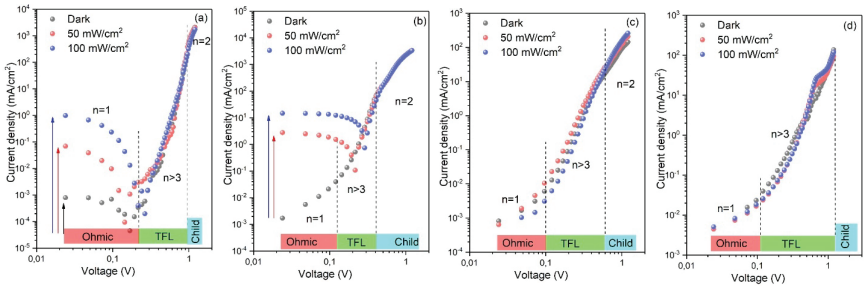

Figure 5. *log(J)-log(V) plots of Al/$CH_3NH_3PbI_{3-x}Cl_x$/n-Si/Al and Al/$CH_3NH_3PbI_{3-x}Cl_x$/p-Si/Al diodes in dark and under different light intensity, respectively.*

On the other hand, the charges excited by electrical field and/or light sweep out from the space charge region and then further injection of carriers from the electrode occurs. As a result of this process, the current density changes rapidly with applied voltage and it is well known that this process is observed by effect of light reached into light-harvesting layer. Interestingly, although the opaque Al rectifier contact, the n-Si based diodes have high light-response as photodiode-like for the Sn-Si and solar cell-like for the Ln-Si diode, and then the log(J)-log(V) curve of the Sn-Si and Ln-Si diodes has increased with increasing reverse-bias voltage at ohmic region due to shift towards positive value of threshold voltage. All the results show that the Al/$CH_3NH_3PbI_{3-x}Cl_x$/n-Si/Al diode has two junctions in single structure while the Al/$CH_3NH_3PbI_{3-x}Cl_x$/p-Si/Al diode has a dominantly junction occurred by Schottky rectifier contact.

To understand the phenomena better, linear J-V characteristics of the Sn-Si and Ln-Si diodes are given in Fig. 6(a) and (b), respectively. It is well known that the turn on voltage for Si-based Schottky diode is 0.2 to 0.3 V whereas for p-n junction diode is 0.6 to 0.7 V. Clearly, the Sn-Si diode having photodiode-like photo-response has turn on voltage range of 0.5 to 0.6V and the Ln-Si diode having solar cell-like photo-response has turn on voltage around 0.3V. It can be attributed that the Al/$CH_3NH_3PbI_{3-x}Cl_x$/n-Si/

Al diode has two junctions in single structure while the Al/$CH_3NH_3PbI_{3-x}Cl_x$/p-Si/Al diode has a dominant junction occurred by Schottky rectifier contact, as mentioned above. Furthermore, Karin et al. have reported that the $CH_3NH_3PbI_{3-x}Cl_x$ thin film are p-type semiconductor confirmed by Hall Effect study [45] and the carrier diffusion length has been reported in the range of nm to a few μm [46]. Therefore, the dominant p-n junction effect may be occurred in the n-Si based diodes rather than p-Si. However, the light cannot be absorbed in the active region due to opaque Al rectifier contact, which determine the active area as the vertical area under contact, and then light absorption in the active area cannot be source of photo-current. However, highly doped interface can generate the anomalous photo-response for the incident photo-energy [23]. Furthermore, to achieve breakdown voltage up to the ideal value of the SBDs, the edge termination techniques are applied to eliminating electric field crowding around the edges of metal contact [47], which is consisting of an overflowed depletion region (ODR) [48], as seen in Fig. 6(c). In other words, the edge termination techniques such as high resistive guard ring reduces the spread of depletion region crowding at the metal edges and then dramatically shift towards the high field region from the metal edge to deep inside the active region, thereby eliminating the effect of surface states [49]. These two phenomena may have occurred in the Al/perovskite interface under solar light. Therefore, when all the sample surface is illuminated, edge electric field effect increases with hot carrier injection by photon absorption and then the depletion layer close to the interface with carriers contribute to the photo-current in reverse polarization. This phenomenon is observed as lower breakdown voltage, increased reverse current and dominant p-n junction behavior with shift from Schottky contact to ohmic-like feature of the rectifier contact, which is observed in the Sn-Si diode. This effect decreases with increasing contact area due to that in small diodes the conductance per unit area decreases with increasing diode area which predicts a thicker barrier for larger interfaces [50]. Therefore, the two junctions feature is observed in the Ln-Si diode with lower turn on voltage and solar cell-like J-V character under solar light, as seen in Fig. 6(b). The Ln-Si based diodes has open circuit voltage (V_{oc}) at around 0.3 V with short circuit current density (J_{sc}) 3.45 and 15.59 mA/cm^2 depend on the light intensity. Consequently, when passivation of overflowed depletion region around contact is performed and only the surface area corresponding to the active area is illuminated, the SBDs having opaque metal contact in the direction of illumination probably will not exhibit optoelectronic device characters such as photodiode and solar cell.

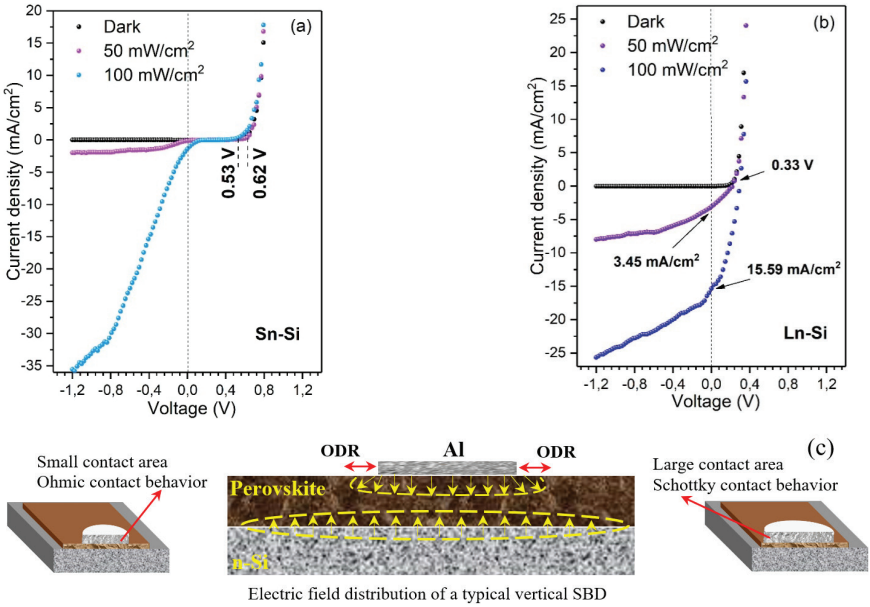

Figure 6. *Linear J-V plots of Al/$CH_3NH_3PbI_{3-x}Cl_x$/n-Si/Al diodes fabricated with different Al contact area; (a) 7.85x10^{-3} cm^2 and (b) 3.14x10^{-2} cm^2, (c) cross-section illustration of Al/ $CH_3NH_3PbI_{3-x}Cl_x$/n-Si junction to show of an overflowed depletion region (ODR) and p-n depletion region.*

Consequently, contrary to generation of photo-current by photons absorbed in active layer covered with circular or liner channel space, grid-line, transparent window and semi-transparent metal contact, the photo-current has been observed at the vertical SBD configuration consisted of the opaque Al metal contact. As seen in Fig. 7, the photo-diode and solar cell-like behavior has been observed at the diodes based on n-Si substrate while the p-Si based diodes showed weak photo-response. This phenomenon is attributed to the presence of two junctions inside the diode fabricated with p-type $CH_3NH_3PbI_{3-x}Cl_x$ thin film having µm scale carrier diffusion length. Furthermore, the presence and effect of electric field crowding around the edges of metal contact which is consisting of an overflowed depletion region has occurred the anomalous photo-current response. The Sn-Si diode showed a dominant p-n junction behavior having turn on voltage shift from 0.62 V to 0.53 V with increasing light intensity, and 1.97 and 33.06 mA/cm^2 reverse-bias photo-current at -1.0 V. Additionally, the Ln-Si diode showed Schottky barrier solar cell-like behavior having V_{oc} value at around 0.3 V with 3.45 and 15.59 mA/cm^2 J_{sc} values depend on the light intensity. However, it is clearly seen that the SBDs having opaque metal contact in the direction of illumination probably will not account for photo-response and will not behave like optoelectronic devices such

as photodiode and solar cell in case of passivation of overflowed depletion region around contact. Therefore, these effects should be considered in device design and characterization, and the use of active area is important in studies where light effects are evaluated.

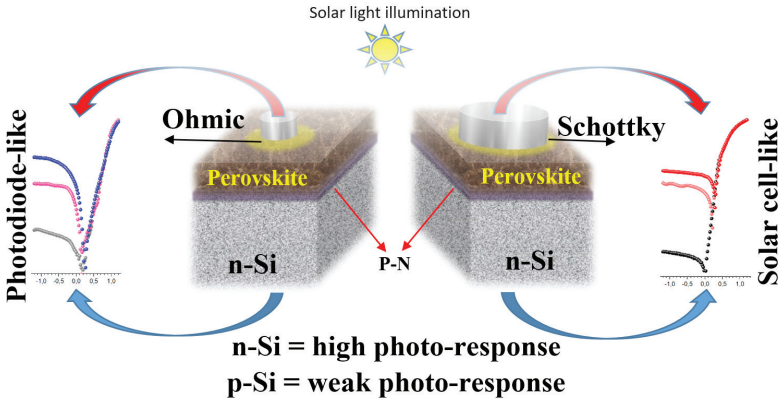

Figure 7. *Graphical abstract of n-Si based the photo-diode and solar cell-like devices.*

Experimental Details

Materials

The wafer substrates (n-Si and p-Si) were purchased from MTI KJ. The methylammonium iodide (MAI) powder (99.99% purity), lead chloride ($PbCl_2$) (99.99% purity) powder and dimethylformamide (DMF) solvent were purchased from Sigma-Aldrich. The chemical solvents; acetone, isopropyl alcohol, hydriodic acid, and hydrochloric acid were purchased from Sigma-Aldrich. ITO substrates were purchased from Delta Tech./(CB–50IN–S111).

Fabrication

Fabrication process was started with chemically cleaning of the (100) Si wafers using the RCA1 and RCA2 procedures, as in reported study [24]. After the cleaning process, the Al ohmic contact was deposited onto the unpolished side of Si wafer by thermal evaporation and annealed at 465 °C under N_2 atmosphere for 5 min. The perovskite precursor solution was prepared as a mixed solution of MAI and $PbCl_2$ with molar ratio of 3:1 (40% w/w) in the DMF solvent. The perovskite thin film was spin coated by one-step spin coating method onto the Si substrates at 5000 rpm for 60 seconds. And then, the perovskite thin films are thermally annealed at 90 °C for 60 minutes. Onto the perovskite/Si/Al structure, the circular Al rectifier contacts were deposited by thermal evaporation using shadow mask having different area 7.85×10^{-3} cm^2 and 3.14×10^{-2} cm^2. Therefore, the 7.85×10^{-3} cm^2 and 3.14×10^{-2} cm^2 are also considered as vertical diode

area. Finally, the diodes having Al/$CH_3NH_3PbI_{3-x}Cl_x$/Si/Al structure has been obtained. Additionally, the perovskite film was spin coated onto PEDOT:PSS/ITO substrate to analyze of the optical absorption spectrum, where the PEDOT:PSS was spin coated onto the ITO at 5000 rpm for 60s and annealed at 125 °C for 25min.

Measurement and Characterization

The measurement systems used are Bruker D2 PHASER XRD with CuKα radiation at λ= 1.54184 Å, Zeiss/Sigma 300 SEM, PerkinElmer Lambda2S UV–visible spectrometer (325–1100 nm), Hitachi 5100N AFM, and KLA Tencor P7 profilometer. For the electrical measurement, Keithley 2400 pico-ammeter/voltage source-meter was used. The solar-light illumination was carried out using a solar simulator system having AM 1.5G with Keithley 2400 source-meter unit. As an illustration, the fabrication and measurement processes were depicted in Fig. 8.

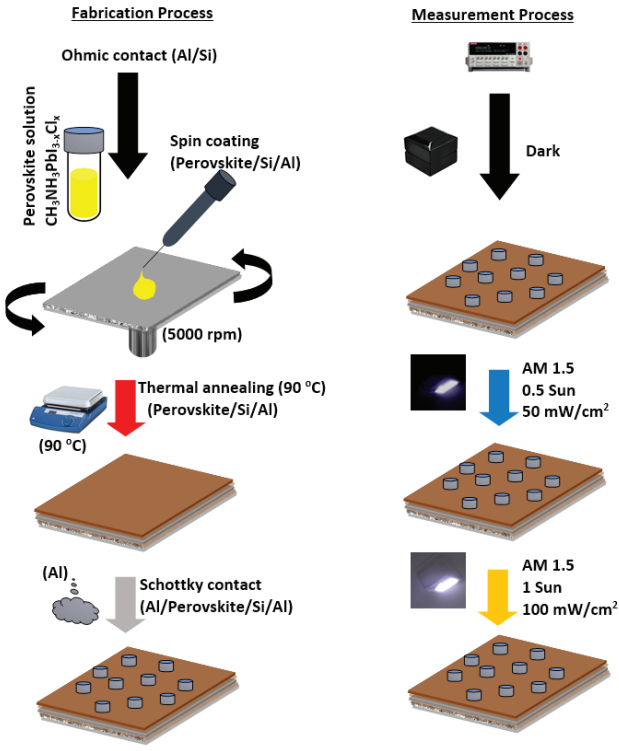

Figure 8. *Illustration of fabrication and measurement processes.*

Acknowledgement

I wish to express gratitude to Assist. Prof. Dr. Ahmet TAŞER for assistance and guidance in the thermal evaporation process.

References

[1] A. Baltakesmez, M. Biber, and S. Tuzemen, Improved perovskite film quality and solar cell performances using dual single solution coating, J. Appl. Phys. 122, 085502 (2017); https://doi.org/10.1063/1.4985826.

[2] S.M.H. Qaid, M.S. Al Sobaie, M.A. Majeed Khan, I.M. Bedja, F. H. Alharbi, M. Khaja Nazeeruddin and A. S. Aldwayyan, Band-gap tuning of lead halide perovskite using a single step spin-coating deposition process, Materials Letters 164 (2016) 498–501; http://dx.doi.org/10.1016/j.matlet.2015.10.135.

[3] X. Chen, H. Lu, Y. Yang and M.C. Beard, Excitonic Effects in Methylammonium Lead Halide Perovskites, J. Phys. Chem. Lett. 2018, 9, 10, 2595–2603; https://doi.org/10.1021/acs.jpclett.8b00526.

[4] Z.L. Zhang, B. Q. Men, Y.F. Liu, H.P. Gao and Y.L. Mao, Effects of precursor solution composition on the performance and I-V hysteresis of perovskite solar cells based on CH3NH3PbI3-xClx, Nanoscale Research Letters (2017) 12:84; https://doi.org/10.1186/s11671-017-1872-8.

[5] J.H. Heo, M.H. Lee, M.H. Jang and S.H. Im, Highly efficient $CH_3NH_3PbI_{3-x}Cl_x$ mixed halide perovskite solar cells prepared by re-dissolution and crystal grain growth *via* spray coating, J. Mater. Chem. A, 2016,4, 17636-17642; https://doi.org/10.1039/C6TA06718B.

[6] Q. Dong, L. Lei, J. Mendes and F. So, Operational stability of perovskite light emitting diodes, J. Phys.: Mater. 3 (2020) 012002; https://doi.org/10.1088/2515-7639/ab60c4.

[7] W. Wu, X. Wang, X. Han, Z. Yang, G. Gao, Y. Zhang, J. Hu, Y. Tan, A. Pan and C. Pan, Flexible Photodetector Arrays Based on Patterned $CH_3NH_3PbI_{3-x}Cl_x$ Perovskite Film for Real-Time Photosensing and Imaging, Adv. Mater. 2019, 31, 1805913; https://doi.org/10.1002/adma.201805913.

[8] T.S. Kao, Yu-H. Hong, Kuo-B. Hong and Tien-C. Lu, Perovskite random lasers: a tunable coherent light source for emerging applications, 2021 Nanotechnology 32 282001; https://doi.org/10.1088/1361-6528/abe907.

[9] D. Ali Aldemir, M. Kaleli, A. Celal Yavru, Electrical and photoelectric properties of Yb/CIGS thin filmSchottky photodiode, Sensors and Actuators A 311 (2020) 112091; https://doi.org/10.1016/j.sna.2020.112091.

[10] H. Uslu, Ş. Altındal, U. Aydemir, I. Dökme, I.M. Afandiyeva, The interface states and series resistance effects on the forward and reverse bias I–V, C–V and G/ω-V characteristics of Al–TiW–Pd_2Si/n-Si Schottky barrier diodes, Journal of Alloys and Compounds 503 (2010) 96–102; https://doi.org/10.1016/j.jallcom.2010.04.210.

[11] A.A.M. Farag, A. Ashery, E.M.A. Ahmed, M.A. Salem, Effect of temperature, illumination and frequency on the electrical characteristics

of Cu/p-Si Schottky diode prepared by liquid phase epitaxy, Journal of Alloys and Compounds 495 (2010) 116–120; https://doi.org/10.1016/j.jallcom.2010.01.098.

[12] A.G. Imer, E. Kaya, A. Dere, A.G. Al-Sehemi, A.A. Al-Ghamdi, A. Karabulut, F. Yakuphanoglu, llumination impact on the electrical characteristics of Au/Sunset Yellow/n-Si/Au hybrid Schottky diode, Journal of Materials Science: Materials in Electronics (2020) 31:14665–14673; https://doi.org/10.1007/s10854-020-04029-8.

[13] D. Rao Lambada, S. Yang, Y. Wang, P. Ji, S. Shafique and F. Wang, Investigation of Illumination Effects on the Electrical Properties of Au/GO/p-InP Heterojunction with a Graphene Oxide Interlayer, Nanomanufacturing and Metrology (2020) 3:269–281; https://doi.org/10.1007/s41871-020-00078-z.

[14] S.O. Tan, H. Uslu Tecimer, O. Çiçek, H. Tecimer, I. Orak, Ş. Altındal, Electrical characterizations of Au/ZnO/n-GaAs Schottky diodes under distinct illumination intensities, J Mater Sci: Mater Electron (2016) 27:8340–8347; https://doi.org/10.1007/s10854-016-4843-4.

[15] A. Baltakesmez, $FAPbI_3$ perovskite thin film having α/δ phase junction and its light harvesting performance in solar cell. J Mater Sci: Mater Electron 31, 17773–17783 (2020); https://doi.org/10.1007/s10854-020-04331-5.

[16] G.M. Ali, Performance analysis of planar Schottky photodiode based on nanostructured ZnO thin film grown by three different techniques, Journal of Alloys and Compounds 831 (2020) 154859; https://doi.org/10.1016/j.jallcom.2020.154859.

[17] R. Ramadan and R. J. Martín-Palma, Electrical Characterization of MIS Schottky Barrier Diodes Based on Nanostructured Porous Silicon and Silver Nanoparticles with Applications in Solar Cells, Energies 2020, 13, 2165; https://doi.org/10.3390/en13092165.

[18] Y. Wang, S. Yang, A. Ballesio, M. Parmeggiani, A. Verna, M. Cocuzza, C. Fabrizio Pirri, and S. Luigi Marasso, The fabrication of Schottky photodiode by monolayer graphene direct-transfer-on-silicon, J. Appl. Phys. 128, 014501 (2020); https://doi.org/10.1063/5.0004242.

[19] J. Gosciniak, F.B. Atar, B. Corbett and M. Rasras, Plasmonic Schottky photodetector with metal stripe embedded into semiconductor and with a CMOS-compatible titanium nitride, Scientific Reports (2019) 9:6048; https://doi.org/10.1038/s41598-019-42663-3.

[20] O.S. Cifci, A. Kocyigit and P. Sun, Perovskite/p-Si photodiode with ultra-thin metal cathode, Superlattices and Microstructures 120 (2018) 492–500; https://doi.org/10.1016/j.spmi.2018.06.009.

[21] S.K. Ravi, W. Sun, D.K. Nandakumar, Y. Zhang and S. Ching Tan, Optical manipulation of work function contrasts on metal thin films, Sci. Adv. 4, eaao6050 (2018); https://doi.org/10.1126/sciadv.aao6050.

[22] N. A. Torkhov, Effect of Photovoltage on Current Flow in Metal–Semiconductor Schottky Barrier Contacts, Semiconductors, 2011, 45 (7), pp. 935–943. https://doi.org/10.1134/S1063782611070220.

[23] B. K. Li, C. Wang, I. K. Sou, W. K. Ge, and J. N. Wang, Anomalous photocurrent observed in an Fe–ZnS:Fe Schottky diode, Applied Physics Letters 91, 172104 (2007); https://doi.org/10.1063/1.2801707.

[24] A. Baltakesmez, S. Tekmen, P. Köç, S. Tüzemen, K. Meral, and Y. Onganer , "UV-visible detector and LED based n-ZnO/p-Si heterojunction formed by electrodeposition", AIP Advances 3, 032125 (2013); https://doi.org/10.1063/1.4795737.

[25] T. Soto-Montero, W. Soltanpoor, and M. Morales-Masis, Pressing challenges of halide perovskite thin film growth, APL Materials 8, 110903 (2020); https://doi.org/10.1063/5.0027573.

[26] Y. Yao, G. Wang, F. Wu, D. Liu, C. Lin, X. Rao, R. Wu, Guangdong Zhou and Qunliang Song, The interface degradation of planar organic– inorganic perovskite solar cell traced by light beam induced current (LBIC), RSC Adv., 2017,7, 42973-42978; https://doi.org/10.1039/C7RA06423C.

[27] C. Zuo and L. Ding, Drop-Casting to Make Efficient Perovskite Solar Cells under High Humidity, Angew. Chem. Int. Ed. 2021, 60, 11242 – 11246; https://doi.org/10.1002/anie.202101868.

[28] S. Luo and W. A.Daoud, Crystal Structure Formation of $CH_3NH_3PbI_{3-x}Cl_x$ Perovskite, Materials 2016, 9(3), 123; https://doi.org/10.3390/ma9030123 .

[29] L. Xinli, C. Yongchao, L. Lihua and H. Jinliang, Perovskite Thin Film Consisting with One-Dimensional Nanowires, Materials 2018, 11(9), 1759; https://doi.org/10.3390/ma11091759.

[30] H. Xu, H. Zhang, Y. Ma, M. Jiang, Y. Zhang, Y. Wu, H. Zhang, R. Xia, Q. Niu, X. Li and W. Huang, Morphology control of organic halide perovskites by adding $BiFeO_3$ nanostructures for efficient solar cell, Scientific Reports (2019) 9:15441; https://doi.org/10.1038/s41598-019-51273-y.

[31] C. Hettiarachchi, N. Valdes, P. Mukherjee and S. Witanachchi, A Novel Single-Step Growth Process for the Deposition of $CH_3NH_3PbI_{3-x}Cl_x$ Perovskite Films from CH_3NH_3Cl and PbI_2 Precursors, Journal of Materials Science and Engineering A 6 (9-10) (2016) 233-242; doi: 10.17265/2161-6213/2016.9-10.001.

[32] E. Klein, R. Lesyuk and C. Klinke, Insights into the formation mechanism of two-dimensional lead halide nanostructures, Nanoscale, 2018,10, 4442-4451; https://doi.org/10.1039/C7NR09564C.

[33] C.L. Hettiarachchi, Organolead Halide Perovskite Solar Absorbers and Ferroelectric Nanocomposites for Harvesting Solar Energy Perovskite Solar Cells View Project Quantum Dot Solar Cells View Project. Ph.D. Thesis, University of South Florida, Tampa, FL, USA, April 2018.

[34] M.J. Cha, Y.J. Park, J.H. Seo and B. Walker, Depth-dependent electronic band structure at the Au/$CH_3NH_3PbI_{3-x}Cl_x$ junction, Phys. Chem. Chem. Phys., 2019,21, 14541-14545; https://doi.org/10.1039/C9CP00834A.

[35] H. Imran, I. Durrani, M. Kamran, T. M. Abdolkader, M. Faryad and N. Z. Butt, "High-Performance Bifacial Perovskite/Silicon Double-Tandem Solar Cell," in IEEE Journal of Photovoltaics, vol. 8, no. 5, pp. 1222-1229, Sept. 2018; doi: 10.1109/JPHOTOV.2018.2846519.

[36] P. H. P. Koller, F. W. M. Vanhelmont, H. Boeve, R. Coehoorn and W. J. M. de Jonge, Oxidation process of AlO_x-based magnetic tunnel junctions studied by photoconductance, Journal of Applied Physics 93, 8549 (2003); https://doi.org/10.1063/1.1555317.

[37] E. Karagöz, S.F. Varol, S. Sayın and Z. Merdan, Electrical characterization of two analogous Schottky contacts produced from *N*-substituted 1,8-naphthalimide, Phys. Chem. Chem. Phys., 2018,20, 30502-30513; https://doi.org/10.1039/C8CP04136A.

[38] **A.** Baltakesmez, A. Taşer, Z. Kudaş, B. Güzeldir, D. Ekinci and M. Sağlam, Barrier Height Modification of n-InP Using a Silver Nanoparticles Loaded Graphene Oxide as an Interlayer in a Wide Temperature Range. Journal of Elec Materi 48, 3169–3182 (2019); https://doi.org/10.1007/s11664-019-07088-8.

[39] V. Mikhelashvili, G. Eisenstein, V. Garber, S. Fainlei, G. Bahir, D. Ritter, M. Orenstein, A. Peer, On the extraction of linear and nonlinear physical parameters in nonideal Diodes, J. Appl. Phys. 85 (1999) 6873–6883; http://dx.doi.org/10.1063/1.370206.

[40] LF. Mao, Physical origins of the ideality factor of the current equation in Schottky junctions. Pramana - J Phys 94, 16 (2020); https://doi.org/10.1007/s12043-019-1868-2.

[41] N.A. Al-Ahmadi, Schottky barrier inhomogeneities at the interface of different epitaxial layer thicknesses of n-GaAs/Ti/Au/Si: Al0.33Ga0.67As. Heliyon. 2020 Sep 16;6(9):e04852. https://doi.org/10.1016/j.heliyon.2020.e04852.

[42] H.C. Card and E.H. Rhoderick, (1971) Studies of tunnel MOS diodes I. Interface effects in silicon Schottky diodes. J Phys D: Appl Phys 4: 1589-1601; https://doi.org/10.1088/0022-3727/4/10/319.

[43] M. Gokcen, M. Yıldırım, A. Demir, A. Allı, S. Allı, B. Hazer, UV illumination effects on electrical characteristics of metal–polymer–semiconductor diodes fabricated with new poly(propylene glycol)-b-polystyrene block copolymer, Composites: Part B 57 (2014) 8–12; http://dx.doi.org/10.1016/j.compositesb.2013.09.038.

[44] S.-Kyo Kim, H. Yang, and Y.-Seog Kim, Control of carrier injection and transport in quantum dot light emitting diodes (QLEDs) via modulating Schottky injection barrier and carrier mobility, J. Appl. Phys. 126, 185702 (2019); https://doi.org/10.1063/1.5123670.

[45] A. M. M.Tanveer Karim, M. K. R. Khan and M. S. Hossain, Temperature dependency of excitonic efective mass and charge carrier conduction mechanism in $CH_3NH_3PbI_{3-x}Cl_x$ thin films, Scientific Reports (2021) 11:10772; https://doi.org/10.1038/s41598-021-90247-x

[46] G. Zhyrair, M. Lenrik, A. Karapet, H. Valeri, A. Eduard and M. Khachatur, Determination of the complete set of optical parameters of micronsized polycrystalline $CH_3NH_3PbI_{3-x}Cl_x$ films from the oscillating transmittance and reflectance spectra, Mater. Res. Express 7 (2020) 016408; https://doi.org/10.1088/2053-1591/ab5c46.

[47] Y. Huang, K. V. A. Jayaprakash and C. Cheung, "Effects of edge termination using dielectric field plates with different dielectric constants, thicknesses and bevel angles," 2014 IEEE Applied Power Electronics Conference and Exposition - APEC 2014, 2014, pp. 2902-2906; doi: 10.1109/APEC.2014.6803716.

[48] S.N. Mohammad, F.J. Kub and C.R. Eddy, Field-plate design for edge termination in silicon carbide high-power Schottky diodes, Journal of Vacuum Science & Technology B 29, 021021 (2011); https://doi.org/10.1116/1.3562276.

[49] S. Roy, A. Bhattacharyya and S. Krishnamoorthy, "Design of a β-Ga_2O_3 Schottky Barrier Diode with p-Type III-Nitride Guard Ring for Enhanced Breakdown," in IEEE Transactions on Electron Devices, vol. 67, no. 11, pp. 4842-4848, Nov. 2020; doi: 10.1109/TED.2020.3025268.

[50] G.D.J. Smit, S. Rogge, and T.M. Klapwijk, Enhanced tunneling across nanometer-scale metal-semiconductor interfaces, Appl. Phys. Lett. 80, 2568 (2002); https://doi.org/10.1063/1.1467980